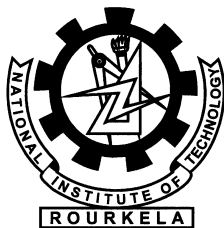


Some Studies on Designs of Planar Antennas for UWB Applications

S. Natarajamani



Department of Electronics and Communication Engineering
National Institute of Technology, Rourkela
Odisha, India-769 008

Some Studies on Designs of Planar Antennas for UWB Applications

*Thesis submitted in partial fulfillment
of the requirements for the degree of*

Doctor of Philosophy

in

Electronics and Communication Engineering

by

S. Natarajamani

(Roll: 508EC104)

under the guidance of

Dr. Santanu Kumar Behera

and

Dr. Sarat Kumar Patra



Department of Electronics and Communication Engineering
National Institute of Technology, Rourkela
Odisha, India-769 008

January 2014

Dedicated to my Appa, Amma and Paati



Department of Electronics and Communication Engg.
National Institute of Technology, Rourkela
Odisha, India-769 008

November 12, 2014

Certificate

This is to certify that the thesis titled *Some Studies on Designs of Planar Antennas for UWB Applications* by *S. Natarajamani* is a record of an original research work carried out under our supervision and guidance in partial fulfillment of the requirements for the award of the degree of Doctor of philosophy in *Electronics and Communication Engineering* during the session 2013-2014. We believe that the thesis fulfills part of the requirements for the award of degree of Doctor of Philosophy. Neither this thesis nor any part of it has been submitted for any degree or academic award elsewhere.

Dr. Santanu Kumar Behera
Associate Professor
Dept. of ECE
National Institute of Technology, Rourkela
Odisha, India - 769 008

Dr. Sarat Kumar Patra
Professor
Dept. of ECE
National Institute of Technology, Rourkela
Odisha, India - 769 008

Acknowledgements

I have been very blessed to receive all the support and encouragement from many people towards the completion of this dissertation. I would like to express my gratitude toward them.

First, I would like to express my sincere gratitude and indebtedness to Prof. S K Behera, Associate Professor, Department of Electronics and Communication, NIT Rourkela. his valuable guidance and constant encouragement were indispensable for the progress and completion of my thesis. It has been really a great privilege to work under him.

My co-adviser Prof. S K Patra guidance, support and motivation have helped me shape this thesis. Also, I would like to thank my committee members, Prof. S.Meher, Prof. K K Mahapatra, Prof. P K Sahu and Prof. S K Jena for serving in as my dissertation committee.

I would like to thank to Prof. K J Vinoy, IISC, Bangalore and Prof. C K Aanandan, CUSAT, Cochin for providing measurement facility in his antenna and microwave lab. Also thanks to Ms. Vijayshree and Mr. Lindo for their support during the measurement. I also wish to thank Dr. S. Sankaralingam, Jadavpur University, Kolkata for he is guidance and encouragement towards my research.

I am very much thankful to my colleague and friend Mr. Yogesh Kumar and Mrs. Runa Kumari Research scholar for their valuable suggestions and support during my research.

I extend my heartfelt thanks to My parents, Mr. Senthilnathan and Mrs. Suganthi, and my sister Mrs. Anitha sureshbabu and my grandmother Mrs. Senthamarai who taught me the virtues of perseverance and hard work; two qualities that have served me well throughout my graduate studentship.

S. Natarajamani

Abstract

In Ultra-Wideband (UWB) wireless system, considerable research efforts have been put into the design of UWB antennas and communication systems. These UWB antennas are essential for providing wireless wideband communications based on the use of very narrow pulses on the order of nanoseconds, covering a very wide bandwidth in the frequency domain and over very short distance at very low power densities. Also it is well known that, in traditional narrow-band communications, multiple antenna systems offer attractive aspects in wireless communication by means of Multiple-Input Multiple-Output (MIMO) techniques. These techniques either give out high channel capacities through spatial multiplexing, or offer an increase of link robustness. The present work deals with four new compact broadband antennas, suitable for portable applications are designed and characterized, namely- octagon shaped monopole, semi-circular disk monopole, semi-octagon shaped diversity, semi-circular diversity. The performances of these designs have been studied using standard simulation tools used in industry or academy and experimentally verified. One of the major contributions of the thesis lies in the analysis of the frequency and time-domain response of the designed UWB antennas to confirm their suitability for portable pulsed-UWB system. A technique to avoid narrow band interference by etching narrow slot resonators on the antenna is also proposed and their effects on a nano-second pulse have been investigated.

Contents

Certificate	ii
Acknowledgment	iv
Abstract	v
Contents	vi
List of Figures	ix
List of Tables	xv
List of acronyms	xvi
List of Symbols	xix
1 Introduction	1
1.1 Introduction	1
1.2 UWB Technology	1
1.2.1 Antenna for UWB systems	3
1.2.2 UWB antenna parameters	4
1.3 Planar Monopole Antenna	5
1.3.1 UWB multiple antennas	7
1.4 Challenges in Antenna Design	8
1.5 Motivation	9
1.6 Problem Statement	10
1.7 Thesis Organization	10
1.8 Summary	11

2	Planar Ultra WideBand Antennas: A state-of-the-art	12
2.1	Introduction	12
2.2	Planar UWB Antenna	13
2.3	Frequency Notched Function in UWB Antenna	16
2.3.1	Inserting slots	16
2.4	Multi Element Antennas	17
2.4.1	Planar diversity antenna	18
2.5	Summary	22
3	Planar Broadband Monopole Antennas	23
3.1	Semi Octagon Shaped Monopole Antenna	24
3.1.1	Antenna design and simulation results	24
3.1.2	Experimental verification	27
3.2	Semi Circular Disc Monopole Antenna	29
3.2.1	Antenna design and simulation results	29
3.2.2	Experimental verification	32
3.3	Band Notch Antenna	34
3.3.1	Band notch octagon shaped monopole antenna	34
3.3.2	Simulation and experimental verification	37
3.3.3	Band notch semi circular disk monopole antenna	40
3.3.4	Simulation and experimental verification	43
3.4	Summary	46
4	Planar Diversity Antenna	48
4.1	Introduction	48
4.2	Semi Octagon Shaped Diversity Antenna	49
4.2.1	Antenna geometry and simulation results	49
4.2.2	Experimental verification	54
4.3	Semi circular shaped diversity antenna	55
4.3.1	Antenna geometry and simulation results	55
4.3.2	Experimental verification	57

4.4	Band-Notched Diversity Antenna	59
4.4.1	Band-notched semi octagon shaped diversity antenna	60
4.4.2	Band-notched semi circular diversity antenna	68
4.5	Summary	74
5	Time Domain Analysis of Planar Antennas	76
5.1	Transfer Function Determination	76
5.1.1	Transient reception and radiation	78
5.1.2	Implementation in CST microwave studio software	78
5.2	Measurements with the Prototype Antennas	80
5.3	Impulse Responses of UWB Antennas	81
5.3.1	Pulse distortion analysis: Fidelity factor	81
5.3.2	Time domain parameters	85
5.4	Summary	87
6	Conclusion and Future Work	89
6.1	Summary	89
6.2	Limitations of the work	92
6.3	Future Work	92
A	Design Methodology	93
A.1	Introduction	93
A.1.1	Numerical and Analytical Approaches	93
A.1.2	Finite Element Method using Ansoft HFSS	95
A.1.3	Finite Integration Technique using CST	97
A.1.4	Antenna Fabrication	100
A.1.5	Input Reflection Coefficient and VSWR	101
A.1.6	Anechoic Chamber	102
A.1.7	Radiation Pattern Measurement	102
A.1.8	Antenna Gain Measurement	104
	Bibliography	105

List of Figures

1.1	Geometry of a monopole antenna	5
1.2	Printed square monopole antenna	6
1.3	Multiple antennas configuration	8
3.1	Geometry of a semi octagon shaped monopole antenna (a) Top layer (b) Bottom layer	24
3.2	Simulated reflection coefficient curve of a semi octagon shaped monopole antenna for different values L_1	25
3.3	Simulated reflection coefficient curve of a semi octagon shaped monopole antenna for different values W_f	26
3.4	Simulated reflection coefficient curve of a semi octagon shaped monopole antenna	27
3.5	Simulated input impedance curve of a semi octagon shaped monopole antenna	27
3.6	Measured reflection coefficient of a semi octagon shaped monopole an- tenna	28
3.7	Measured radiation patterns at 4.2GHz, 7.8GHz, and 10GHz (a) E- plane, (b) H-plane	28
3.8	Geometry of a semi circular disk monopole antenna	29
3.9	Simulated reflection coefficient of a semi circular disk monopole antenna	30
3.10	Simulated reflection coefficients of a semi circular disk monopole an- tenna for different feed gap ' d '	31

3.11	Simulated reflection coefficients of a semi circular disk monopole antenna for different feed gap ' r '	31
3.12	Simulated input impedance curve of a semi circular disk monopole antenna	32
3.13	Simulated surface currents distribution of a semi circular disk monopole antenna along with its simulated radiation patterns at (a) 3.8GHz, (b) 4.8GHz, (c) 6GHz and (d) 8.5GHz.	33
3.14	Measured reflection coefficient of a semi circular disk monopole antenna	34
3.15	Measured radiation of a semi circular disk monopole antenna at (a) 3.8GHz (b) 4.8GHz (c) 6GHz and (d) 8.5GHz	35
3.16	Geometry of a notched octagon shaped monopole antenna	36
3.17	Simulated VSWR results for different values W_1 for octagon shaped monopole antenna	37
3.18	Simulated impedance curve of a octagon shaped monopole antenna	37
3.19	Simulated results of the surface current distributions for the antenna (a) 3.5GHz (b) 5.5GHz and (c) 8.2GHz	38
3.20	Measured and simulated reflection coefficient of a octagon shaped monopole antenna	39
3.21	Measured radiation patterns at 4GHz, 7GHz, and 10GHz (a) E-plane (b) H-plane	39
3.22	Photograph of proposed semi octagon shaped monopole antenna (a) without bandnotch (b) with bandnotch	40
3.23	Measured gain of the octagon shape monopole antenna with and without bandnotch	41
3.24	Geometry of a notched semi circular disk monopole antenna	42
3.25	(a) Optimization of SLR by changing S_3 Value. (b) Optimization of integrated microstrip resonators by changing L_{S1} and L_{S2} value.	43
3.26	Simulated impedance of the notched disk monopole antenna	43
3.27	Simulated and measured reflection coefficient performances	44

3.28	Measured radiation patterns of the notched semi circular disk monopole antenna in (a) 4.5GHz (b) 6.5GHz (c) 8.5GHz frequencies.	45
3.29	Photograph of proposed semi octagon shaped diversity antenna (a) without bandnotch (b) with bandnotch	46
3.30	Measured gain of the semi circular disk monopole antenna with and without resonator	46
4.1	Geometry of the semi octagon shaped diversity antenna (a) Front view (b) 3D view	50
4.2	Simulated reflection coefficient and isolation coefficient for different with branches (a) $ S_{11} $ and $ S_{22} $ (b) $ S_{12} $ and $ S_{21} $	52
4.3	Simulated reflection coefficient and isolation coefficient for different values of 'd' (a) $ S_{11} $ and $ S_{22} $ (b) $ S_{12} $ and $ S_{21} $	52
4.4	Simulated reflection coefficient and isolation coefficient for different values of 'W _g ' (a) $ S_{11} $ and $ S_{22} $ (b) $ S_{12} $ and $ S_{21} $	52
4.5	Simulated reflection coefficient and isolation coefficient for different values of 'L _g ' (a) $ S_{11} $ and $ S_{22} $ (b) $ S_{12} $ and $ S_{21} $	53
4.6	Simulated surface currents distribution of the diversity antenna (a) Antenna 1 at 3.6 GHz and 7.8 GHz, (b) Antenna 2 at 3.6GHz and 7.8GHz	53
4.7	Simulated 3D gain radiation patterns for the antenna 1 and antenna 2: (a) and (b) at 3.6GHz, (c) and (d) at 5.8GHz, (e) and (f) at 7.8GHz and (g) and (h) at 10.2GHz	54
4.8	Measured and simulated reflection coefficient and isolation curves (a) $ S_{11} $, (b) $ S_{21} $	55
4.9	Measured radiation patterns of the antenna 1 in X-Z and Y-Z plane at (a) 3.6GHz, (b) 7.8GHz and (c) 10.2GHz	55
4.10	Geometry of the 2 element semi circular shaped diversity antenna (a) Top layer (b) Bottom layer (c) Top View	56

4.11 Simulated reflection coefficient and isolation coefficient curves for different ‘d’ values (a) $ S_{11} $ and $ S_{22} $ (b) $ S_{12} $ and $ S_{21} $	57
4.12 Simulated reflection coefficient and isolation coefficient curves for different iterations (a) $ S_{11} $ and $ S_{22} $ (b) $ S_{12} $ and $ S_{21} $	58
4.13 Simulated surface current distributions with port 1 excitation at (a) 3.4GHz, (b) 5GHz and (c) 7GHz	58
4.14 Measured and simulated (a) reflection and (b) isolation coefficients of semi circular diversity antenna	59
4.15 Measured radiation patterns of the antenna 1 in X-Z and Y-Z plane at (a) 3.4GHz, (b) 5GHz, and (c) 7GHz	59
4.16 Geometry of a notched semi octagon shaped diversity antenna	60
4.17 Simulated reflection coefficient with frequency for different values of (a) L_s , and (b) W_s	61
4.18 Simulated radiation patterns of a notched semi octagon shaped diversity antenna1 at (a) 3.5GHz, (b) 4.2 GHz, (c) 10.2GHz and (d) the current distribution at 3.5GHz	62
4.19 Simulated radiation patterns of a notched semi octagon shaped diversity antenna2 at (a) 3.5GHz, (b) 4.2 GHz, (c) 10.2GHz and (d) the current distribution at 3.5GHz	62
4.20 Measured reflection coefficient with frequency for notched semi octagon shaped diversity antenna 1	63
4.21 Measured radiation patterns of the antenna1 in X-Z and Y-Z plane at (a) 4GHz, (b) 6GHz and (c) 9.2GHz	63
4.22 Photograph of proposed semi octagon shaped diversity antenna (a) without bandnotch, (b) with bandnotch	64
4.23 Measured peak gains of semi octagon shaped diversity antenna	65
4.24 Simulated and measured (a) Envelope correlation coefficient(ECC) without bandnotched (b) Envelope correlation coefficient(ECC) with bandnotched.	67

4.25	Simulated and measured (a) Capacity loss antenna without bandnotched (b) Capacity loss antenna with bandnotched	67
4.26	Geometry of a notched semi circular diversity antenna	68
4.27	Simulated reflection coefficient and isolation coefficient with frequency for different values of S_2 and t	69
4.28	Simulated radiation patterns of a notched semi circular diversity antenna1 at (a) 3.3GHz, (b)5.8 GHz, (c) 8.6 GHz and (d) the current distribution at 5.8GHz	70
4.29	Simulated radiation patterns of a notched semi circular diversity antenna2 at (a) 3.3GHz, (b)5.8 GHz, (c) 8.6 GHz and (d) the current distribution at 5.8GHz	70
4.30	Measured reflection coefficient for a notched semi circular diversity antenna	71
4.31	Measured radiation patterns of the antenna 1 in X-Z and Y-Z plane at (a) 3.3GHz, (b) 4.5GHz and (c) 8GHz	71
4.32	Simulated and measured (a) Envelope correlation coefficient (ECC) without bandnotched, (b) Envelope correlation coefficient(ECC) with bandnotched.	72
4.33	Simulated and measured (a) Capacity loss antenna without bandnotched, (b) Capacity loss antenna with bandnotched	72
4.34	Photograph of proposed semi circular diversity antenna (a) without bandnotch, (b) with bandnotch	73
4.35	Measured peak realized gain of semi circular diversity antenna	73
5.1	UWB channel model (a) classical (b) contemporary	77
5.2	UWB channel model (a) Input pulse (b) Power spectral density	79
5.3	(a) System set-up (b) Antenna orientation: Face to Face and Side by Side	81

5.4	The measured transfer function in the face to face and side by side planes of the (a) octagon shaped monopole antenna (b) band notched octagon shaped monopole antenna (c) semi circular disk monopole antenna (d) band notched semi circular disk monopole antenna (e) semi octagon shaped diversity antenna (f) band notched semi octagon shaped diversity antenna (g) semi circular diversity antenna (h) band notched semi circular diversity antenna	82
5.5	The measured group delays in the face to face and side by side planes of the (a) octagon shaped monopole antenna (b) band notched octagon shaped monopole antenna (c) semi circular disk monopole antenna (d) band notched semi circular disk monopole antenna (e) semi octagon shaped diversity antenna (f) band notched semi octagon shaped diversity antenna (g) semi circular diversity antenna (h) band notched semi circular diversity antenna	83
5.6	Simulated and measured transmitted pulses by two identical antennas in their face to face and side by side orientations (a) octagon shaped monopole antenna (b) band notched octagon shaped monopole antenna (c) semi circular disk monopole antenna (d) band notched semi circular disk monopole antenna (e) semi octagon shaped diversity antenna (f) band notched semi octagon shaped diversity antenna (g) semi circular diversity antenna (h) band notched semi circular diversity antenna.	84
5.7	Impulse response, its envelope and time domain related parameters	86
A.1	Antenna structure in Ansoft HFSS.	96
A.2	A single mesh shape used in Ansoft HFSS	96
A.3	Antenna structure in CST MW studio	98
A.4	A single (a) hexahedral, (b) tetrahedral and (c) surface mesh element used in CST MW Studio.	98
A.5	Various steps involved in the fabrication process	100
A.6	Antenna measurement setup	103

List of Tables

1.1	Frequency range for various types of UWB systems under -41.3dBm EIRP emission limits	2
3.1	Dimensions of octagon shaped monopole antenna	25
3.2	semi circular disk monopole antenna parameters	30
3.3	Dimensions of notched octagon shaped monopole antenna	36
3.4	Dimensions of notched semi circular shaped monopole antenna	42
3.5	Comparison between proposed works with existing works.	47
4.1	The ratio of the branch lengths to the total length of structure	51
4.2	Dimensions of semi octagon shaped diversity antenna	51
4.3	Dimensions of 2 element semi circular shaped diversity antenna	56
4.4	Comparison between proposed works with existing works.	74
5.1	Measured fidelity of the transmitted pulses	85
5.2	<i>FWHM</i> and ringing in face to face and side by side planes	87

List of acronyms

Here are the main acronyms used in this document. The meaning of an acronym is usually indicated once, when it first occurs in the text.

AUT	Antenna Under Test
BW	Bandwidth
CAD	Computer Aided Design
CPW	Coplanar Waveguide
CST MWS	Computer Simulation Technology Microwave Studio
CELC	Complementary Electric Inductive Capacitive
CSRR	Complementary Split-Ring Resonator
dB	Decibel
dBi	Decibel Isotropic
EBG	Electromagnetic Band-Gap
ECC	Envelope Correlation Coefficient
EIRP	Effective Isotropic Radiated Power
EMC	Electromagnetic Compatibility
FCC	Federal Communication Commission
FDTD	Finite Differentiation Time Domain
FEM	Finite Element Method
FIT	Finite Integration Technique
FWHM	Full Width Half Maximum
GPS	Global Positioning System
GPRS	General Packet Radio Service
GSM	Global System Mobile
HFSS	High Frequency Structural Simulator
I-UWB	Impulse UWB
IEEE	Institute of Electrical and Electronics Engineers
ITM	International Mobile Telecommunications
ISM	Industrial Scientific Medical

ISI	Inter Symbol Interference
LTI	Linear Time Invariant
MIC	Microwave Integrated Circuit
MIMO	Multiple Input Multiple Output
MoM	Method of Moment
MPA	Microstrip Patch Antenna
MIMO	Multiple Input Multi Output
MISO	Multiple Input Single Output
NBI	Narrow Band Interference
PCB	Printed Circuit Board
PDA	Personal Digital Assistant
PSD	Power Spectral Density
PIFA	Printed Inverted F Antenna
PIFA	Printed Inverted L Antenna
RF	Radio Frequency
RL	Return Loss
RC	Reflection Coefficient
SPA	Suspended Plate Antenna
SAP	Shorted Annular Patch
SNR	Signal to Noise Ratio
SMA	Sub Miniature Architecture
SISO	Single Input Single Output
SIMO	Single Input Multiple Output
TSA	Tapered Slot Antenna
UHF	Ultra High Frequency
USB	Universal Serial Bus
UWB	Ultra Wide-Band
VHF	Very High Frequency
VNA	Vector Network Analyzer

VSWR	Voltage Standing Wave Ratio
UV	Ultra Violet
WiMax	Worldwide Interoperability for Microwave Access
WLAN	Wireless Local Area Network
WPAN	Wireless Personal Area Network

List of symbols

ρ_c	Envelope correlation coefficient
λ	Wavelength
λ_0	Free-space Wavelength
λ_g	Guided Wavelength
τ	Scaling Factor
$\tan\delta$	Loss tangent
c	Speed of light in free space
γ	Propagation Constant
α	Attenuation Constant
β	Phase Constant
Γ	Return loss
τ_r	Ringling
τ_g	Group Delay
ϵ_{eff}	Effective Permittivity
ψ^R	Receiving antenna correlation matrix
\vec{E}	Electric field intensity
\vec{H}	Magnetic field intensity
\vec{D}	Electric flux density
\vec{B}	Magnetic flux density
φ_E	Scalar quantities of electric flux
φ_B	Scalar quantities of magnetic flux
\vec{x}	Electric field vector
Δt	Maximum time step
f_c	Center frequency
G_t	Gain of the transmitting antenna
G_r	Gain of the receiving antenna
P_t	Transmitted power
P_r	Received power

CHAPTER 1

Introduction

1.1 Introduction

Ultra-wideband (UWB) technology is one of the most promising technologies for high data rate wireless communications ($\geq 100\text{Mbits/s}$ in 15m distance), high accuracy radars application and imaging systems. Compared to conventional broadband wireless communication systems, the UWB system operates with an extremely wide bandwidth in the microwave band along with a very low emission limit. Due to the system features and unique applications, antenna design for UWB has a variety of challenging issues such as broadband response in terms of impedance, gain, radiation patterns as well as small or compact physical size. This chapter discusses the antenna design issues in UWB systems. Firstly, the UWB technology and regulatory environment are briefly introduced, followed by a review of antenna in UWB system. Finally, a description of the stimulus behind the current investigations is presented.

1.2 UWB Technology

UWB is a wireless technology for transmitting digital data over a wide spectrum with very low power and has the ability to carry huge amounts of data over short distance. The Shannon's equation shows that increasing channel capacity 'C' demands a linear increase in bandwidth with signal to noise ratio (SNR) remaining constant.

$$C = B * \log_2(1 + \text{SNR}) \tag{1.1}$$

Equation (1.1) illustrates that the transmission data rate can be raised by enhancing the bandwidth or SNR. SNR can be general improved by increasing signal power. Nevertheless, the signal power cannot be increased as many portable devices are powered by battery and potential interference with other radio systems should also be suppressed. Therefore, bandwidth enhancement is the solution to realize a higher data rate. Relation among transmitted power, received power and distance in free space is given in (1.2)

$$d \propto \sqrt{\frac{p_t}{p_r}} \quad (1.2)$$

where ‘ d ’ denotes the distance, ‘ p_t ’ the transmitted power and ‘ p_r ’ the received power. Equations (1.1) and (1.2) together suggest that, it is more efficient to achieve higher capacity by increasing the bandwidth instead of power, but it is equally difficult to achieve in longer transmission range. Thus, UWB has been primarily designed for high data rate technology with short transmission range systems. In 2002, the United States Federal Communications Commission (FCC) adopted the first report that validated the commercial operation of Ultra Wideband (UWB) technology [1]. The intention was to provide efficient use of frequency spectra for short-range high data-rate Wireless Personal Area Network (WPAN). It was also envisioned to provide long-range low data-rate wireless connectivity applications along with radar and imaging systems as shown in Table 1.1

Table 1.1: Frequency range for various types of UWB systems under -41.3dBm EIRP emission limits

Applications	Frequency range(GHz)
Indoor communication systems	3.1-10.6
Ground-penetrating radar, wall imaging	3.1-10.6
Through-wall imaging systems	1.61-10.6
Surveillance systems	1.99-10.6
Medical imaging systems	3.1-10.6
Vehicular radar systems	22-29

UWB signal occupies extremely large bandwidth where the Radio Frequency (RF) energy spreads over enormous spectrum. It’s spectrum is wider than any incumbent

narrow band wireless systems in terms of magnitude and its emitted power. If the full 7.5GHz band allocated for UWB is optimally utilized then the maximum achievable power to UWB transmitters is limited to 0.556mW. This is barely a fraction of available transmitted power in the Industrial, Scientific and Medical (ISM) bands, like the Wireless Local Area Network (WLAN). This effectively confines the UWB scheme to indoor and short-range communications at high data rates or mid-range communications at low data rates. Applications, such as wireless Universal Serial Bus (USB) and Wireless Personal Area Network (WPANs) have been proposed spreading across hundreds of Mbps to several Gbps data rates with a coverage distance ranging from 1 to 4 meters [2]. For ranges beyond 20 meters, the achievable data rate by UWB is inferior for existing WLAN systems.

1.2.1 Antenna for UWB systems

With the advancement of UWB communications, there have been considerable research carried out in evaluation of effectiveness of UWB antennas for commercial applications [3]. Historically, there have been three different classes of broadband antennas. The first is the *DC-to-daylight class*. These antennas are designed to have maximal bandwidth. Typical applications include ground penetrating radars, field measurement or electromagnetic compatibility radar and impulse radar. The design goal of these antennas is to receive as wide spectrum as possible.

Horn antennas: A horn antenna is an electromagnetic funnel directing energy in a particular direction [4]. Horn antennas have high gain and relatively narrow beams. However, they tend to be larger and bulkier. These antennas are well suited for point-to-point communication applications where a narrow beam width is required.

Reflector antennas: Reflector antennas direct energy in a particular direction similar to horn antennas. Reflector antennas are generally easier to modify and adjust by manipulating the feed. Examples of these include the Hertz's parabolic cylinder reflector [5].

Frequency-independent antennas: Frequency independent antennas are based upon a variation in geometry from a smaller to a larger scale portion [6]. The smaller scale

portion contributes to higher frequencies while the larger one contributes to lower frequencies. Practically, the effective source of the radiated fields varies with frequency, giving a disperse behavior. Examples of this type of antenna are the spiral antenna, log periodic antenna and conical spiral antennas.

Small antennas: Small antennas tend to be small, omnidirectional or quasi omnidirectional. Examples include the Lodge's biconical antenna [7] bow tie antenna, and diamond dipole [8].

The growing significance of UWB communication, encouraged researchers to investigate on small antennas, since in many applications the antenna has to be small enough to be integrated into portable devices. Two families of compact antennas have emerged to provide this solutions. The first originated from biconical antennas, but in planar configuration which includes bow-tie, diamond, circular and elliptical disc dipoles. The second one originated from the development of monopole elements. A number of UWB monopole based upon different planar elements like circular, square, elliptical etc, have been demonstrated to provide UWB characteristics. According to classical resonating theory, these kinds of antennas is no more suitable. Schantz et.al suggested the dipole mode and high-order modes to account for the operation of UWB planar antennas [9].

1.2.2 UWB antenna parameters

Depending on the application, UWB antenna parameters for frequency or time domains can be selected. Inverse Fourier transform is used to switch from the frequency domain to time domain. The following are the important parameters of UWB antenna.

Peak value of the impulse response $P(\theta, \phi)$ is the maximal value of the strongest peak of the antenna transient response.

Pulse width is a measure of describing the broadening of the radiated impulse. This value is limited to a few hundred picoseconds in order to ensure high data rates in communication.

Ringling (τ_r) is an undesired effect in UWB antenna. The energy storage or multiple

reflections in the antenna result in oscillation of the radiated pulse after the main peak. This energy is of no use and lowers the peak value. The duration of ringing (τ_r) is expressed as the time until the pulse amplitude has fallen from the peak value to below a certain lower limit α . The ringing is expressed in nano seconds (ns) and should be small, i.e. less than a few pulse widths.

Group delay (τ_g) quantitatively evaluates the disperse performance of the antenna. It is defined in frequency domain as in (1.3)

$$\tau_g(\omega) = -\frac{d\psi(\omega)}{d(\omega)} = -\frac{d\psi(f)}{2\pi df} \quad (1.3)$$

Fidelity of an antenna is a measure of how accurately the received voltage available at the antenna terminal reproduces the behavior of transient field incident upon the antenna. For the transmitting, it is a measure of how accurately the time integral of the transmitted field reproduces the behavior of the voltage applied to the antenna terminals. It is to be noted that the antenna fidelity is waveform specific; i.e, an antenna may provide a high-fidelity reproduction for some waveforms and be unable to provide equivalent fidelity for many other waveforms [10].

1.3 Planar Monopole Antenna

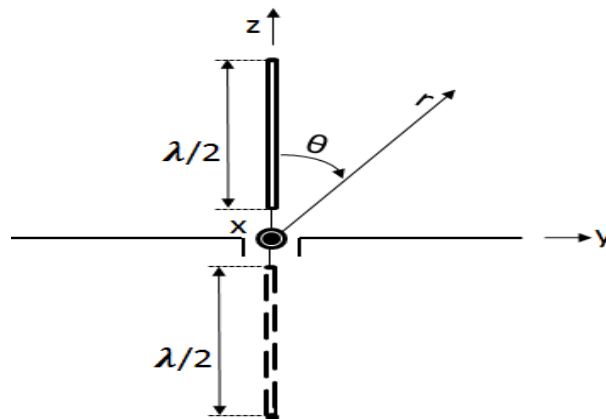


Figure 1.1: Geometry of a monopole antenna

When one arm of the dipole is replaced with a large ground plane, the new arrangement is a monopole antenna as shown in Figure 1.1. If the ground plane is large enough, the monopole radiation matches the dipole radiation behavior, since the ground plane acts as electric mirror and creates the other half. A monopole antenna is inherently unbalanced. Hence, it is suitable to be connected directly to the center conductor of a coaxial cable and grounded to the outer shield. Comparing with the dipole, just half of the power is radiated above the ground in terms of radiation resistance and directivity respectively.

The demand for broadband antennas that are capable of supporting high data speeds and multiband operations for modern wireless communication systems have increased significantly. These systems need low cost solutions with desired performance in terms of impedance bandwidth, polarization and gain. Planar antennas play an important role in various wireless communication applications due to their unique merits, such as small volume, low manufacturing cost and easy integration into planar circuits.

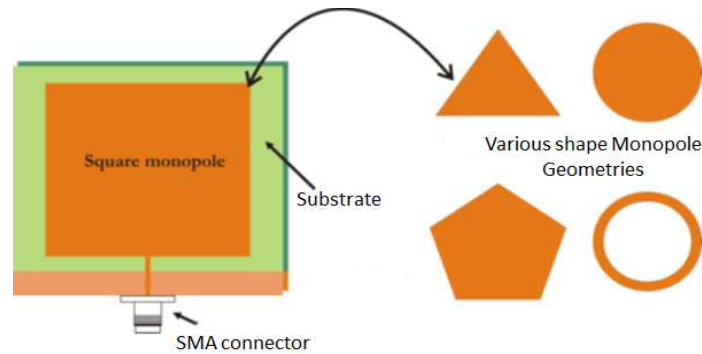


Figure 1.2: Printed square monopole antenna

With respect to radiation performance, the planar antennas can usually be categorized in terms of radiation performance into microstrip patch antenna, suspended plate antenna (SPA), planar inverted antenna and planar monopole antenna [11, 12]. Generally, the changes in such antenna design are made in terms of specific requirements of applications. The microstrip patch antenna, in its basic form has a low profile.

Due to conformal design, it suffers from narrow impedance bandwidth. In contrast, the planar monopoles usually have a high profile above a ground plane with broad bandwidth. The geometry of a monopole antenna is depicted in Figure 1.2.

Considering the antenna profile, impedance and radiation performance, the SPAs is a good option for fixed base stations in wireless communication systems, whereas planar monopole is more suitable for mobile wireless terminals. A variety of techniques have been developed to further enhance the broadband performance of the SPAs and planar monopoles. Due to the merits of acceptable performance, low profile and particularly low manufacturing cost, the SPAs and planar monopoles have been widely applied to high-speed wireless communication systems.

1.3.1 UWB multiple antennas

The use of multiple antennas are derived from the theoretical works done by Winders et al [13], Foschine et al [14]. The original idea was to use multiple antennas at both receiver and transmitter sides to increase the capacity of the wireless channel. Consequently, there was a growing interest towards the development of codes and schemes to enable the systems to approach the limit. On the other hand, works by Tarokhe et al [15], and Alamouti et al [16] on space-time block coding, demonstrated the possibility to obtain transmit diversity without channel state information at the transmitter and boosted research in that direction.

An important stimulus was given by the researches at Bell Laboratories on layered space-time techniques [14], showing high spectral efficiency. When multiple antennas are employed at both receiver and transmitter, Multiple-Input Multiple-Output (MIMO) systems come into picture. Single Input Single-Output (SISO) is the usual configuration with one antenna at both ends. Single-Input Multiple-Output (SIMO) uses a single transmitting antenna and multiple receiving antennas. Multiple-Input Single-Output (MISO) employs multiple transmitting antennas and a single receiving antenna as shown in Figure 1.3. Single Input Single-Output (SISO) is the usual configuration with one antenna at both ends. Single-Input Multiple-Output (SIMO) uses a single transmitting antenna and multiple receiving antennas. Multiple-Input

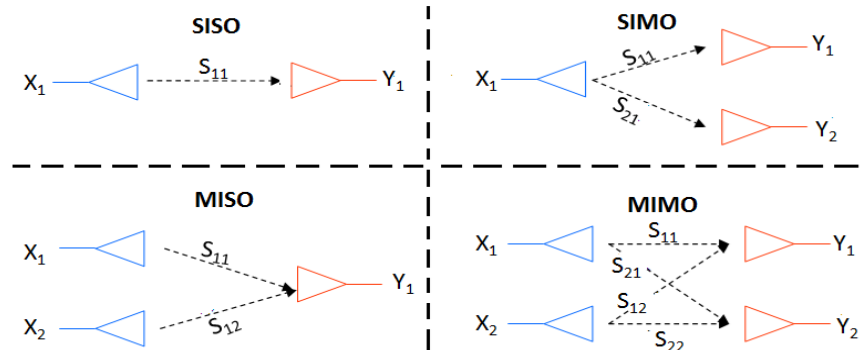


Figure 1.3: Multiple antennas configuration

Single-Output (MISO) employs multiple transmitting antennas and a single receiving antenna as shown in Figure 1.3.

1.4 Challenges in Antenna Design

Modern wireless communication industry is advancing rapidly since all the communication systems are integrating multiple applications, such as WLAN, Bluetooth etc, and large number of hand held devices are being introduced. In the near future, most of the wireless protocols will be employed in the mobile devices. Antenna isolation is a very difficult problem to solve due to close proximity between the antennas in space limited devices, particularly in MIMO devices.

Another challenge is the availability of space in a mobile device. In order to overcome this challenge, there is need for multiband designs with consistent radiation patterns, efficiency and polarization over the wide frequency band. Generally, most of the multiband antennas meet the return loss requirements but the radiation performance degrades at higher frequency ranges. Electronically tunable antennas have been potential solution for application areas like DVD-H. Antenna planning and placement is another challenge, which involves selection and placement of antenna efficiently in a system by considering both electrical and mechanical requirements. The UWB antennas are used for short range application and cannot be as highly effi-

cient as the WiMax and WLAN antennas and can be fabricated as a low-efficient chip antenna. The WiMax and WLAN antennas should provide much higher efficiency since they have long range application and in most of the cases, there should have certification from the service provider.

Ground plane of the antenna plays an important role in its design. The ground plane is generally symbolized as the return path for the current in the patch. In case of whip antennas, the ground plane can be treated as the other half of the dipole to the antenna.

In case of large antennas, the challenge in design is to realize ultra-low side-lobes and to reduce electromagnetic interference. The modeling of the large antennas to predict its performance is another difficult task. Currently, commercial softwares are quite limited in their ability to handle the structures which require a problem description with a very large number of meshes because of their complexity, multi-scale characteristics and homogeneous nature.

1.5 Motivation

With the growing demand of high speed data transfer and internet access, the communication systems with wideband applications are becoming more prevalent. The motivation for the proposed work comes from the need of compact, highly efficient, low cost antenna suitable for broadband operation. The diversity antenna design for portable devices in consumer electronics such as PCs and mobile devices will be challenging due to the space constraint. It is essential to maintain low mutual coupling when the antenna elements are placed in close proximity to each other and stable radiation performance across a broad operating bandwidth. The interference between wideband devices with other existing narrow band communication networks can be sorted by implementing filters to notch out the required frequency bands. However, since additional filters would increase the size of the devices, embedded filter on the antenna is preferred. To meet some of these challenging demands, this thesis work promotes the study and design of planar antennas. The aim of the thesis is to inves-

investigate the requirements for a wide band behavior of compact planar antenna designs. This work looks at the wideband performance of the monopole and diversity antennas in detail. Several designs using commercially available microwave substrates are proposed that could be successfully implemented in consumer electronics applications. It is important to characterize the designed UWB antennas in terms of their transient performances.

1.6 Problem Statement

With the motivation mentioned in section 1.5, we take up the problem for the doctoral research, which is stated as follows:

To design and develop

- (i) Planar broadband monopole antennas,
 - (ii) Planar diversity antennas,
 - (iii) Planar antennas with time domain characteristics,
- for UWB applications.

1.7 Thesis Organization

Chapter 1 of this thesis presents an overall introduction to UWB systems and discusses scope of research in field of antennas for UWB. Finally, a description of the stimulus behind the present investigations is presented and this chapter concludes with the details of the organization of the present thesis.

Chapter 2: This chapter is devoted to the literature on the present work. Recent development of UWB technology, review on monopole and diversity antenna for UWB applications are discussed. Finally, the chapter is summarized in Section 2.5.

Chapter 3: In this chapter, two novel compact designs of planar monopole antennas are presented. These antennas perform well in terms of its impedance matching and gain, over a wide band and easily comply with the FCC UWB frequency band. The operating principle of the antenna is addressed based on the investigation of the antenna performance and characteristics. A technique to prevent Narrow Band

Interference (NBI) is also discussed. Experimental results in the frequency domain are presented followed by conclusions.

Chapter 4: The frequency domain performance of planar diversity antennas are detailed in this chapter. The diversity characteristics of the proposed antenna evaluated by envelope correlation coefficients are computed from the reflection coefficient values. The antenna structure is compact and performs well over UWB frequency band. The inverted L-shape stub and Complementary Electric Inductive-Capacitive (CELC) resonator are introduced in the radiator without changing the patch size for notched narrow frequency band.

Chapter 5: This chapter investigates the influence of the antenna on radiation of a UWB pulse to confirm its suitability for Indoor-UWB applications. The transfer function measurements are performed for both the face to face and side by side plane and their impulse responses are deduced. From the impulse responses, parameters such as Full Width Half Maximum (FWHM) and ringing are computed and compared. The influence of the antenna on pulse transmissions is evaluated by convolution of the impulse response with a UWB pulse. The time domain distortion for the different designs is then characterized in terms of mathematically tractable parameter like fidelity.

Chapter 6: This chapter presents the summary and conclusion of the overall work, brief descriptions as well as the scope for future investigations are also sketched out. In the Appendix, the methodology for developing the antennas, Viz. Simulation studies; fabrication and measurement done with the test set up are discussed.

1.8 Summary

This chapter provides a brief introduction to UWB technology and planar antennas. This chapter also systematically outlines the motivation behind this work and the problem statement of the thesis. A concise presentation of research work carried out in each chapter has been dealt with. In essence, this chapter provides an overview of the thesis in a comprehensive manner.

CHAPTER 2

Planar Ultra WideBand Antennas: A state-of-the-art

2.1 Introduction

Microstrip patch antennas in their basic forms are considered as narrow band antenna (bandwidth typically between 1% to 10%). This essentially limits the application of this type of antenna. For this reason, much effort has been devoted to the development of broadband techniques. The techniques can be categorized in to two main groups: Impedance matching techniques and introduction to multiple resonances. By incorporating broadband impedance matching technique between the antenna and the feed line, a good matching over a broad frequency range can be attained. The matching network can be a quarter-wavelength impedance transformer, tuning stubs, active components and many more combinations [17]. Alternately, if closely distributed resonances are well excited simultaneously, the bandwidth can be enhanced. The simple configuration based on this approach would be the use of multiple parasitic elements to add extra resonant path and therefore increase the bandwidth [18].

UWB antennas are the key components of the UWB systems. They have received significant attention from research in recent years. With increasing popularity of UWB systems, there have been breakthroughs in the design of UWB antennas. Due to their wide frequency impedance bandwidth, simple structure, easy of fabrication on printed circuit boards (PCBs) and Omni-directional radiation patterns there has been a breakthrough in the design of UWB antennas. PCB versions of

planar monopole antenna are considered to be promising entrant for the applications of UWB communication. However, there are several existing narrow band communication systems operating below 10.6GHz in the same UWB frequency band and may cause interference with the UWB systems such as IEEE 802.11a WLAN systems or HIPERLAN/2 wireless systems or WiMAX wireless systems. These systems operate at 3.5GHz or 5.15GHz-5.825GHz which may cause interference with a UWB system. To avoid the interference with the existing wireless systems, a filter with bandstop characteristics may be integrated with the UWB antennas to achieve a notch function at the interfering frequency band.

This chapter discusses the background information and literature review related to the planar antennas for UWB applications. This chapter is organized as follows. Section 2.2 presents a brief introduction on planar UWB antenna. Section 2.3 gives detail information related to the band notch antennas. Various diversity antennas are reviewed in Section 2.4, followed by a summary in Section 2.5.

2.2 Planar UWB Antenna

In 1898, Oliver Lodge had developed spherical dipoles, square plate dipoles, bi-conical dipoles and bowtie dipoles [7] and had introduced the concept of a monopole antenna with earth as the ground. A renewed interest in the wide band antennas led to the rediscovery of biconical and conical monopoles by carter in 1939 [19]. Carter improved upon Lodge's original design by incorporating a broadband transition between the feed lines and radiating elements. The complete analysis of these antennas can be found in [20].

Another remarkable invention is the classic volcano smoke antenna that is developed by Kraus in 1945, a detailed discussion can be found in [21]. This antenna topology offers exceptional bandwidth and azimuthal Omni directionality. Sleeve monopole configurations [20] are excited using a coaxial transmission line and exhibit broad band radiation behavior. The sleeve exterior acts as a radiating element, while its interior acts as the outer conductor of the feed coaxial transmission line.

Stohr et al. proposed the use of ellipsoidal monopoles and dipoles [22] which were re-discovered in [23]. This study describes the extensive analysis carried out on square, rectangular and hexagonal disc monopole antennas in addition to the elliptical design. Square or rectangular monopole antennas are inherently bandwidth limited and in order to improve the bandwidth, various techniques were proposed. In [24], it was demonstrated that when a shorting pin is added to a planar monopole antenna, an additional mode is excited below the fundamental mode. By optimizing the dimensions, 50% size reduction can be obtained compared to an equivalent planar monopole without a shorting pin. In [25] two techniques are presented: offset feeding and use of orthogonal square monopoles on a circular base to obtain wide band response and omnidirectional radiation.

The use of beveling technique [26] and that of a shorting pin can improve the overall impedance bandwidth of square monopole antennas in [27]. The use of double feeding and trident shaped feeding in [28] are proposed to improve the impedance bandwidth of such antennas. The different radiator types that have been reported are semi-circular base [29], trapezoidal [30], triangular [31], steeped rectangular patch [32], circular [33] and elliptical [34]. The radiator edge near the ground is an important parameter which affects the antenna performances and they have even been characterized by binomial functions for ultra-wideband performance [35]. Even though such curved radiators along with straight ground edge gives wide band performance, the antenna size can be reduced by making ground plane and feed modifications. The ground edges have been slotted [36], curved and hexagonal shaped [37], trident shaped [38] or with slits on the ground plane for improved bandwidth performance [39].

Although various shapes and types of feeding have been examined in literature, most of the antennas in this class operate on one principle that is overlapping of closely distributed several resonance modes. Investigations show that the first resonance is determined by the overall height of the radiator. This implies that, at the lower end of the frequency band, the antenna operates in an oscillating mode i.e. standing wave mode. At the high frequency end, the slot formed by the lower edge of the radiator and the top edge of the ground plane supports the traveling wave. In the middle of

the band the antenna operated in a hybrid mode of standing and traveling waves.

Thomas et al. [40], proposed a new ultra wideband sleeved transmission in line-fed rectangular planar disc monopole antenna with a small ground plane. Objective of the study was to design a monopole antenna with improved radiation performance than the existing ones. The antenna offers an ultra-broadband performance with a VSWR of less than 2.5:1. Certain UWB applications such as a wireless dongle required antenna limited in space [41]. This compact antenna comprises an L-shaped rectangular monopole element and a matching section and is relatively easy to fabricate. In [42] the antenna is mounted at the top portion of the PCB and one end of the radiating arm is short-circuited to the system ground plane. With the proposed antenna structure, wide operating bandwidth of larger than 7.6GHz is obtained which easily covers the 3.1GHz and 10.6GHz.

In [43], an elliptic-card ultra-wideband planar antenna has been proposed. The design consists of an elliptical radiating element and feeding structure which are mounted on the back and front surfaces respectively. The structure of the antenna is miniaturized by optimizing its elliptic profile. The required ground plane size is only 22mm×40mm.

In [44], a semi elliptical dipole antenna is proposed. This antenna has large bandwidth covering the frequency band of 3.1GHz to 10.6GHz, and radiation patterns are similar to conventional dipole antenna. A compact omnidirectional monopole antenna is presented in [45]. This monopole antenna sequentially embeds several pairs of rectangular notches in two corners of the radiation patch. With this stability of the H-plane patterns are improved, especially at the higher frequencies between 11GHz to 17GHz.

A low profile slot antenna is presented in [46]. This antenna is constructed by etching a T-shaped open-ended slot in the ground plane that is excited by a microstrip feed line. Multiple resonant frequencies are excited and merged to provide a return loss of -10dB [47–54].

The review of the planar monopole antennas confirms the requirement for a tapered transformation from the feed to the antenna edges so as to have a gradual impedance

variation among the different resonant mode excitation. The ground and radiator edges basically operate as a pair of opposing tapered slot lines which makes them inherently wide band. However, their radiation patterns may deviate from the desired omnidirectional behavior as the tapered slot line antennas are relatively directional.

2.3 Frequency Notched Function in UWB Antenna

UWB systems must share their operational frequency band with existing systems such as WLAN, WiMAX and so on due to its wideband characteristic. So it is necessary to avoid interference with nearby communication systems. While it was accomplished by a conventional filter in the radio frequency receiver front end, it is possible to design UWB antennas with a band notch characteristic to aid in narrow band signal rejection. This section presents different methods to notch some frequency bands such as inserting slots and removing narrow band resonant structure. In addition, the techniques to control the notched band and to notch multiple bands are discussed.

2.3.1 Inserting slots

To obtain the frequency band notched function in UWB antenna, the well known method is to insert the slots. Various notched UWB antennas studied by many researchers can be classified according to slot's locations such as radiating elements, ground plane, feeding line and vicinity of the radiating element. UWB antennas have slot on the various radiation elements. [55]

Farrokh et al. [56] have designed band-notched antenna. By embedding two L-shaped slits at the edge of the open radiating slots, a tunable notched band for avoiding interference between the UWB and WLAN systems was achieved. The realized slot antenna operates over (2.6-13.6)GHz for $VSWR \leq 2$ and has a band rejection of (4.9-5.85)GHz. Monopole antenna with dual band-notched characteristics is presented by Liu [57]. One complementary split-ring resonator (CSRR) is etched inside the patch on the monopole antenna to achieve dual notch frequency bands. A novel antenna is presented by Seungwoo et al. [58] for lower WLAN band and upper WLAN band

notches. Here, one antenna is designed for single band notch with separated strip to cover the 5.15GHz-5.825GHz band. The second antenna is designed for dual band notches using two separated strips to cover the (5.15-5.35)GHz band and 5.725GHz-5.825GHz band. A planar monopole antenna with triple band-notched characteristics is proposed by Li et al. [59], triple notched bands are realized by using an ‘ Ω ’ shaped slot in the radiating patch, a semi-octagon shaped resonator on the back side, and a defected grounded structure. Kim et al. [60] proposed triple-band notched UWB antenna, the essence of the design strategy is embedding the three notched elements onto the primitive antenna to serve as respective stop band filters. Tang et al. [61,62] have designed multiple band notches antenna. This antenna is designed for rejection of interference of WiMAX, lower and upper WLAN with covering of three notched bands.

2.4 Multi Element Antennas

An alternative approach to design antennas suitable for multi standard radio applications is to employ several antennas. A dual port antenna for operation at an international mobile telecommunications-2000 (IMT-2000), global positioning system (GPS) and wireless local area network (WLAN) was proposed in [63]. It consists of two radiating elements, planar inverted-F antenna (PIFA) with folded branches for GPS and WLAN band, and planar inverted-L antenna (PILA) for IMA-2000 band. These two antennas were printed next to each other on the top layer of the substrate. This approach might be effective when there is less limitation on antenna space requirements. Furthermore, the close proximity of the ports could be resulting in mutual coupling between the ports. A more efficient approach was presented in [64], where the two slot of the antenna was combined together. The outer slot antenna operates at 2.37GHz to 2.55GHz and the inner slot operates at 3.5GHz worldwide interoperability for microwave access (WiMAX) and 5.125GHz to 6GHz bands. Low port mutual coupling was achieved by the specific configuration of the ports. This approach is not only limited to wireless radio applications. A dual feed broadband

antenna is introduced in [65, 66] which is suitable for high frequency (VHF/UHF) communication or electromagnetic compatibility (EMC) applications. The antenna comprises of monopole and a disc-cone antenna. Two coaxial cables were used for feeding. The first cable is inserted in the center canal and connected to the disk-cone structure; bended sleeve is fixed under the ground plane. The second cable fed to the monopole with the aid of the sleeve. This technique is also very popular for designing reconfigurable antennas where each element can be tuned independently [67, 68]. For instance in [67] a PIFA is combined with a monopole with the space taken by the PIFA and also a switch is used in the PIFA for frequency reconfiguration.

2.4.1 Planar diversity antenna

In multi standard radio systems with simultaneously operating antennas, excellent isolation between antenna ports are required. In case the operating frequency bands are widely separated, embedded or external filtering structures can be used to provide the required isolation. On the other hand, there are applications where bands have to be closely spaced or even have to occupy the same band such as multiple input multiple output system (MIMO) where the demanded isolation cannot be achieved with microwave filters or where isolation provided by filters is not sufficient. Various port decoupling techniques have been reported in the literature [69, 70]. High antenna port isolation is well-known to be available from widely spaced antennas. Good isolation can be achieved by separating antennas by much more than half a wavelength. To achieve maximum separation for instance in a typical mobile phone or laptop the antennas are distributed around the periphery of the devices. When multiple antennas are grouped on a single device some factors such as the antenna position relative to each other and the ground influence the radiation. Moreover, in applications such as in mobile phones, the ground plane or device chassis is considered as part of the antenna and therefore contributes to the radiation. Hence, it is important to find the appropriate configuration of antennas which can satisfy all the system requirements. Wong et al. [71], have designed diversity antenna, which consists of two truncated square monopole antenna printed orthogonally and symmetrically on two sides of a

T-shaped protruded ground plane. This antenna is capable of operating in a very wide bandwidth, defined by return loss of -10dB at 5.4GHz bandwidth.

Chi et al. [72], have designed integrated dual band diversity antenna. The two ports of this antenna show high isolation and good impedance matching for frequency across the 2.4GHz and 5.2GHz for WLAN bands. This antenna can also provide spatial diversity which is capable of combating multipath fading for WLAN application.

Printed ultra wideband diversity antenna presented by Liu et.al [73], consisting of two orthogonal half circles with radiator placed symmetrically with respect to a protruded T-shaped ground plane. This antenna has good port isolation with $|S_{21}| \leq -20dB$ in the frequency of 3.1GHz-5.8GHz. A study of reduction of the mutual coupling between two mobile phone is presented by A. Diallo et al. [74]. This study shows, the process of optimally integrating in a mobile phone with two PIFAs working in close radio communication standards.

Chiu et al. [75] have designed simple ground plane structure that can reduce mutual coupling between closely-packed antennas. Measured results show that isolation coefficient of more than -20dB can be achieved between two antennas by sharing a common ground plane with inter-antenna spacing of $0.116\lambda_0$.

A novel dual-band printed diversity antenna is proposed by Ding et al. [76]. This antenna consists of two back-to-back monopoles with symmetric configuration and is printed on a PCB. The effects of some important parameters of the antenna are deeply analyzed. The measured radiation patterns of the two monopoles in general cover complementary space regions and also diversity performance is evaluated by calculating the envelope correlation coefficient.

A 2-element diversity planar antenna for MIMO is proposed by Hong et al. [77] to reduce the mutual coupling between two radiating elements where three stubs are inserted on the ground plane. The measured impedance bandwidth of the antenna ranges from 2.27GHz-10.2GHz. Good impedance matching and improved isolation characteristics are observed.

Lee et al. [78] have designed ultra-wideband MIMO antenna for Personal Digital Assistant (PDA). To improve the impedance bandwidth, a connecting strip is used

on each antenna element. The isolation is improved by inserting two T-shaped stubs. The designed antenna has a 10-dB return loss bandwidth of 9GHz.

A compact 2-element antenna with both pattern and polarization diversity and high isolation for WLAN application is reported by Wang et.al [79]. This antenna is composed of low profile monopole and a pair of inverted-L antenna fed by 180° out-of-phase excitation. The measured isolation is better than -29dB across the required bandwidth.

A study of UWB diversity antenna is presented by See et al. [80]. This antenna is designed on a PCB slab, which consists of two notched triangular radiating elements with two feeding ports. The shape of the ground plane is optimized to improve the isolation between the ports as well as impedance matching. This antenna achieved broad impedance bandwidth with good isolation performance $|S_{21}| \leq -20\text{dB}$. The correlation between the radiation patterns shows consistent diversity performance across the UWB bandwidth.

A novel tri-band MIMO monopole antenna is presented by Nezhad et al. [81]. The proposed antenna can create a single resonance within the WLAN range. Placement of two slots in the radiating element creates two extra resonances. The MIMO antenna array provides better than -14dB mutual coupling, envelope correlation of lower than 0.002 and stable omnidirectional patterns at all three frequencies.

In order to enhance the wideband isolation, a tree-like structure used in the antenna is presented by Zhang et al. [82]. Measured S-parameters show that the isolation is better than -16dB across the UWB band. The radiation patterns, gain and envelope correlation coefficients are also analyzed.

A planar MIMO antenna array is presented by Baek et al. [83]. This antenna array is composed of two orthogonal polarized elements which act as electric and magnetic loop antennas. A high isolation of -20dB between the two antennas are achieved at 2.3GHz. The calculated envelope correlation coefficient is 0.00035.

Reconfigurable dual-band monopole antenna array with high isolation is presented by Luo et al. [84]. This antenna array contains two C-Shaped monopoles with a shorting line, on which two RF switches were integrated. By changing states of RF

switches, high isolation coefficient at 2.4GHz or 5.2GHz are achieved. Sonkki et al. [85] have designed low mutual coupling between monopole antenna by using two half-wave length slots. The structure has two half-wavelength slots cut into the ground plane between the monopoles. The improvement in measured total efficiencies with the slotted ground plane against the reference ground plane is between 2.8% and 24.3%. A compact broad band printed diversity antenna is presented by Kang et al. [86]. This antenna has been designed for covering WLAN applications. The isolation of the diversity antenna is higher than -14.8dB. The patterns can cover complementary space regions. The diversity performance is also evaluated by calculating the envelope correlation coefficient. A novel MIMO antenna array for wireless devices is presented in Ling et al. [87]. This antenna array consists of two back-to-back monopole elements with an edge-to-edge distance of 0.096λ . Shorting strip and isolation stub are used to reduce the mutual coupling between the two elements. The measured isolation values are lower than -25dB and -20dB at the frequency of 2.45GHz and 5.8GHz band.

A two element polarized diversity antenna with band-notch function is presented by H.K. Yoon et al. [88]. This antenna consists of two octagonal monopoles that are orthogonally and symmetrical aligned with extended ground planes. The antenna covers UWB frequency with good isolation of less than -20dB. Also, it has a band-notch function to avoid overlap with 5GHz wireless local area network band. Both the time-domain and frequency-domain characteristics of the antenna have been investigated by using normalized antenna transfer function.

A novel stub structure with UWB-MIMO antenna is presented by Najam et al. [89], here two circular disc monopole antenna elements constitute a UWB-MIMO antenna operating over the frequency band 3.2GHz-10.6GHz. The isolation between the antenna ports have been enhanced by more than -15dB throughout the frequency band. Novel diversity or MIMO PIFA antenna with broadband circular polarization was presented by Yao.et al [90]. The circular polarization characteristic of the antenna is achieved by cross branch at its corner of the ground. Good isolation of -14dB between the two elements over the whole band is achieved.

2.5 Summary

In this chapter, state of the art literatures of planar monopole antennas for UWB application has been presented. The chapter starts with the introduction of planar UWB antenna, followed by investigated research work related to wideband antenna designs. The chapter also presents several research works related to UWB band notch antennas and UWB diversity antennas. It is found that the present communication system needs more compact and wideband antennas.

CHAPTER 3

Planar Broadband Monopole Antennas

Monopole antennas are used in communication systems at a wide range of frequencies. Electrical properties of these antennas are dependent on the geometry of both the monopole element and the ground plane. The monopole element is either electrically short with length much less than a quarter-wavelength with length approximately a quarter-wavelength. Normally, a monopole geometry consists of a vertical cylindrical element at the center of a perfectly conducting infinitely thin, circular ground plane in free space. Electrical characteristics of such antennas are primarily a function of only three parameters: element length, element radius and ground plane radius, when each is normalized to the excitation wavelength. Radiation patterns of such antennas are uniform in the azimuthal direction.

There are two novel designs of compact planar monopole antennas presented in this chapter: semi octagon shaped monopole and semi circular disk monopole antenna. These antennas perform well in terms of its impedance match and gain, over a wide band and easily comply with the FCC approved UWB frequencies of 3.1GHz to 10.6GHz. The slot resonators are engraved on either or both the radiator and ground plane to disable the antenna from functioning at the selected narrow band frequencies. The antennas have been shown to be suitable for broadband mobile applications in terms of their physical requirements and wide band characteristics. Their suitability for pulsed UWB applications are confirmed by investigating their effects on large fractional bandwidth pulses and this work is carried out in Chapter 5.

3.1 Semi Octagon Shaped Monopole Antenna

The octagon monopole is used to maintain the characteristics of the fat monopole such as a rectangular monopole and it has a smaller size than a rectangular monopole. This makes it possible to have a compact size for UWB, while maintaining omni directional radiation patterns. Theoretically, the radiators of the planar monopole antennas can be of any shape for broad operating bandwidth. Small and gradual discontinuities are desired for a reflection less transducer action over wide frequencies. The planar monopole antennas with octagon shaped radiating elements are known to operate effectively over a wide frequency band making them natural candidates for broadband application [91].

3.1.1 Antenna design and simulation results

The geometry of the octagon shaped monopole is shown in Figure 3.1. It consists of octagon shape radiator patch and an ground plane with a rectangular slot. The 50Ω line-fed monopole antenna was printed on FR4 substrate with thickness ‘h’ with relative permittivity $\epsilon_r = 4.4$.

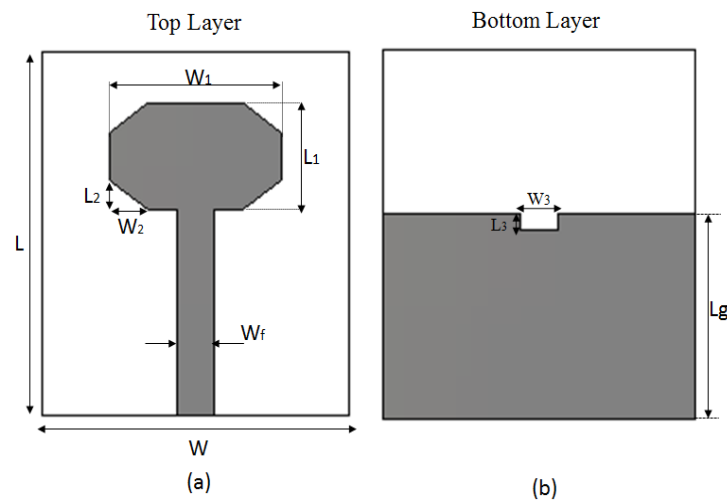


Figure 3.1: Geometry of a semi octagon shaped monopole antenna (a) Top layer (b) Bottom layer

Table 3.1: Dimensions of octagon shaped monopole antenna

L	W	h	L_g	W_f	L_1	W_1	L_2	W_2	L_3	W_3
36mm	32mm	1.6mm	20mm	3.8mm	10mm	18mm	3mm	4mm	0.5mm	3.8mm

The antenna performance was obtained by carrying out a detailed parametric analysis. Figure 3.2 shows the simulated reflection coefficient curves for different antenna dimensions. A significant observation from the plots is that a wide band impedance matching ($S_{11} \leq -10\text{dB}$) is inherently achieved for the octagon shaped monopole antenna considered, in spite of variations in its parameters. However, it shows a shift in the lowest resonance frequency f_{r1} with the parameter L_1 and W_f .

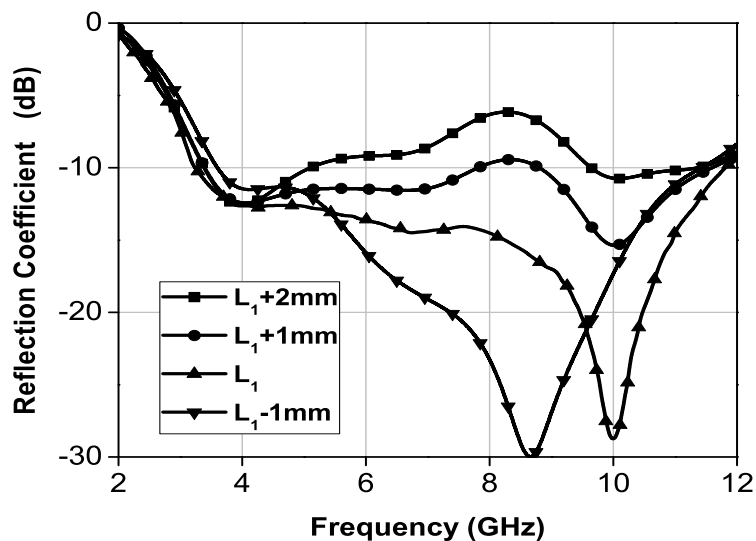


Figure 3.2: Simulated reflection coefficient curve of a semi octagon shaped monopole antenna for different values L_1

Figure 3.2 plots the antenna reflection coefficient by varying L_1 . A shift in the antenna frequencies towards a higher range can be noted with a distinct increase in f_{r1} . This confirms the monopole type operations of the antenna, where decrease in the radiator length increases the resonant frequency. Figure 3.3 show the variation in f_{r1} against frequency for different values of W_f .

The planar octagon shaped monopole antenna is a very wide band design where the lowest resonance is found to be critically determined by the antenna dimensions.

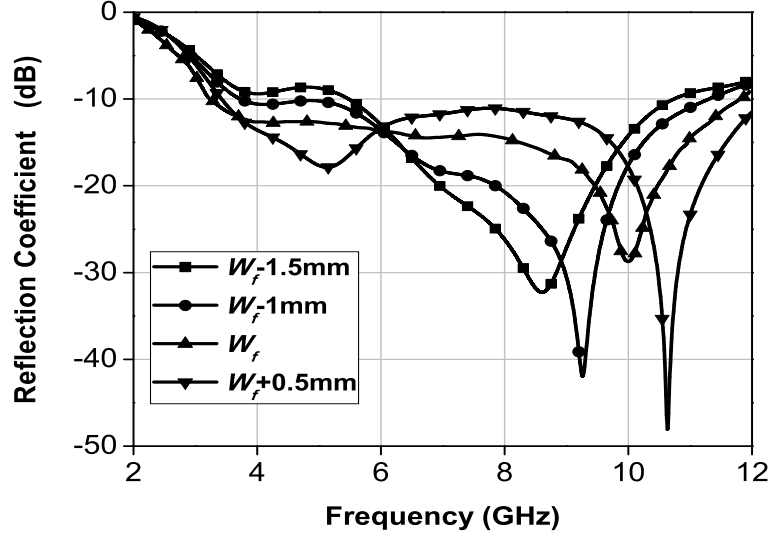


Figure 3.3: Simulated reflection coefficient curve of a semi octagon shaped monopole antenna for different values W_f

Hence, an approximate relation for f_{r1} is deduced as resonant frequency from (3.1).

$$f_{r1} = 7.2 / ((L_g + r + g) \times k) \quad (3.1)$$

where ' L_g ' is the length and ' r ' is the effective radius of an equivalent cylindrical monopole antenna and ' g ' is the length of the feed line. The factor ' k ' has a significance of an effective dielectric constant, as the configuration is printed on a substrate. The empirical values of $k=1.15$, for FR4 substrate with $\epsilon_r = 4.4$, $h = 1.6$ mm. Figure 3.4 illustrates the simulated reflection coefficient ($S_{11}(\text{dB}) = -\text{Reflection coefficient in dB}$) of an optimal design of the antenna with parameters as in Table 3.1, the simulated -10dB bandwidth appears to span an extremely wide frequency range from 3.4GHz to more than 11GHz. In order to identify the resonance modes of the antenna, its input impedance is plotted against frequency in Figure 3.5. Generally, the zero crossings on the reactance curve are identified as resonances which in this case compares well with the dips in the reflection coefficient curve.

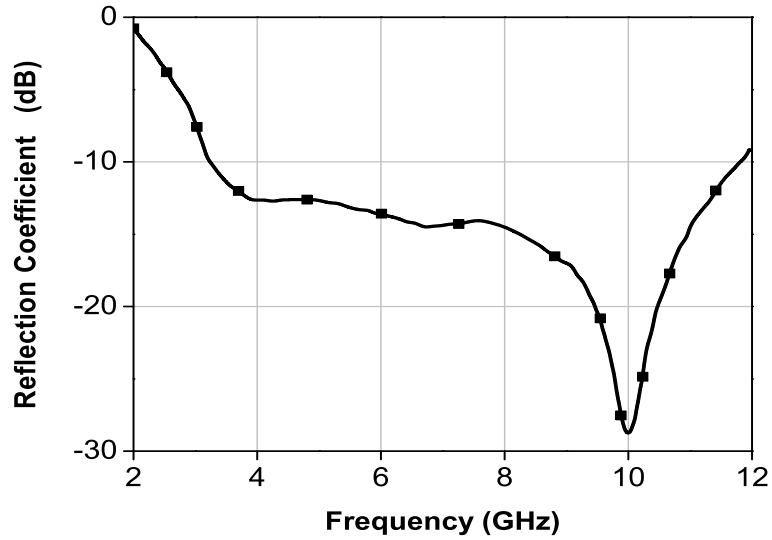


Figure 3.4: Simulated reflection coefficient curve of a semi octagon shaped monopole antenna

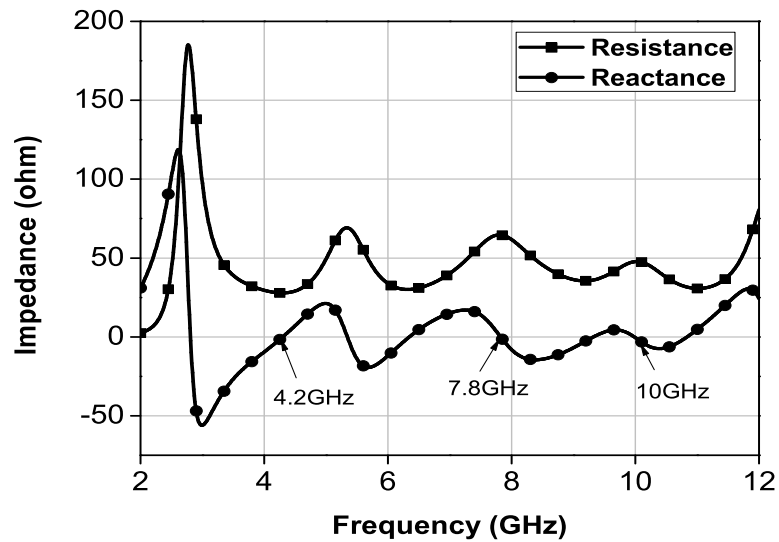


Figure 3.5: Simulated input impedance curve of a semi octagon shaped monopole antenna

3.1.2 Experimental verification

A prototype of the antenna was fabricated on a substrate of $\epsilon_r = 4.4$ and $h = 1.6\text{mm}$ with the parameters in Table 3.1

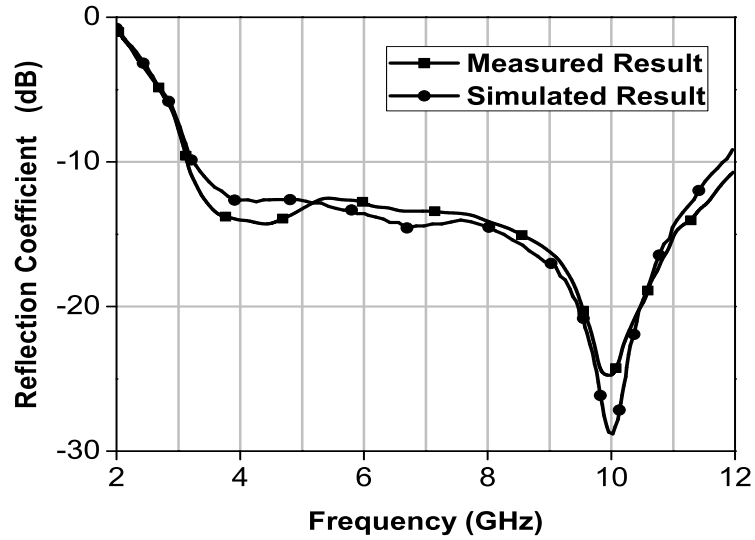


Figure 3.6: Measured reflection coefficient of a semi octagon shaped monopole antenna

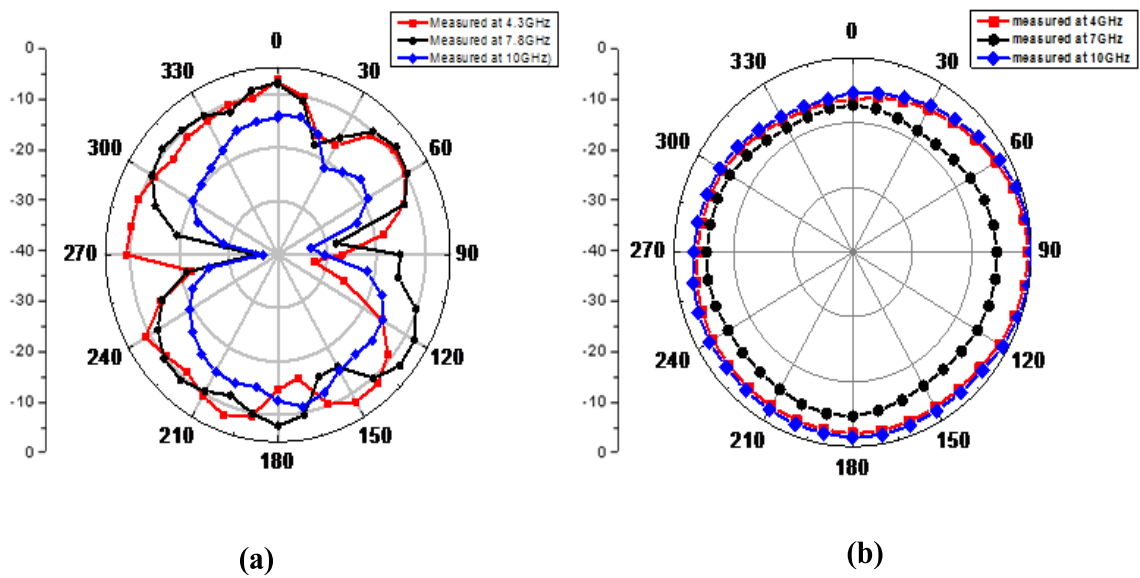


Figure 3.7: Measured radiation patterns at 4.2GHz, 7.8GHz, and 10GHz (a) E-plane, (b) H-plane

Reflection coefficient measurements indicate a wide band width from 3GHz to more than 12GHz, which is validated by simulations as shown in Figure 3.6. The normalized radiation patterns of the antenna for E and H planes for three different frequencies are shown in Figure 3.7. The patterns are stable throughout the band and resembles that of a monopole; omnidirectional in the azimuth (X-Y) and bidirectional in the elevation (Y-Z) at lower resonance frequency.

3.2 Semi Circular Disc Monopole Antenna

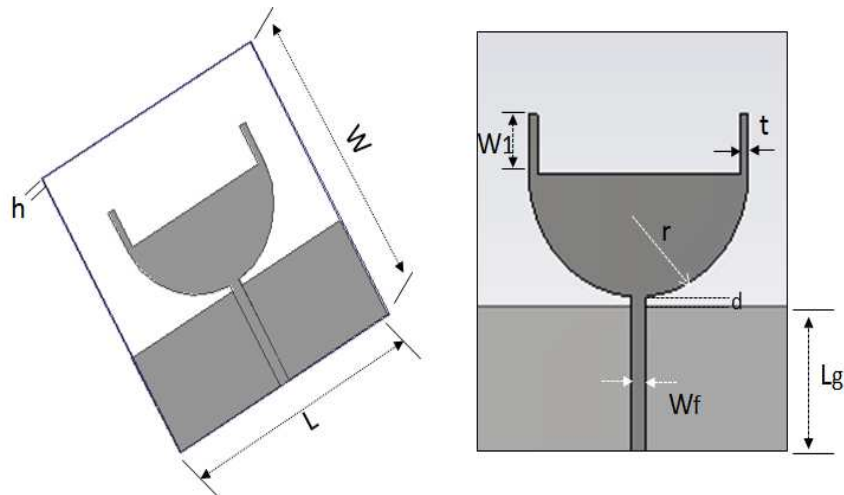


Figure 3.8: Geometry of a semi circular disc monopole antenna

3.2.1 Antenna design and simulation results

Figure 3.8 shows the geometry of the proposed semi circular disc monopole antenna. The proposed antenna is printed on substrate of thickness(h) 1.6mm with dielectric constant 4.4 and loss tangent 0.0018. A semi-circular patch of radius ' r ' is printed on the front side of the substrate. The radiator is excited via 50Ω microstrip line of 1.5mm width (W_f). With insertion of two stubs above the radiating elements, additional resonance is excited and hence the band width increases. A small gap ' d ' is introduced to achieve impedance matching.

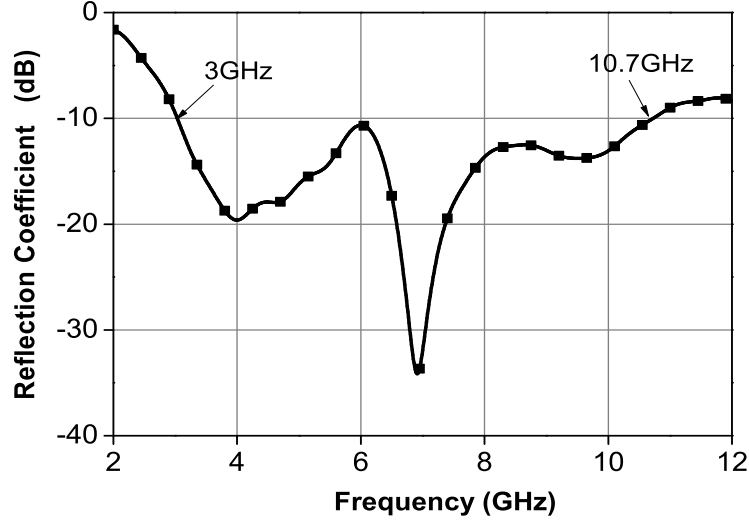


Figure 3.9: Simulated reflection coefficient of a semi circular disk monopole antenna

The design equation is deduced for the first resonance f_{r1} for an semi circular disk monopole antenna from relationship (3.2).

$$f_{r1} = \frac{150}{L_g \times \sqrt{\epsilon_{eff} + d + h}} \quad (3.2)$$

where ' d ' is gap between radiator and ground element, ' l_g ' is length of the ground. The performance of the antenna is investigated through EM simulation. Figure 3.9 illustrates the simulated reflection coefficient of an optimal design of the antenna with parameters as in Table 3.2, where all the antenna dimensions are in mm. The simulated -10dB bandwidth appears to span an extremely wide frequency range from 3GHz to 10.7 GHz.

Table 3.2: semi circular disk monopole antenna parameters

L	W	h	L_g	W_f	W_1	r	t	d
38mm	43.5mm	1.6mm	15.25mm	1.5mm	6.5mm	12.5mm	1mm	0.5mm

Figure 3.10 shows the simulated reflection coefficient as function of gap ' d ' for the proposed antenna. The first resonant mode of the antenna is shifted to higher frequency as ' d ' increased and impedance bandwidth for the lower band is enhanced.

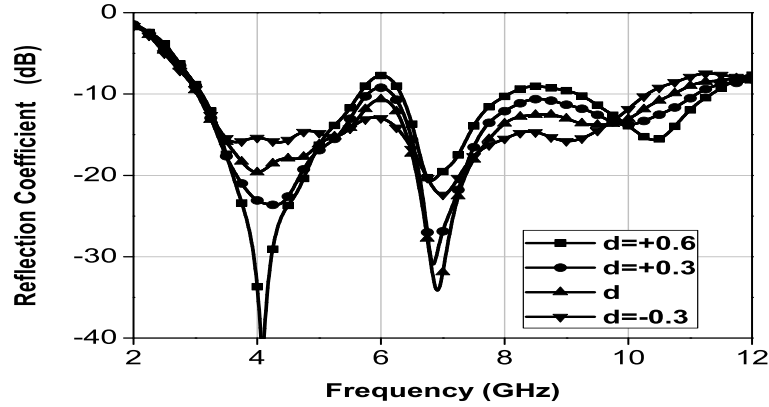


Figure 3.10: Simulated reflection coefficients of a semi circular disk monopole antenna for different feed gap ' d '

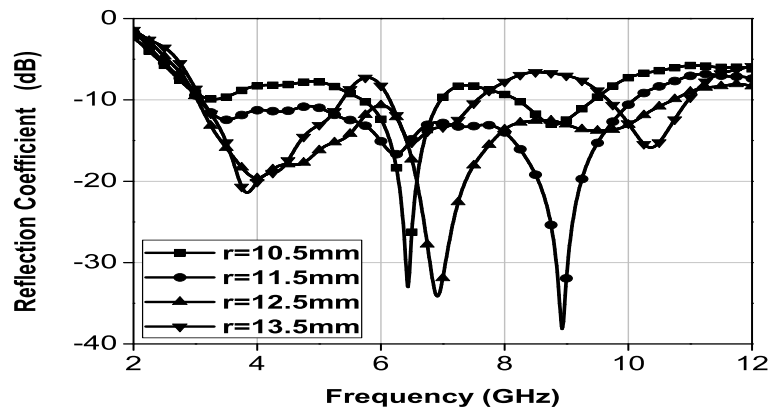


Figure 3.11: Simulated reflection coefficients of a semi circular disk monopole antenna for different feed gap ' r '

For the upper band, the bandwidth is affected slightly. Effects of the different radius of the radiating elements as shown in Figure 3.11 with ' r ' varying from 10.5mm to 13.5mm. In this case the effect of ' r ' on the impedance matching of the first and third resonant mode is larger than that on the second resonant mode.

In order to identify the resonance modes of the antenna, its input impedance is plotted against frequency in Figure 3.12. Traditionally, the zero crossings on the reactance curve are identified as resonances. Four resonance frequencies are identified from the plots, viz. 3.8GHz, then 4.8GHz, 6GHz, and 8.5GHz frequencies.

The reflection coefficient of the input impedance can only described the behavior

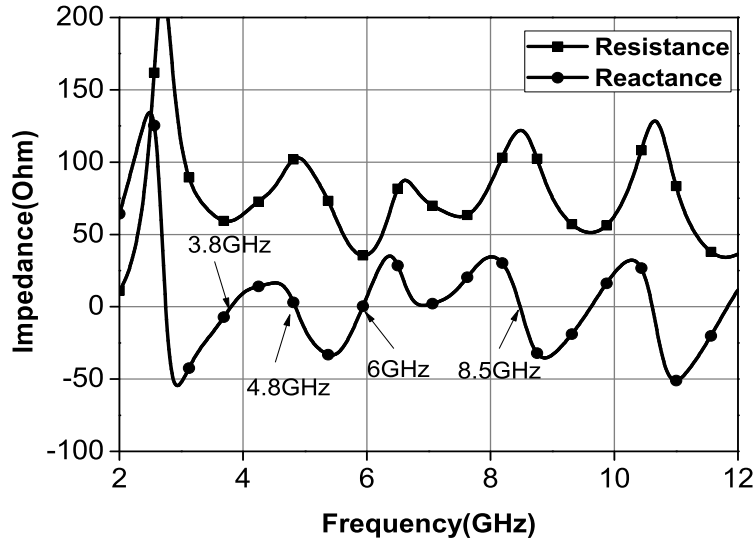


Figure 3.12: Simulated input impedance curve of a semi circular disk monopole antenna

of an antenna as a lumped load at the end of a feed line. The detailed EM behavior of the antenna is revealed by examining the surface current distributions and the radiation patterns. The surface current distribution of the antenna substrate close to the resonance frequencies and their corresponding simulated 3D radiation patterns are plotted in Figure 3.13. At the first (3.8GHz) and next (4.8GHz) resonance frequencies, the currents are mainly concentrated near the edge of the ground plane, while on top of the structure currents are primarily distributed along the periphery of the disc edge and feed line. This is why the first resonant frequency is associated with the dimension of the disc.

3.2.2 Experimental verification

The prototypes of semi circular disc monopole antenna was fabricated and tested in the Antenna Measurement Laboratory at Indian Institute of Science, Bangalore. The reflection coefficients are measured with the help of network analyzer (Agilent model no: N5230A). Reflection coefficient indicates a wide band width operation from 3GHz to 12GHz, which validates the simulation results presented in Figure 3.14. The slight deviation of results at higher frequencies could be due to the soldering

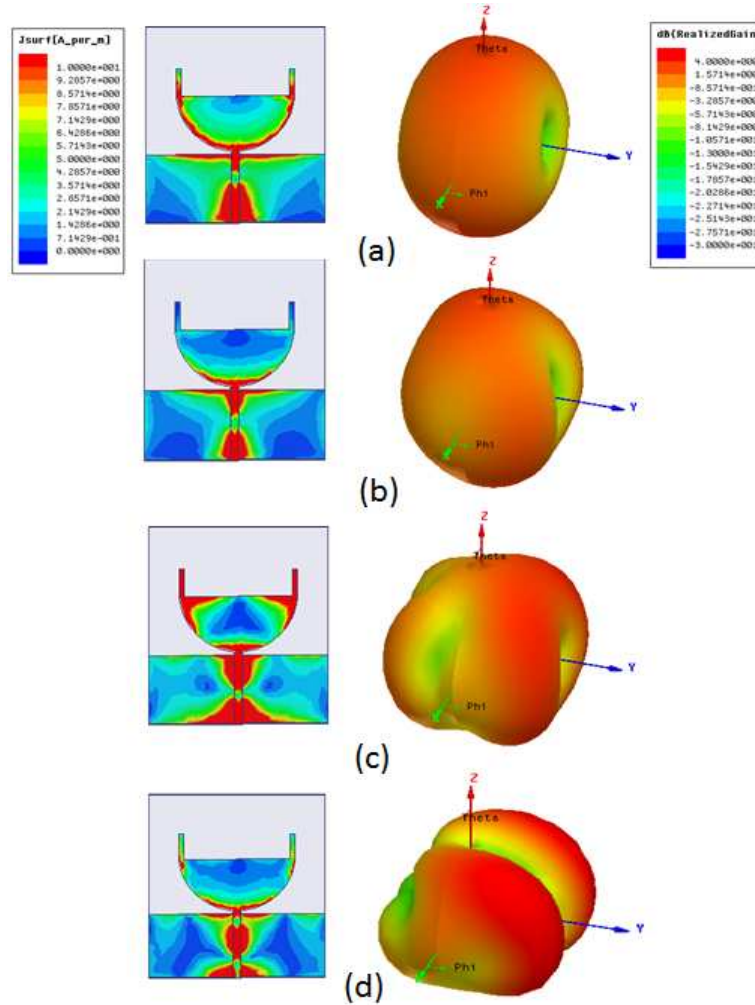


Figure 3.13: Simulated surface currents distribution of a semi circular disk monopole antenna along with its simulated radiation patterns at (a) 3.8GHz, (b) 4.8GHz, (c) 6GHz and (d) 8.5GHz.

effect of the SMA connector and its mechanical tolerance on the finite ground plane current distribution which is not accounted in the simulation. Figure 3.15 shows the measured E- and H- plane radiation patterns at 3.8GHz, 4.8GHz, 6GHz and 8.5GHz. In XZ(Co-pol. and Cross-pol) plane the patterns are close to omnidirectional.

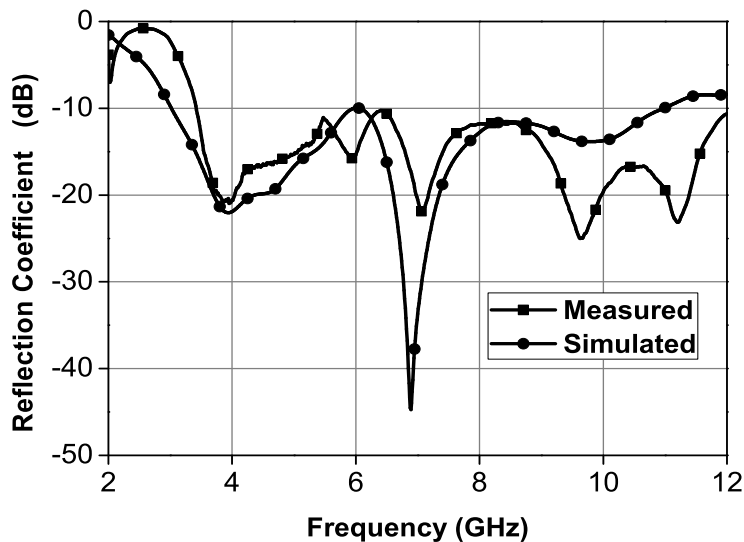


Figure 3.14: Measured reflection coefficient of a semi circular disk monopole antenna

3.3 Band Notch Antenna

3.3.1 Band notch octagon shaped monopole antenna

The radiating monopole and feeding mechanism are printed on the topside of the substrate, while the ground plane is printed on the bottom side. The antenna is printed on $32 \text{ mm} \times 36 \text{ mm}$, FR4 substrate with dielectric constant of 4.4 and substrate thickness of 1.6mm. The width of the microstrip feed line was fixed at 3.8mm to achieve 50 ohm characteristic impedance. The geometry of the proposed band notch antenna is shown in Figure 3.16.

Antenna with C-Shape Slots:

By etching C-shaped slots in the octagon shape radiating patch of antenna a frequency band notch is created. Each slot acts as a resonator and the band-notch frequency mainly depends on the length of the slot. The length of the slot is about a half of the wavelength corresponding to the desired center frequency of the rejection band. The required rejection of bands are at frequencies 3.4GHz-3.7GHz and 5.15GHz-5.825GHz. Hence the designed center frequencies of the rejection are set to be at 3.5GHz and 5.5GHz. The wavelength corresponding to notched frequency λ_r

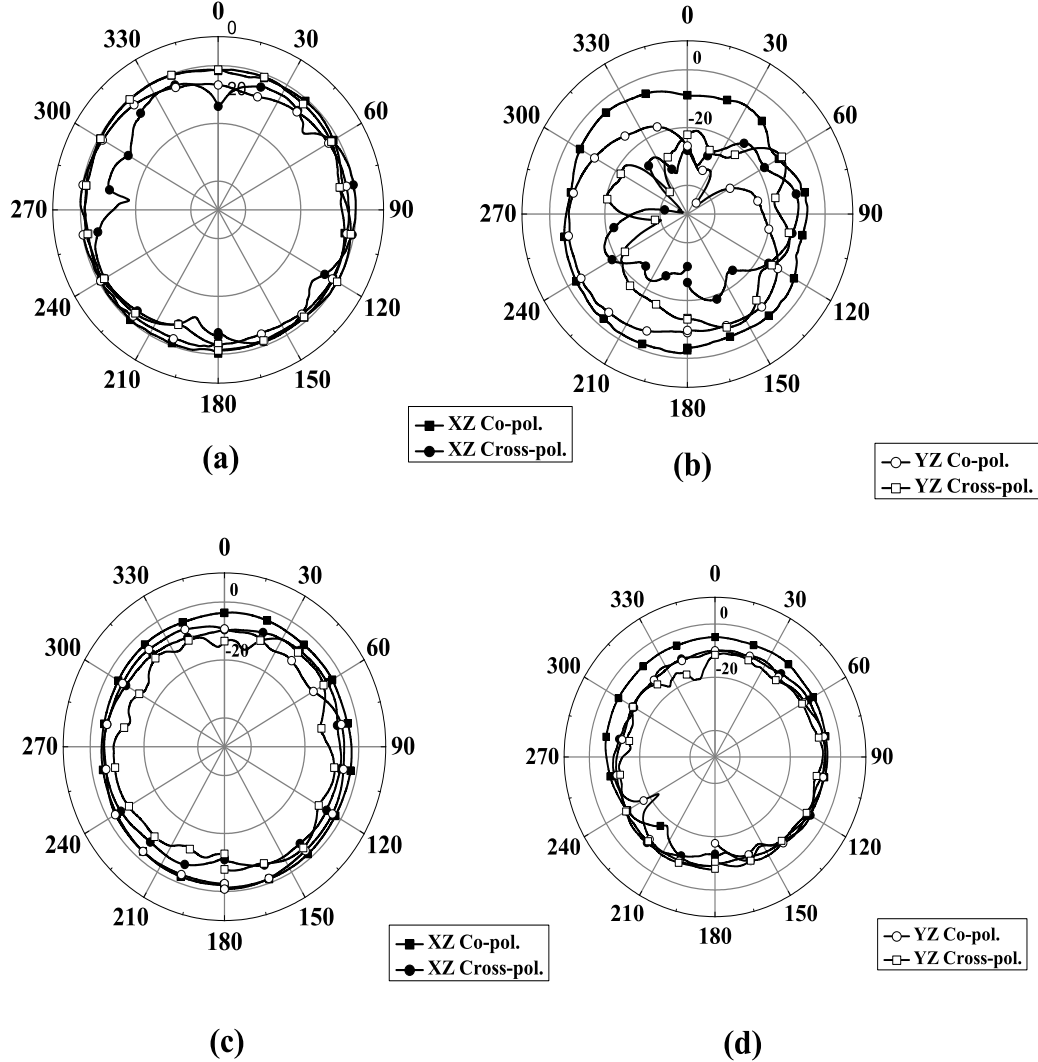


Figure 3.15: Measured radiation of a semi circular disk monopole antenna at (a) 3.8GHz (b) 4.8GHz (c) 6GHz and (d) 8.5GHz

can be calculated by $\lambda_r = \lambda / \sqrt{\epsilon_{eff}}$, where ϵ_{eff} is effective dielectric constant.

The geometry of the antenna with band rejected functions are shown in Figure 3.16. The desired interior C-shaped slot makes a notch band at 5.5 GHz and the exterior C-shaped slot makes another notch band at 3.5 GHz. The length of the interior C-shaped can be deduced by Equation (3.3),

$$L(slot1) = W_{s1} + L_{s1} \approx \frac{\lambda_r}{2} \quad (3.3)$$

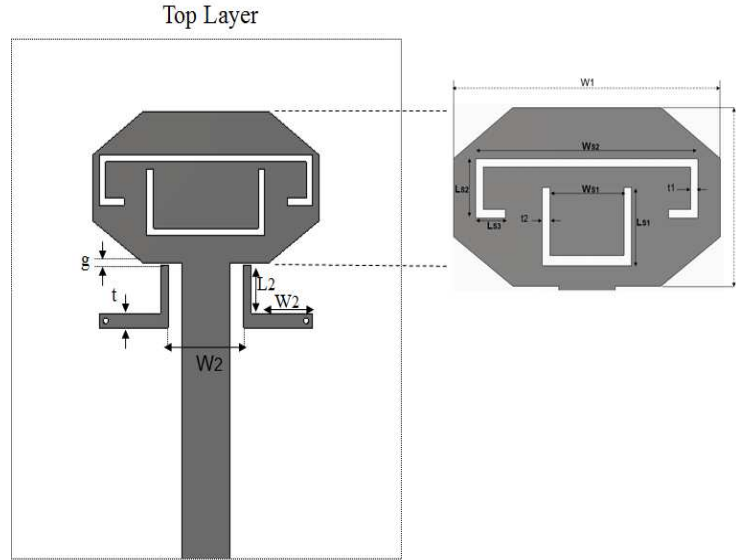


Figure 3.16: Geometry of a notched octagon shaped monopole antenna

Table 3.3: Dimensions of notched octagon shaped monopole antenna

W_{S1}	L_{S1}	W_{S2}	L_{S2}	L_{S3}	g	t_1	t_2	t_3
9.3mm	4.3mm	17mm	3mm	3mm	0.12mm	0.5mm	0.5mm	1mm

The length of the exterior C-shaped can be deduced by Equation (3.4)

$$L(\text{slot2}) = W_{s2} + L_{s2} + L_{s3} \approx \frac{\lambda_r}{2} \quad (3.4)$$

Antenna with Folded Strips:

A pair of end shorted folded strips are printed on the front surface of the substrate to achieve the triple band-notch characteristics. The overall resonator is L-shaped in order to minimize the space occupied and is short circuited to the ground plane via hole connection (radius=0.25mm). The two arms are of 0.25mm width and coupled with the ground plane. The lengths of both strips are closed to each other at the desired center frequency of the rejection. Here 'g' is the coupling gap between the resonator and the radiating patch. The two arms act as resonators and introduce capacitive coupling to offer series resonance for band stop function. The main line

is effectively shorted at resonant frequency and thus no power is delivered to the radiating patch. The optimal dimensions of the designed antenna are shown in table 3.3.

3.3.2 Simulation and experimental verification

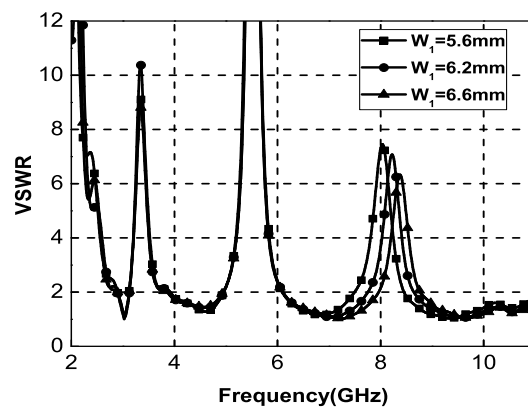


Figure 3.17: Simulated VSWR results for different values W_1 for octagon shaped monopole antenna

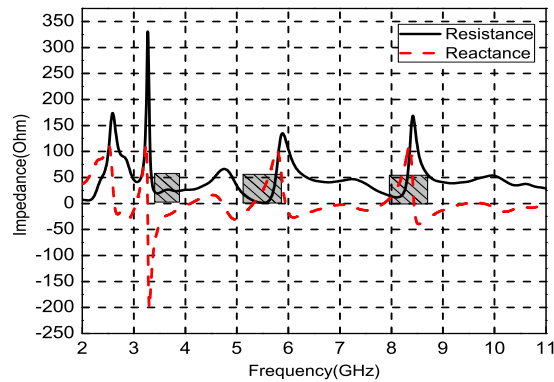


Figure 3.18: Simulated impedance curve of a octagon shaped monopole antenna

In this section, the planar monopole antenna performance with various design parameters is discussed. The proposed antenna is designed using CST microwave studio. Figure 3.17 shows simulated VSWR for different values of W_1 . The center frequency and bandwidth of the notch band is varied from 8GHz to 8.8GHz.

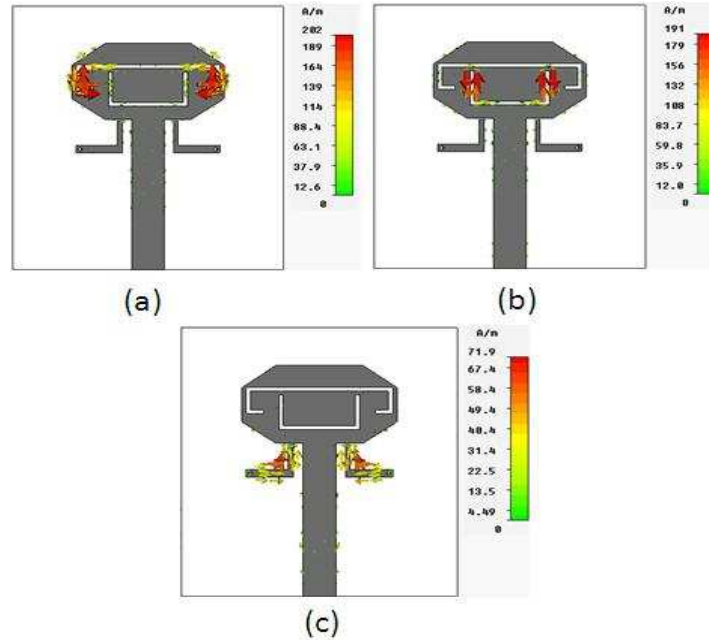


Figure 3.19: Simulated results of the surface current distributions for the antenna (a) 3.5GHz (b) 5.5GHz and (c) 8.2GHz

The simulated impedance of the octagon shaped monopole antenna shown in Figure 3.18. The resistance part of the impedance fluctuates around 50Ω over the UWB band except the band rejection frequency. It is observed that the resistance part of the impedance is very high, while the reactance part is almost zero.

Figure 3.19 shows the simulated current distributions at different frequencies. In this figure the flow of current is more dominated around the filter structure (Interior, Exterior C-shape slot and L shape arms) and they are oppositely directed between the interior and exterior edges. The resultant radiated fields cancel out and provides high attenuation near the notch frequency.

The measured performance for a fabricated prototype of the antenna using optimum simulated design parameters are presented here. The impedance bandwidth of the antenna is measured by using network analyzer(Agilent model no: E8363B). Figure 3.20 shows the performances of the measured and simulated reflection coefficient of UWB antenna with triple band notch characteristics.

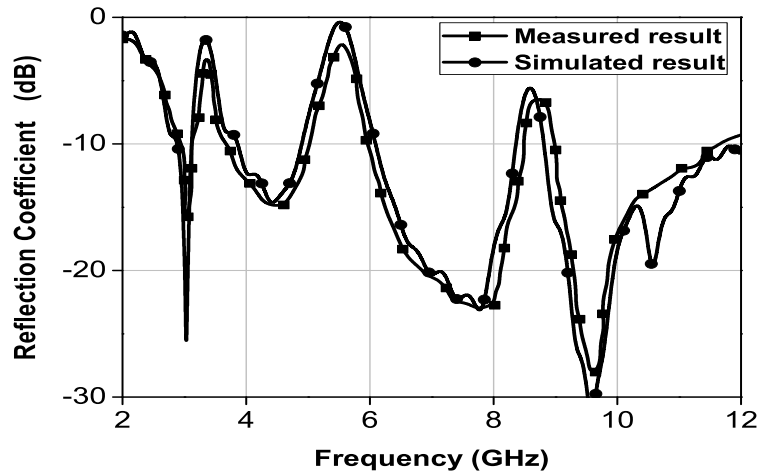


Figure 3.20: Measured and simulated reflection coefficient of an octagon-shaped monopole antenna

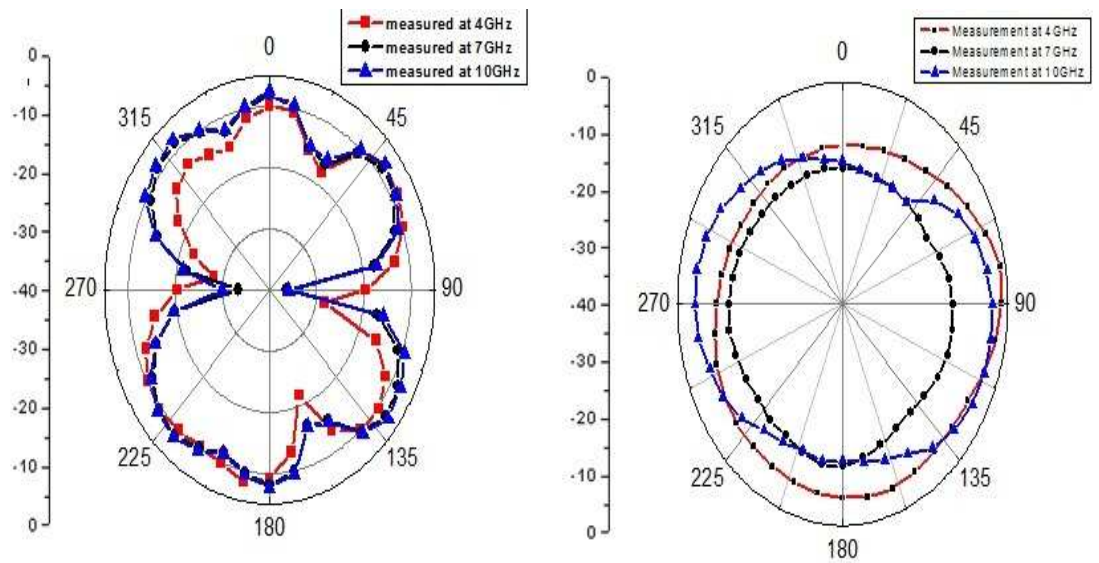


Figure 3.21: Measured radiation patterns at 4GHz, 7GHz, and 10GHz (a) E-plane (b) H-plane

Figure 3.21 illustrates the measured radiation patterns in the E-plane and H-plane at the frequencies of 4GHz, 7GHz and 10GHz of the UWB band. The radiation

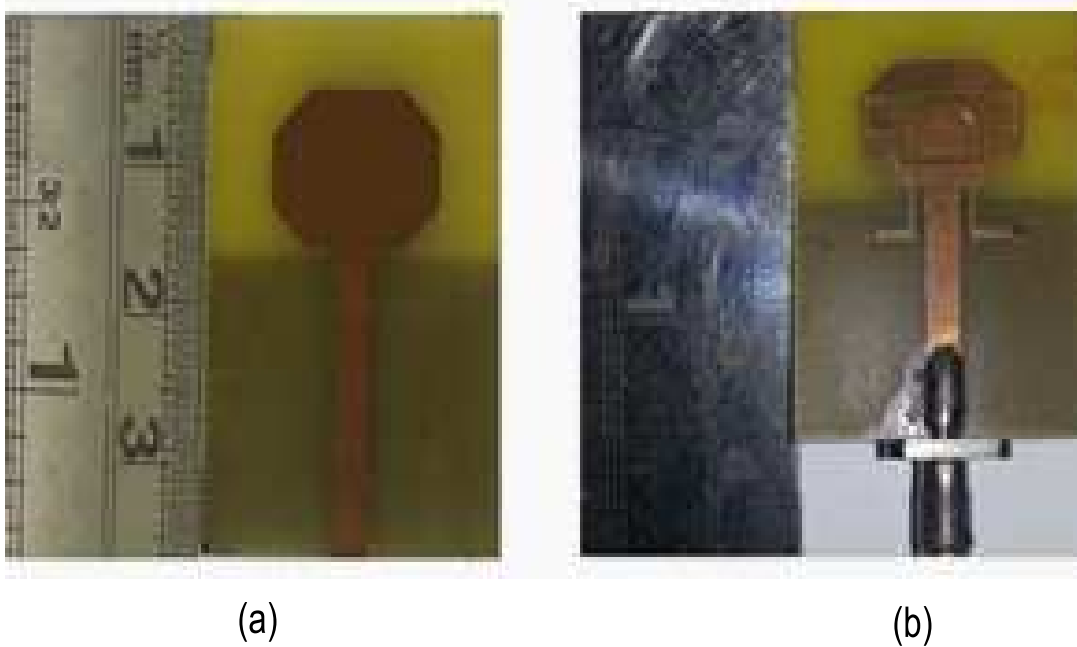


Figure 3.22: Photograph of proposed semi octagon shaped monopole antenna (a) without bandnotch (b) with bandnotch

patterns in the H-plane (YZ plane) are nearly omnidirectional for three frequency bands. The photographs of the proposed antenna with and without bandnotch are shown in Figure 3.22. The measured realized gain with and without bandnotch are presented in Figure 3.23. It is observed that gain variations are within 2dBi to 6dBi.

3.3.3 Band notch semi circular disk monopole antenna

Antenna with Spiral Loop Resonator:

A pair of symmetrical Spiral Loop Resonator (SLR) is printed on the front surface of the substrate merge with radiating element to achieve the band notch characteristics. The dimensions of the resonator are electrically small due to spiral type stub-wavelength structure. High level compactness can be achieved in this antenna by using SLR structure. As number of turns increased in the SLR, the equivalent interaction between the spiral inductance and spiral capacitance cause the resonant

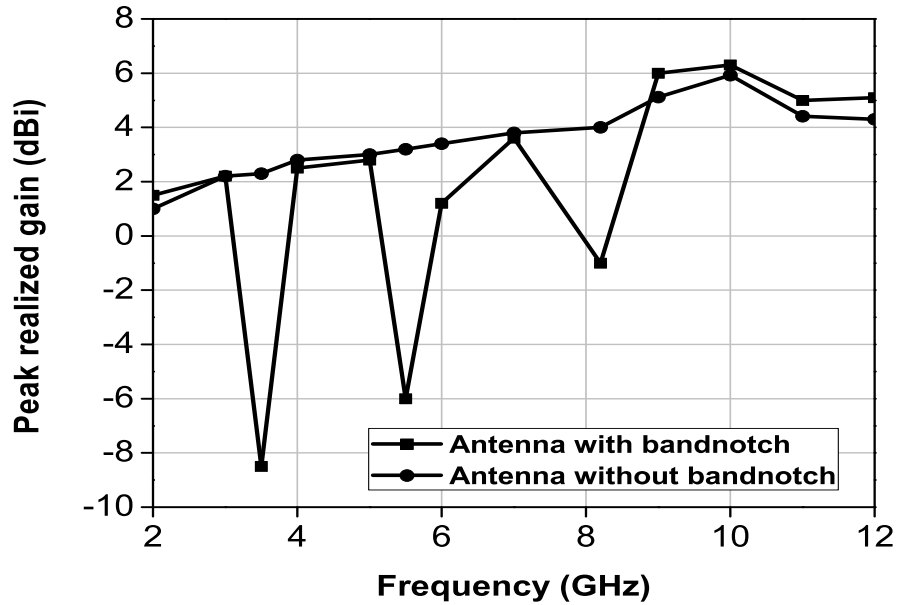


Figure 3.23: Measured gain of the octagon shape monopole antenna with and without bandnotch

behavior.

$$f_{SLR} = \frac{1}{2\pi\sqrt{L_{spiral} \times C_{spiral}}} \quad (3.5)$$

Notched frequency (f_{SLR}) of the SLR is calculated from distributed capacitance and inductance of the spiral loop. Using (3.5), the rough size of the desired SLR can be estimated and turning process need to be implemented by full wave EM simulation software to determine the optimal size of SLR. After tuning the distance between pair of SLR, spurious notched bands in undesired frequency can be eliminated. The optimal dimensions of the designed antenna are shown in Table 3.4

Antenna with Integrated Microstrip Resonators:

As shown in Figure 3.24 two types of microstrip resonators are used. These are (i) open loop resonator (OLR) (ii) open circuit resonator (OCR). These two resonators are placed on the opposite side of the planar antenna and coupled to a return signal on the ground of the planar antenna. The OCR makes one band notch at 5.2GHz-5.4GHz and other OLR makes second band notch at 5.7GHz-6GHz. At notch frequency, current is concentrated around the edge of the resonators and is oppositely directed

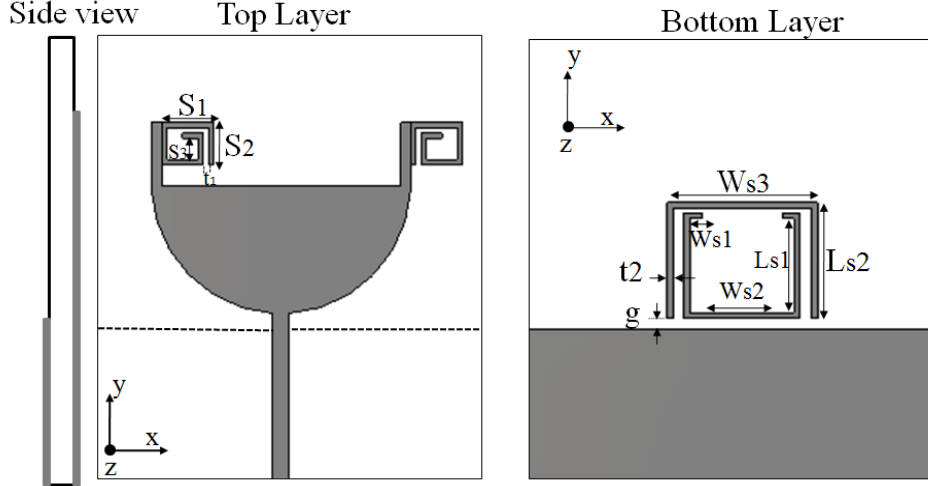


Figure 3.24: Geometry of a notched semi circular disk monopole antenna

between the interior and exterior of the resonator. This affects the antenna to operate in transmission line mode, which transfers the high impedance at the top of the band notch. Due to this effect nearly zero impedance is found at antenna feed point. This creates high attenuation near the notch frequency.

$$f_{OLR} \approx \frac{c}{(2L_{s1} + 2W_{s1} + W_{s2}) \times \sqrt{\epsilon_{eff}}} \quad (3.6)$$

$$f_{OCR} \approx \frac{c}{(2L_{s2} + W_{s3}) \times \sqrt{\epsilon_{eff}}} \quad (3.7)$$

Where 'c' is speed of light in free space, $\epsilon_{eff} \approx (\epsilon_{eff} + 1)/2 = 2.7$ therefore, desired notch frequency is calculated by relationship (3.6) and (3.7). The optimal dimensions of the designed resonator are as shown in Table 3.4.

Table 3.4: Dimensions of notched semi circular shaped monopole antenna

S_1	S_2	S_3	t_1	d	W_{s1}	L_{s1}	W_{s2}	L_{s2}	W_{s3}	t	g
5mm	4mm	2mm	0.5mm	1mm	1.5mm	9.5mm	7mm	10.5mm	13mm	1mm	0.5mm

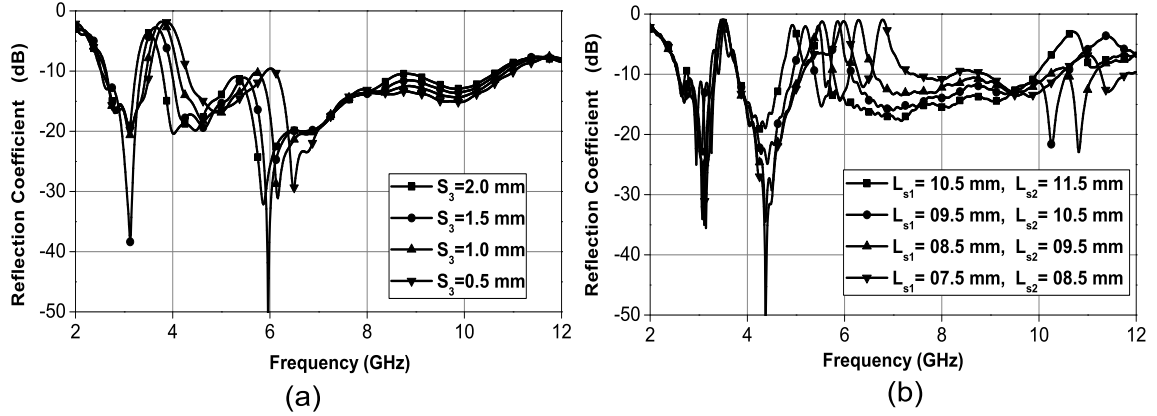


Figure 3.25: (a) Optimization of SLR by changing S_3 Value. (b) Optimization of integrated microstrip resonators by changing L_{S1} and L_{S2} value.

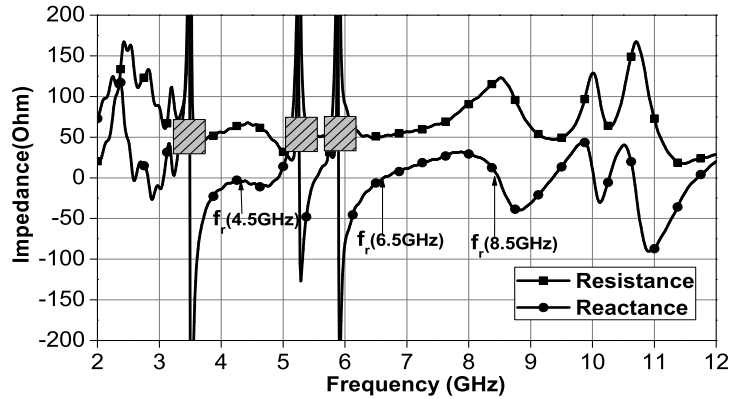


Figure 3.26: Simulated impedance of the notched disk monopole antenna

3.3.4 Simulation and experimental verification

Figure 3.25 (a) shows the S_{11} for the different lengths of the square loop resonator (S_3). It is clearly seen that the length of SLR has a significant effect on the notch frequency. The notch frequency shifted from 3.4GHz to 3.8GHz, as the length of the SLR changes from 2mm to 0.5mm. This is due to the fact that the notch frequency of the SLR is proportional to the length of the resonator. The parameters L_{S1} and L_{S2} mainly determine the second and third notched bands. Figure 3.25 (b) illustrates the impact of the parameters L_{S1} and L_{S2} . The value of L_{s1} and L_{s2} are decrease keeping

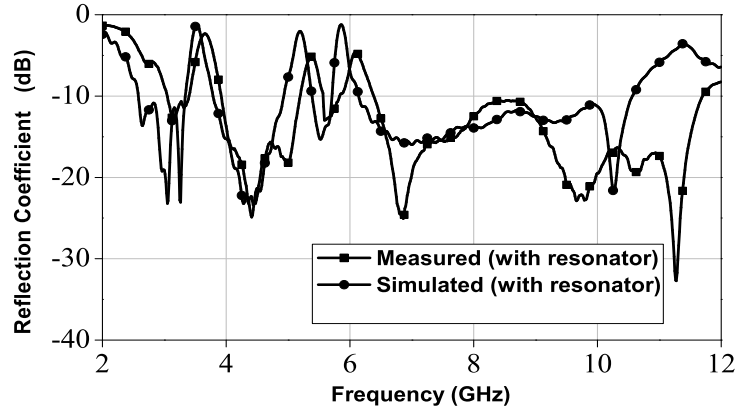


Figure 3.27: Simulated and measured reflection coefficient performances

other parameters constant. The second and third notched band also moves to higher frequency. Thus, the size of the resonator structures has a serious impact on the position and bandwidth of the notched frequency. The simulated impedance of the proposed antenna is shown in Figure 3.26. It is found that the resistance part of the impedance is around 50Ω over the UWB band except the band rejection frequency. It is also observed that the resistance part of the impedance is very high, whereas the reactance part is negative. This means that the proposed antenna is stopping the propagation of the wave at band rejection frequency. From the Figure 3.26, it is also observed that the zero crossing on the reactance curve is identified as resonance frequencies occurring at 4.5GHz, 6.5GHz and 8.5GHz.

A prototype for the proposed UWB antenna was fabricated and tested. A vector network analyzer (Agilent model no: N5230A) was utilized to measure and verify the antenna performance. Figure 3.27 illustrates the simulated and measured $|S_{11}|$ performances against frequency of the antenna. Fairly good agreement between the simulated and measured results has been seen. As observed, the measured impedance bandwidth of the proposed antenna is 8.6GHz (over 3.05GHz-11.7GHz), rejecting frequency band of about 3.4GHz-3.8GHz (WiMAX), 5.2GHz-5.4GHz (Lower WLAN) and 5.7GHz-6GHz (Upper WLAN).

The effect of frequency interference is well avoided. The measured far-field radiation patterns of the proposed antenna at 4.5GHz, 6.5GHz, and 8.5GHz are investi-

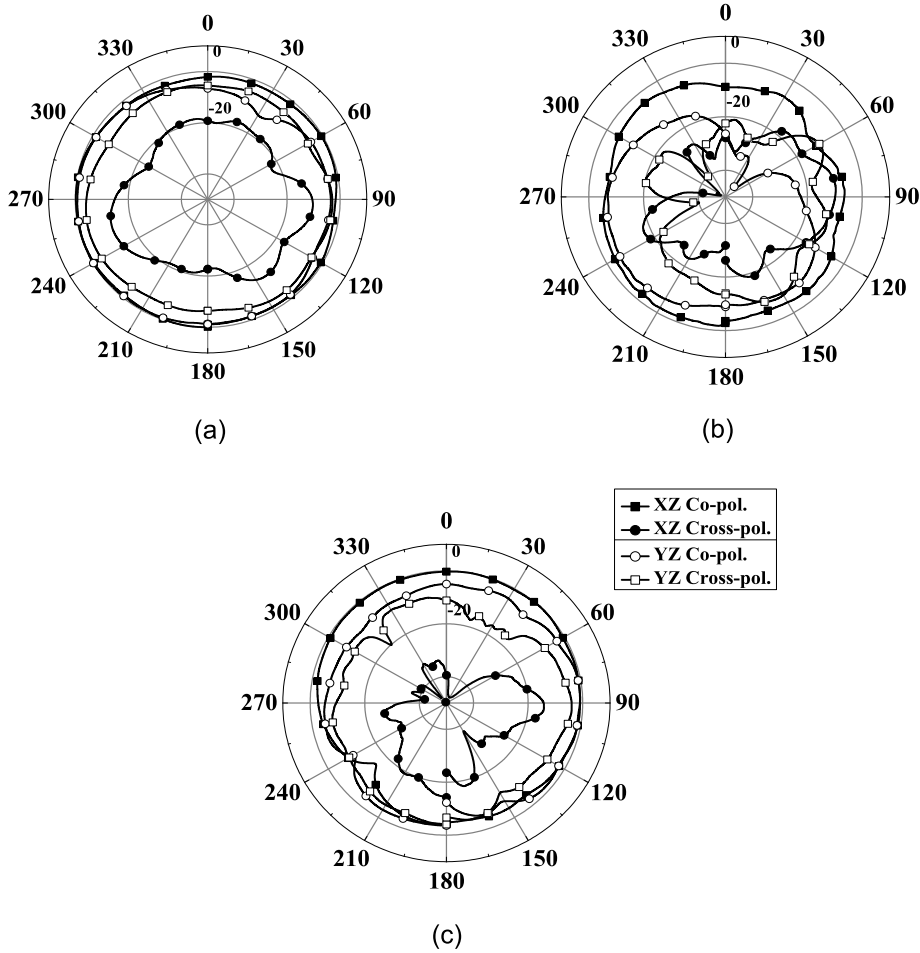


Figure 3.28: Measured radiation patterns of the notched semi circular disk monopole antenna in (a) 4.5GHz (b) 6.5GHz (c) 8.5GHz frequencies.

gated and presented in Figure 3.28. The antenna has nearly monopole like pattern in E-plane and omni directional radiation pattern in H-plane. The photographs of the proposed antenna with and without bandnotch are shown in Figure 3.29. The measured realized gain with and without resonator are presented in Figure 3.30. It is observed that the gain variations are within 2.8dBi to 6dBi using with and without resonators, except the notch frequency. Table 3.5 presents the comparison of the proposed works with existing works.

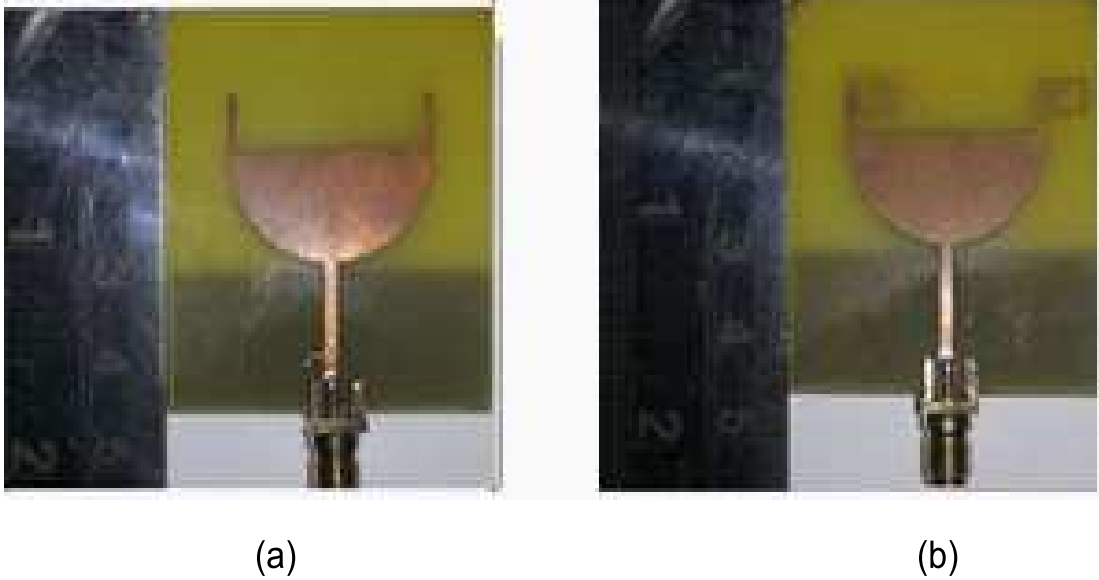


Figure 3.29: Photograph of proposed semi octagon shaped diversity antenna (a) without bandnotch (b) with bandnotch

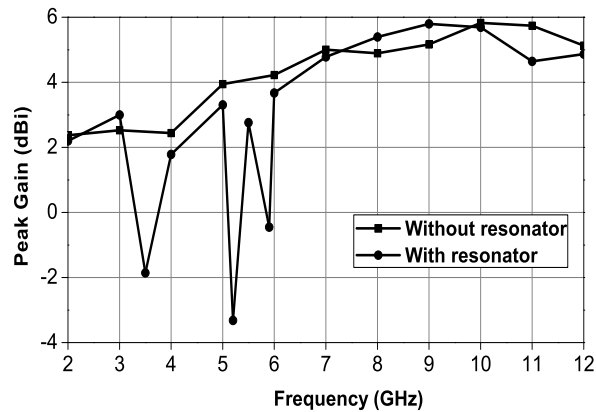


Figure 3.30: Measured gain of the semi circular disk monopole antenna with and without resonator

3.4 Summary

In this chapter, we have presented two designs of broadband planar monopole antennas, namely the octagon shaped monopole and semi circular disk monopole. The planar octagon monopole antenna has a wide band operation (3GHz to 12GHz), sim-

Table 3.5: Comparison between proposed works with existing works.

Antenna type	Size(mm)	Bandwidth	Gain
Simple Ultrawideband Planar Rectangular antenna [74]	30×18×0.76	3.1GHz - 11GHz stop band at 5.5GHz	upto 5dBi
Novel Band-Notched Planar Monopole antenna [75]	22×20×1.6	3.1GHz-11GHz stop band at 5.5GHz	3.8dBi
Compact Ultrawideband Antenna [76]	30×3.5×1.6	3.1GHz to 10.6GHz dual stop band 3.5GHz/5.5GHz	4.5dBi
Semi octagon shaped diversity antenna	36×32×1.6	3GHz-12GHz multiple stop band at 3.5GHz/5.5GHz/7.2GHz	upto 6.2dBi
Semi circular diversity antenna	38×43.5×1.6	3.05GHz to 11.7GHz multiple stop band 3.5GHz/5.2GHz/5.8GHz	6dBi

ple structure and nearly omnidirectional radiation patterns at the lower frequency. The semi circular disk monopole antenna presented in the following sections, provide wide band operation (3.05GHz to 11.7GHz). It appears to be perfectly ideal for UWB band application with a compact size, stable and omnidirectional antenna pattern. In final section of this chapter, the designed wide band antennas are adapted to coexist with existing WLAN bands with minimum interference. The time domain performance of these antennas for assessing their suitability in UWB has been presented in Chapter 5.

CHAPTER 4

Planar Diversity Antenna

4.1 Introduction

In the previous chapter, two geometries based on monopole antenna were discussed for UWB applications with band-notched characteristics. In this chapter, monopole antennas for diversity performance are investigated. The antennas are mostly line-fed used for ease of fabrication and better integration. The surface field distributions on the antenna and their radiation patterns at the resonant modes are analyzed in detail. Here, the antenna designs are followed from previous chapter to obtain diversity characteristics.

An UWB diversity antenna is a promising candidate to combat the multipath fading problem in an indoor UWB wireless communication system. Both MIMO and diversity UWB systems require an increase of the isolation among antennas. In this chapter, two novel designs of planar diversity antenna with stub are presented: semi octagon shaped diversity antenna and semi circular diversity antenna are presented. These antennas perform well in terms of its impedance matching, gain over a wide band and easily comply with FCC approved UWB frequency of 3.1GHz to 10.6GHz. The important parameters which affect the antenna performances are investigated both numerically and experimentally to obtain some quantitative guidelines for designing this type of antennas. Further, to notch out the selected narrow band frequencies in the wide operating band, thin resonators are embedded in the antenna. Such adaptations are incorporated, optimized and experimentally verified for all the

proposed designs. The antennas are seen to be suitable for broadband mobile applications in terms of their physical requirements and wide band characteristics. Their suitability for pulse UWB applications are verified by investigating their effects on large fractional bandwidth pulses and this is carried out in Chapter 5.

This chapter is organized as follows, Section 4.2 shows the 2-element semi octagon shaped antenna with diversity implementation. Section 4.3 shows the 2-element semi circular shaped monopole antenna with diversity characteristics. Section 4.4 describes band notch characteristics for WiMax and WLAN application. Finally, Section 4.5 summarizes the chapter.

4.2 Semi Octagon Shaped Diversity Antenna

Mobile communication using MIMO/diversity processing has emerged as a breakthrough for wireless systems of revolutionary importance. All wireless technologies face the challenges of signal fading, multi-path, increasing interference and limited spectrum. This section deals with diversity antenna for UWB applications. It presents the defined objectives and consequent approaches to achieve the goal. The analysis and evaluation of performances of these proposed designs are considered taking special parameters into account which are necessary to characterize MIMO/diversity antennas. Finally, solution to enhance isolation with reduced antenna size, envelope correlation coefficient and capacity loss are presented.

4.2.1 Antenna geometry and simulation results

The configuration of the semi octagon shaped diversity antenna shown in Figure.4.1. The antenna consists of two symmetrical rectangular patches with three bevels cutting on the edge shaped radiator. It is printed on the upper part of the FR4 substrate with dimensions $L \text{ mm} \times W_g \text{ mm} \times h \text{ mm}$ and relative permittivity of 4.4. Two radiators are separated by distance ' d ' from each other and are symmetrically positioned with respect to the y-axis. The radiators are excited via 50Ω microstrip line of width (W_f).

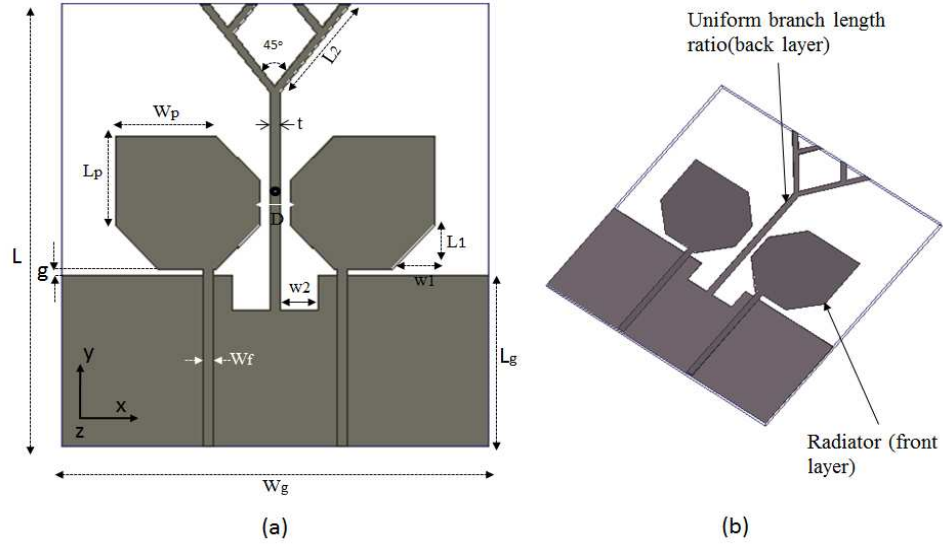


Figure 4.1: Geometry of the semi octagon shaped diversity antenna (a) Front view (b) 3D view

The wideband isolation between the two radiators can be efficiently enhanced by using uniform branch length ratio structure that extends from the ground plane. Wide band isolation can be achieved with uniform branch length ratio structure analyzed by isolation coefficients $|S_{12}|$ and $|S_{21}|$. The antenna branch lengths are equal to the double of the previous branches from the point 'o' in the ground plane. During 1st iteration, the branch 1 can be viewed as a reflector, which can reduce the wideband mutual coupling through separating the radiation patterns of the two radiators. It is clear that increase in number of the iterations, the mutual coupling is further weakened. The ratio of the branch length to the total length is given in Table 4.1. The antenna is designed according to the geometry shown in Figure 4.1 and angle between the two radiating elements is 45° .

A parametric study is carried out to investigate the effects of the important parameters on the impedance matching and isolation. In Figure 4.2 improvement of the isolation across the operating band is observed, when total number of the branches in-

Table 4.1: The ratio of the branch lengths to the total length of structure

Iteration	0	1	2
Branch 1	1	1/3	1/7
Branch 2		2/3	2/7
Branch 3			4/7

Table 4.2: Dimensions of semi octagon shaped diversity antenna

L	W_g	W_f	L_p	W_p	L1
40mm	40mm	0.8mm	08mm	9.5mm	10mm
W_1	L_2	W_2	h	t	d
4mm	10mm	3.5mm	0.8mm	01mm	03mm

creases from one to three. The branches 1, 2 and 3 are mainly affected low, at middle and high frequencies respectively. The effects of varying the separation (d) between the two radiators, length (l_g) and (w_g) of the ground plane are studied. The values of the parameters are the same as that shown in Table 4.2 except for the parameters under investigation. As observed from Figure 4.3, when the distance (d) between the radiator is increased, there is an upward shift in the lower edge frequency. The isolation is mainly affected at the lower and upper edges of the pass-band. The overall size of the antenna is dependent on the length (l_g) and width (w_g) of the ground plane. Figure 4.4, shows that increase in the width of the ground plane, the upper resonance decreases such that the matching and isolation are achieved at center frequency. From Figure 4.5, it is seen that when the length of the ground plane is varied, good impedance matching and high isolation are achieved. When upper resonance decrease such that the impedance matches at the center frequency. From Figure 4.5, it is seen that when the length of the ground plane is varied, good impedance matching and high isolation can still be achieved.

This shows that the ground plane effect of the proposed antenna is minimized. To further investigate the effect of the uniform branch length ratio structure, the surface current distributions at 3.6GHz and 7.8GHz are shown in Figure 4.6. When port 1 is excited, the current from the radiator tend to couple the port 2 has been blocked by the uniform branch length ratio structure and cannot flow to the other radiator

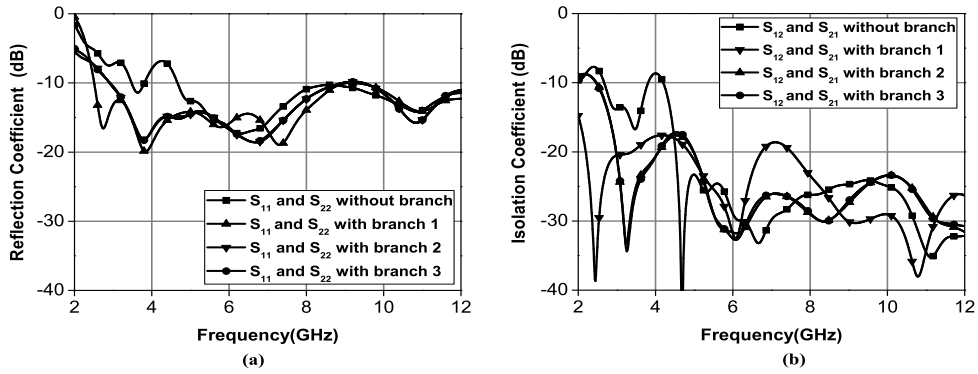


Figure 4.2: Simulated reflection coefficient and isolation coefficient for different with branches (a) $|S_{11}|$ and $|S_{22}|$ (b) $|S_{12}|$ and $|S_{21}|$

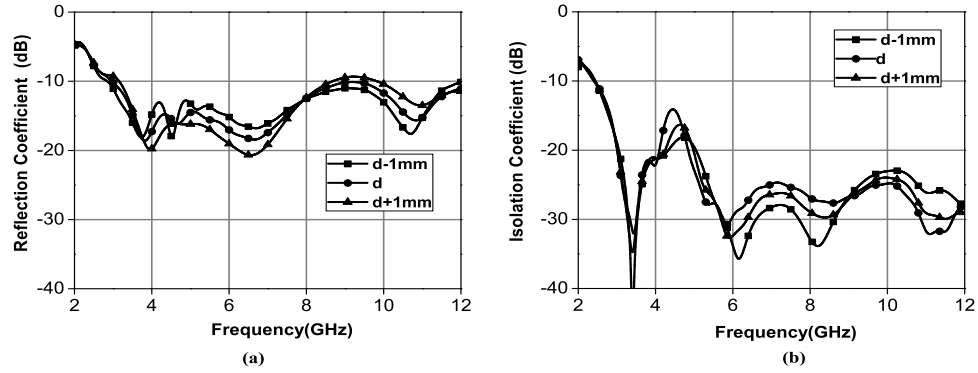


Figure 4.3: Simulated reflection coefficient and isolation coefficient for different values of 'd' (a) $|S_{11}|$ and $|S_{22}|$ (b) $|S_{12}|$ and $|S_{21}|$

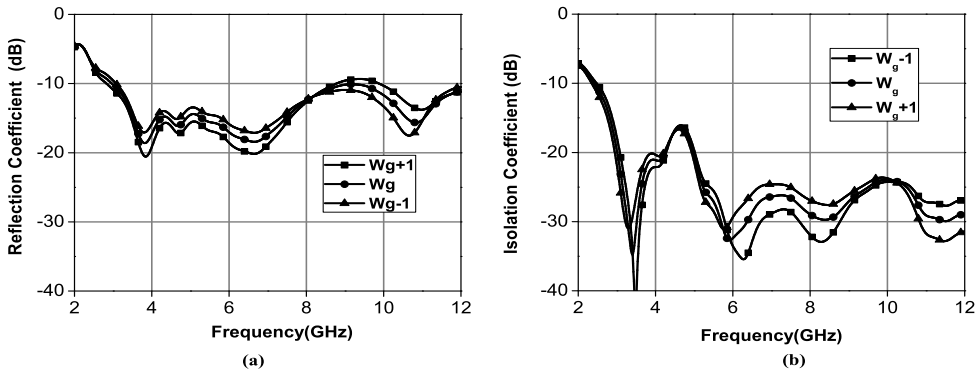


Figure 4.4: Simulated reflection coefficient and isolation coefficient for different values of ' W_g ' (a) $|S_{11}|$ and $|S_{22}|$ (b) $|S_{12}|$ and $|S_{21}|$

through the common ground plane at all these frequencies. The effect is same, when port 2 is excited. This shows that the designed antenna can efficiently enhance the

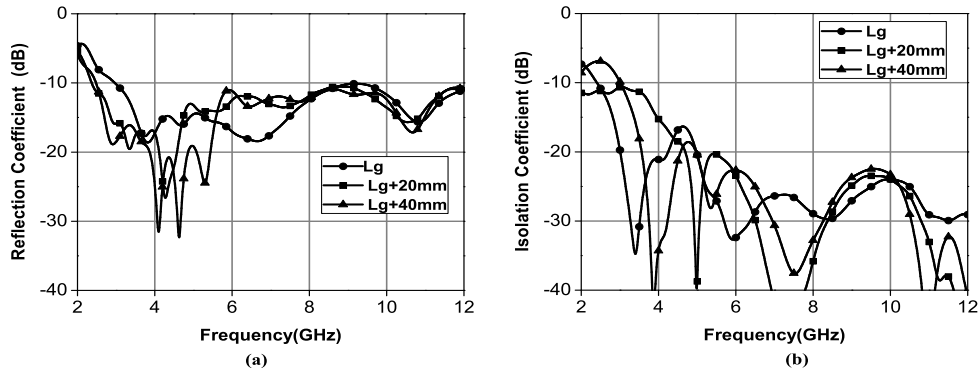


Figure 4.5: Simulated reflection coefficient and isolation coefficient for different values of ' L_g ' (a) $|S_{11}|$ and $|S_{22}|$ (b) $|S_{12}|$ and $|S_{21}|$

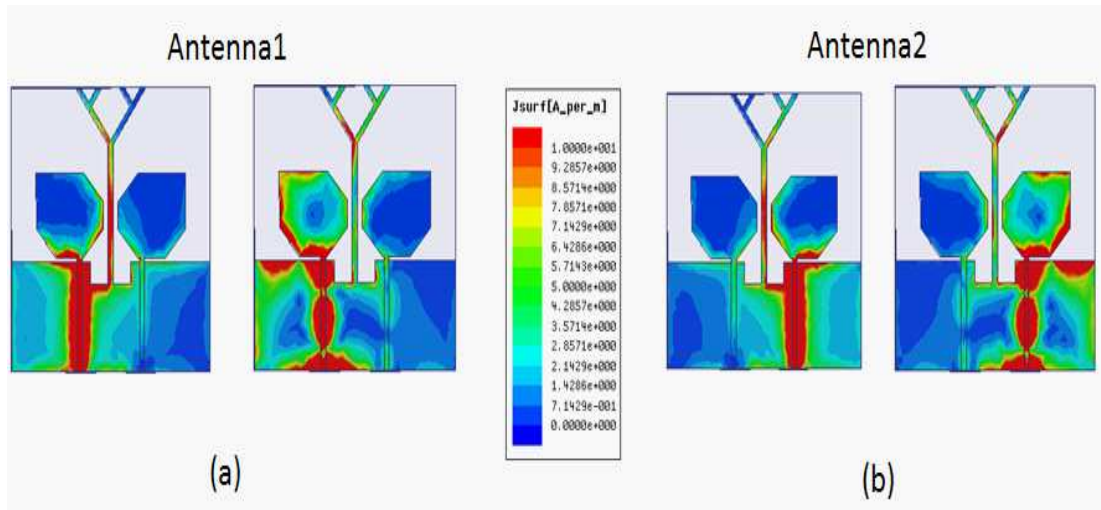


Figure 4.6: Simulated surface currents distribution of the diversity antenna (a) Antenna 1 at 3.6 GHz and 7.8 GHz, (b) Antenna 2 at 3.6GHz and 7.8GHz

isolation between the radiators across the whole UWB. Figure 4.7 shows the simulated 3D radiation patterns for the antenna 1 and antenna 2 at 3.6GHz, 5.8GHz, 7.8GHz and 10.2GHz. It can be noticed that the gain of the proposed monopole antenna at all the frequencies within the bands is more than 2dBi. The 3D radiation patterns are Omni-directional towards the lower frequency band and remain nearly Omni-directional with multiple lobes towards the higher frequency band.

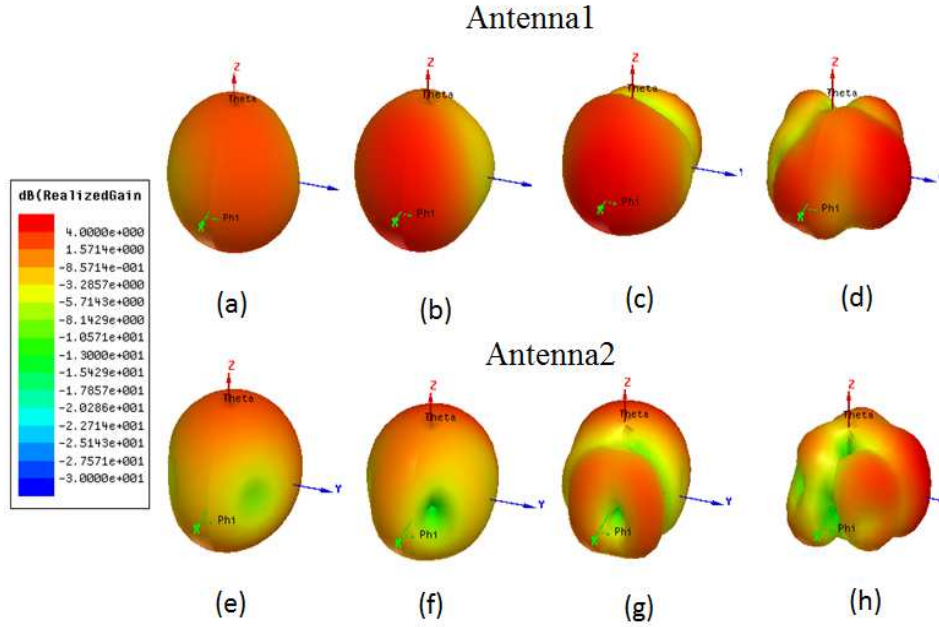


Figure 4.7: Simulated 3D gain radiation patterns for the antenna 1 and antenna 2: (a) and (b) at 3.6GHz, (c) and (d) at 5.8GHz, (e) and (f) at 7.8GHz and (g) and (h) at 10.2GHz

4.2.2 Experimental verification

The measured impedance bandwidths for $|S_{11}|$ and isolation $|S_{21}|$ using vector network analyzer (Agilent Model no.: N5230A) is shown in Figure 4.8. The measured impedance bandwidths ($|S_{11}| \leq -10dB$) cover the whole UWB band. The port 2 has same impedance response ($|S_{22}|$) as that of port 1. The isolation within the impedance bandwidth is greater than -20dB.

Radiation performance at operating frequency across the impedance bandwidth (3.1GHz and 10.6GHz) has been evaluated. At frequencies of 3.6GHz, 7.8GHz and 10.2GHz both X-Z and Y-Z planes were measured and is shown in Figure 4.9. During measurement, only port 1 is excited, while port 2 is terminated with 50Ω load and vice versa. It is seen that the radiation patterns tend to cover complementary space region, which provide spatial diversity for the system. The system switches between

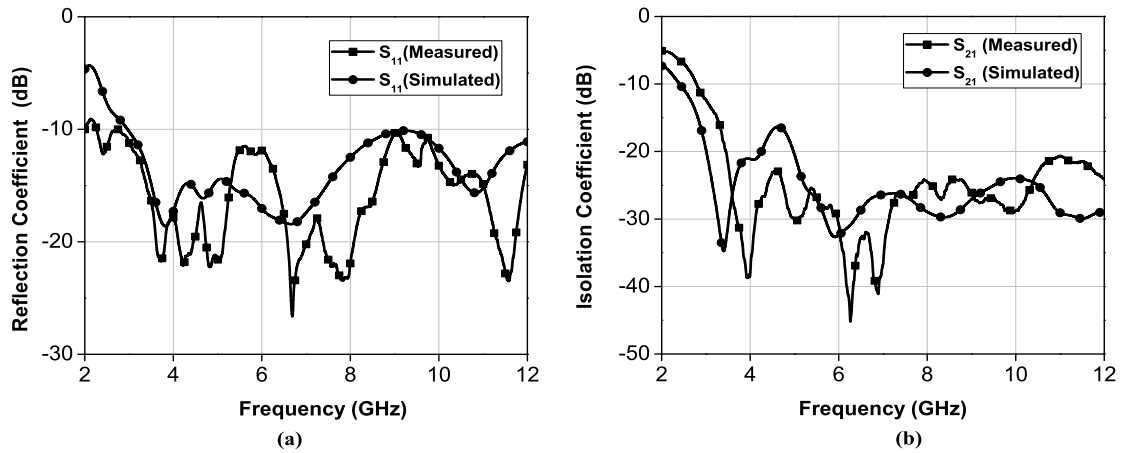


Figure 4.8: Measured and simulated reflection coefficient and isolation curves (a) $|S_{11}|$, (b) $|S_{21}|$

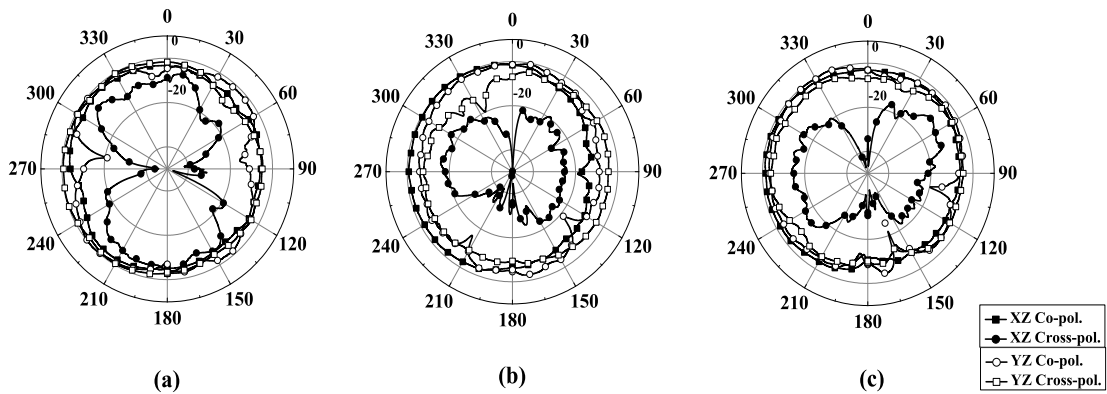


Figure 4.9: Measured radiation patterns of the antenna 1 in X-Z and Y-Z plane at (a) 3.6GHz, (b) 7.8GHz and (c) 10.2GHz

the two monopoles to obtain maximum signal strength. This operation overcomes the multipath fading problem and enhances the systems performance.

4.3 Semi circular shaped diversity antenna

4.3.1 Antenna geometry and simulation results

The configuration of the proposed UWB antenna is shown in Figure 4.10. The diversity antenna consists of two symmetric semi-circular shaped radiators. It is printed

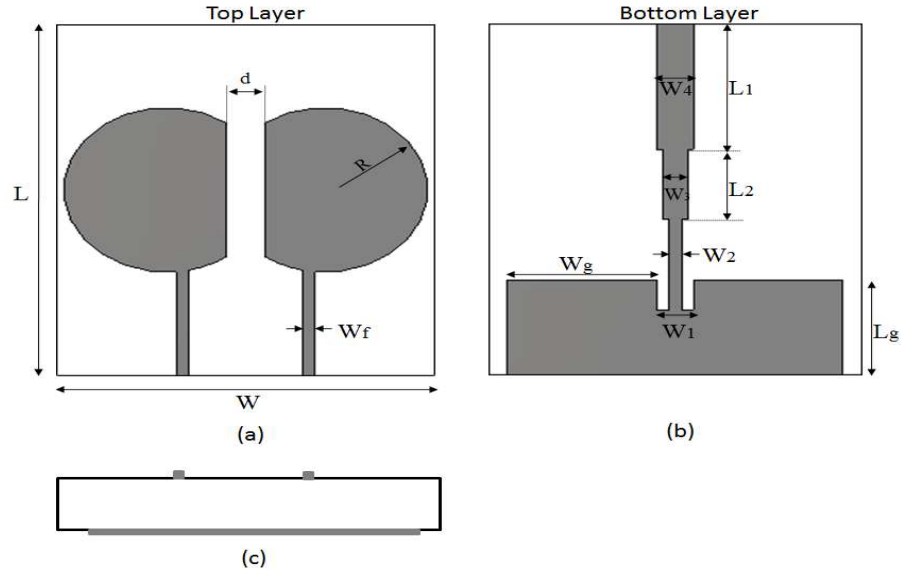


Figure 4.10: Geometry of the 2 element semi circular shaped diversity antenna (a) Top layer (b) Bottom layer (c) Top View

Table 4.3: Dimensions of 2 element semi circular shaped diversity antenna

L	W	L ₁	W ₁	L ₂	W ₂	L ₃
35mm	30mm	09mm	3mm	07mm	01mm	12.5mm
W ₃	L _g	W ₄	W _f	W _g	R	d
02mm	9.5mm	03mm	01mm	12mm	4.2mm	3mm

on upper part of the substrate with dimensions L mm \times W mm \times h mm and the substrate had a relative permittivity 2.4. Two radiators are separated by 3mm from each other and are symmetrically positioned with respect to the Y-axis. The radiators are excited via 50Ω microstrip lines of 1.5mm width. The wideband isolation between the two UWB radiators can be efficiently enhanced by using central strip that extends vertically from the ground plane printed on backside of the substrate. The central strip located at the center of the ground element. It suppresses direct coupling between two antenna elements. The central strip acts as alternate current path, allowing the current to flow through arms of the strip.

As the distance ' d ' between the radiators increased, there is an upward shift in the

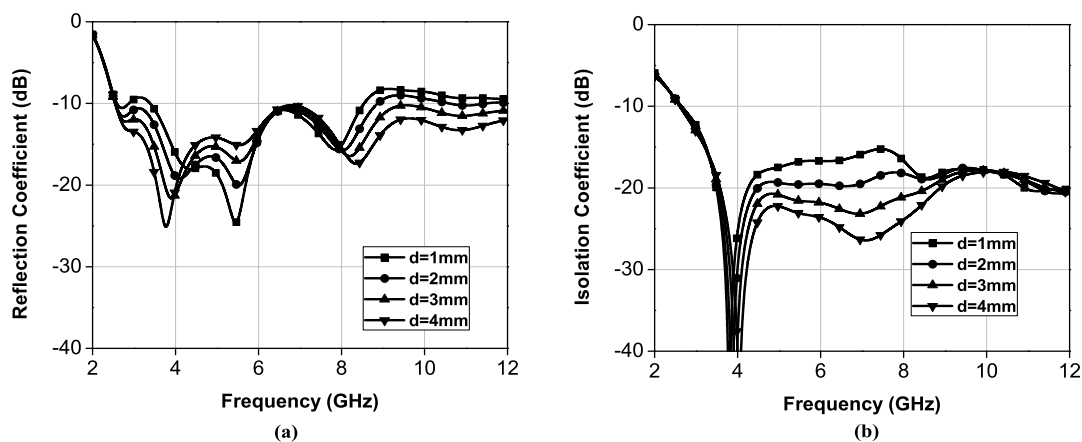


Figure 4.11: Simulated reflection coefficient and isolation coefficient curves for different 'd' values (a) $|S_{11}|$ and $|S_{22}|$ (b) $|S_{12}|$ and $|S_{21}|$

higher edge frequency. The isolation is mainly affected at the lower and upper edges of the pass-band as shown in Figure 4.11. Figure 4.12 illustrate simulated reflection coefficients $|S_{11}|$ $|S_{22}|$ and $|S_{21}|$ $|S_{12}|$ using electromagnetic software. It is observed that the isolation characteristic is improved significantly by increasing the stub size above the ground plane. The optimal dimensions of the designed antenna are listed in Table.4.3

In Figure.4.13, the surface current distributions at 3.4GHz, 5GHz and 7GHz are shown. Port 1 is excited while port 2 is terminated with 50Ω load and vice versa. The current distribution near the radiator 2 is much smaller than those in the antenna without the stub. It is clear from the Figure.4.13 that the current distribution in the stub is very strong. This arrangement reduces the mutual coupling and increases isolation between the two monopole radiating elements.

4.3.2 Experimental verification

The measured $|S_{11}|$ and isolation coefficient $|S_{21}|$ are measured using vector network analyzer and is presented in Figure 4.14. According to the measurement results, the impedance bandwidth ($|S_{11}| \leq -10\text{dB}$) covers the whole operating band. The port 2 has the same impedance response ($|S_{22}|$) as that of port 1. The isolation within the impedance bandwidth is -18dB. The measured E-plane(XZ, Co-pol.and Cross-

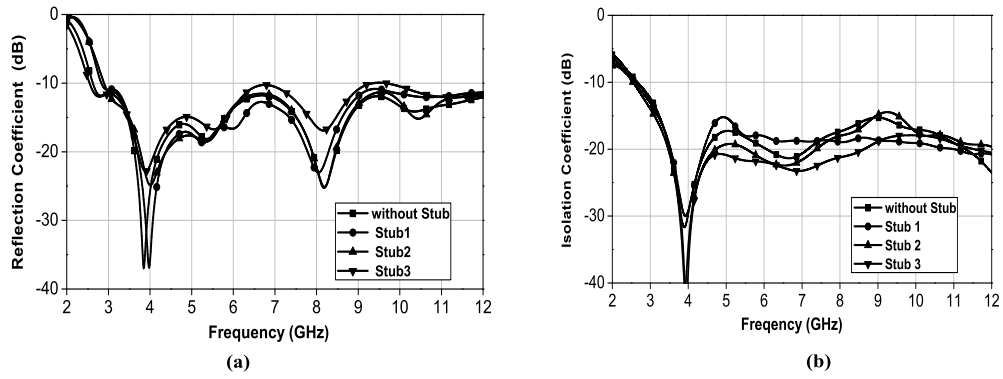


Figure 4.12: Simulated reflection coefficient and isolation coefficient curves for different iterations (a) $|S_{11}|$ and $|S_{22}|$ (b) $|S_{12}|$ and $|S_{21}|$

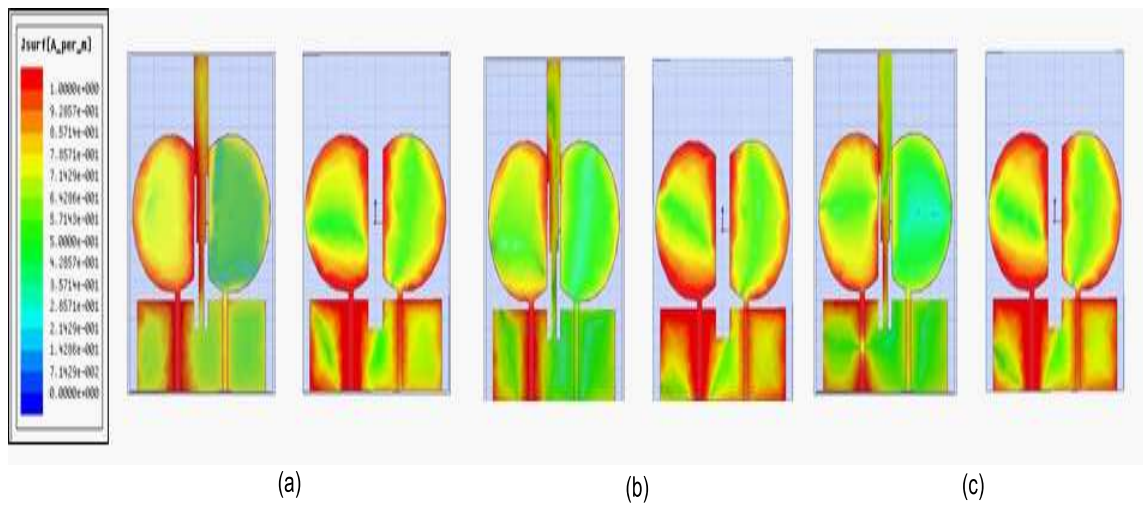


Figure 4.13: Simulated surface current distributions with port 1 excitation at (a) 3.4GHz, (b) 5GHz and (c) 7GHz

pol.) and H-plane(YZ, Co-pol. and Cross pol) radiation patterns at three frequencies 3.4GHz, 5GHz and 7GHz are shown in Figure 4.15. During measurement, only port 1 is excited, while port 2 is terminated with 50Ω load. The antenna radiation patterns are omnidirectional in lower resonant frequency band and nearly omnidirectional in higher resonant frequency band.

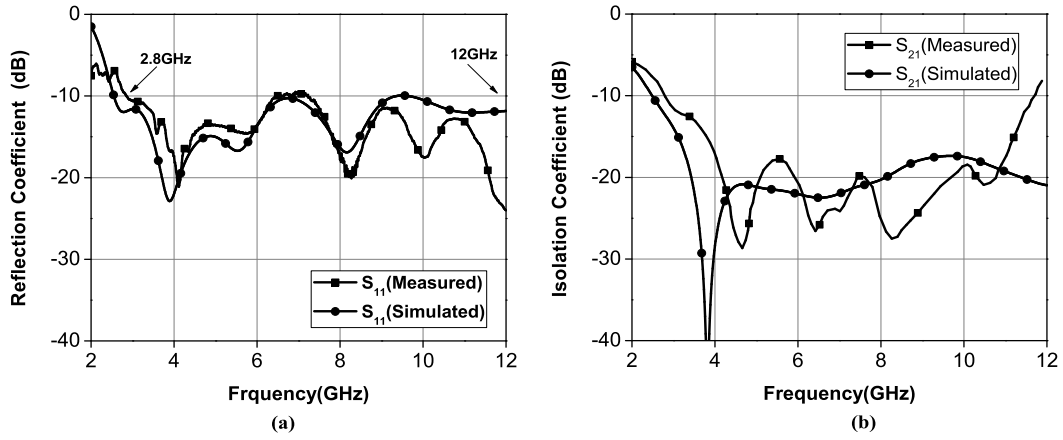


Figure 4.14: Measured and simulated (a) reflection and (b) isolation coefficients of semi circular diversity antenna

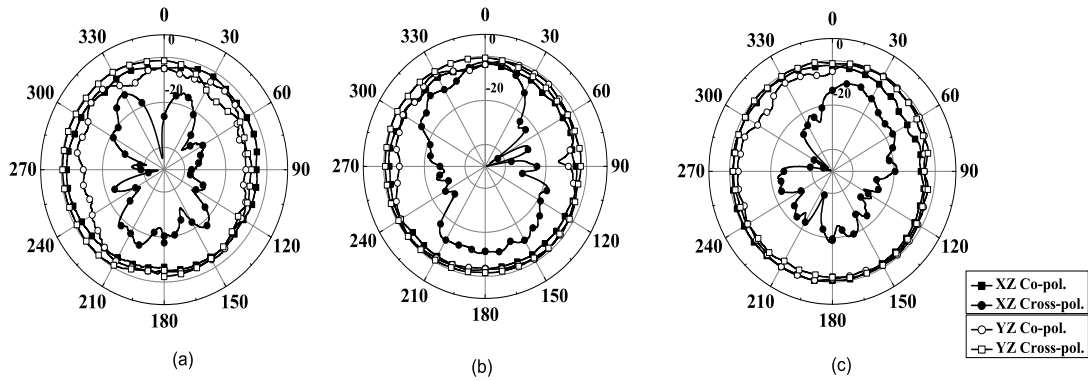


Figure 4.15: Measured radiation patterns of the antenna 1 in X-Z and Y-Z plane at (a) 3.4GHz, (b) 5GHz, and (c) 7GHz

4.4 Band-Notched Diversity Antenna

In this section, thin slot resonators are incorporated within the semi octagon shaped diversity radiator patch and radiating plane of the semi circle antenna to notch out the 3.5 and 5.5 GHz WLAN bands. The investigations include a parametric analysis by varying the slot dimensions. The slot parameters control the center frequency, width of the rejection band as well as the peak $|S_{11}|$ of the rejection band.

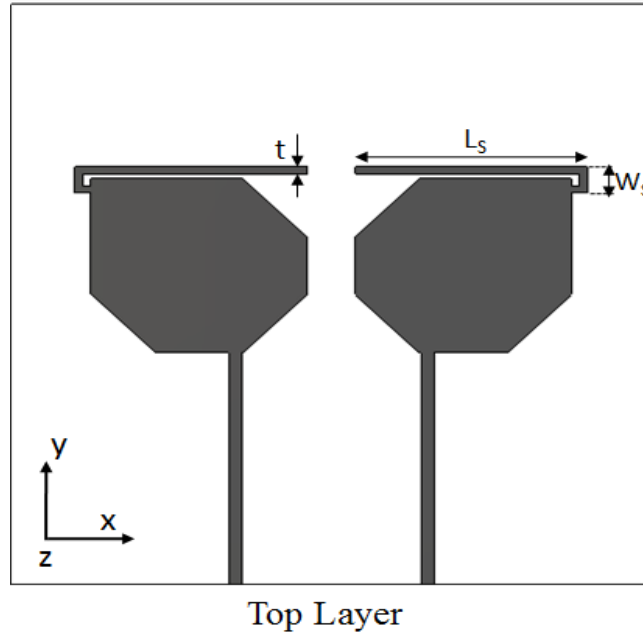


Figure 4.16: Geometry of a notched semi octagon shaped diversity antenna

4.4.1 Band-notched semi octagon shaped diversity antenna

The inverted L-shaped stub is symmetrically placed on the semi octagon shaped diversity antenna, which filters out the undesired frequency without disturbing the antenna characteristics in the rest of the band. The stubs are placed at distance of 0.5mm from the top end of the radiating element. The stubs consist of two orthogonally connected segments with length (L_S) and width (W_S). The total length of each stub is approximately $\lambda_g/4$ at 3.5GHz . At the notch frequency (f_N), the current is flowing on the stubs in opposite directions (out-of phase) as the current on the antenna edges. This affects the antenna to operate in transmission line mode, which transfers high impedance at the top of the notch band. Due to this effect, nearly zero impedance is found at the feed point. This creates high attenuation near the notch frequency. Figure 4.16 shows the geometry of the band-notched semi octagon shaped diversity antenna.

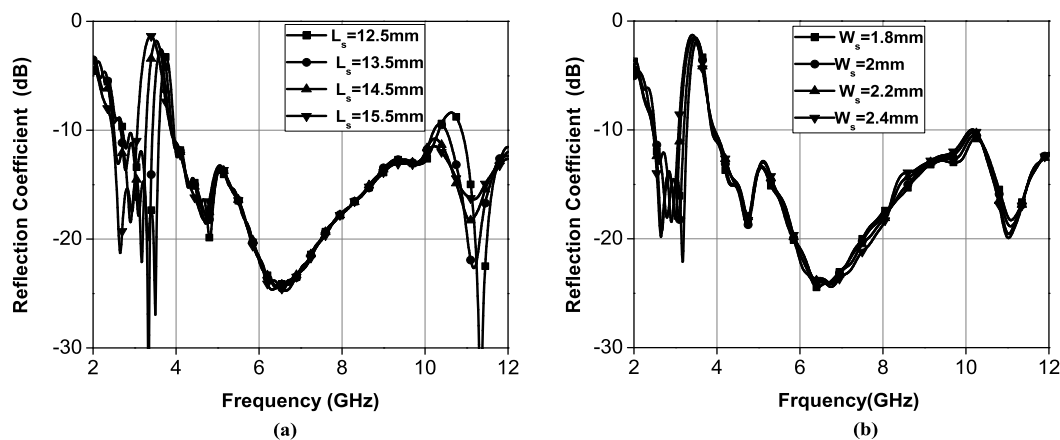


Figure 4.17: Simulated reflection coefficient with frequency for different values of (a) L_s , and (b) W_s

Simulated and Measured Results

Figure 4.17 (a) and (b) depicts the $|S_{11}|$ for various lengths of the inverted L-shape stub. The length of the stub has a significant effect on the notched frequency. The notched frequency shifts from 3GHz to 3.5GHz as the length of the inverted L-shape changes around L_s varying from 12.5mm to 15.5mm ($W_s=2.2$ mm) where as W_s varying from 1.8mm to 2.4mm ($L_s=14.5$ mm). This is because of the fact that the notched frequency of inverted L-shape stub is inversely proportional to the length of the resonator. The band-notched property is also observed in radiation patterns at Figure 4.18 and Figure 4.19, where the simulated 3D radiation patterns are plotted at 3.5GHz, 4.2GHz and 10.2GHz. At 3.5GHz a distinct reduction in radiation pattern is around 10dB along all directions. Figure 4.18 (d) shows that the surface current distribution appears stronger around the stub at the notched frequency 3.5GHz. It is more concentrated at the farthest sides of the slot and is oppositely directed along its lower and upper edges. This leads to destructive interference of the excited surface currents in the patch

Figure 4.20 shows the measured reflection coefficient of the antenna which shows reasonable comparison with simulated plots. The antenna exhibits the band-notched performance in the frequency range of 3.3GHz to 3.8GHz. The measured radiation patterns of the antenna are plotted in Figure 4.21 at 4GHz, 7GHz and 9.2GHz in

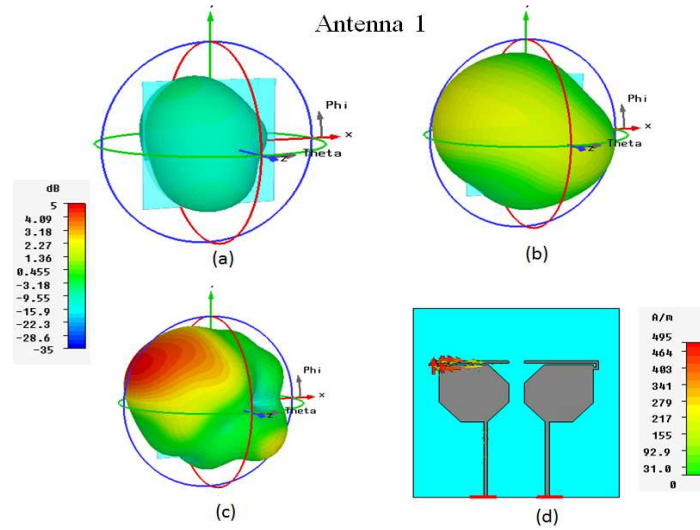


Figure 4.18: Simulated radiation patterns of a notched semi octagon shaped diversity antenna1 at (a) 3.5GHz, (b) 4.2 GHz, (c) 10.2GHz and (d) the current distribution at 3.5GHz

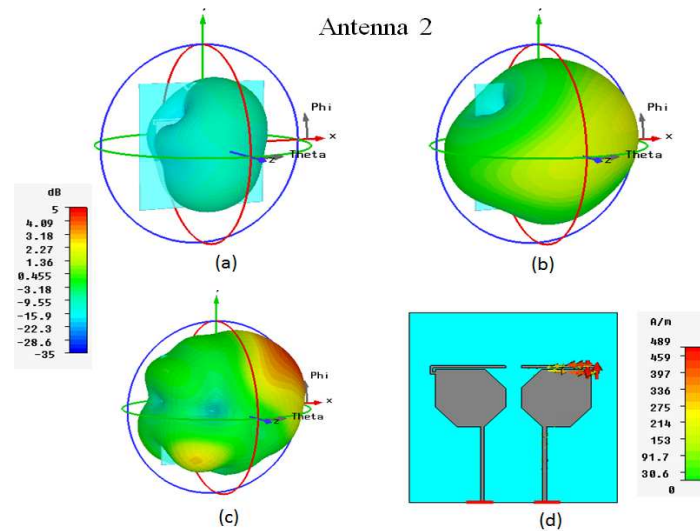


Figure 4.19: Simulated radiation patterns of a notched semi octagon shaped diversity antenna2 at (a) 3.5GHz, (b) 4.2 GHz, (c) 10.2GHz and (d) the current distribution at 3.5GHz

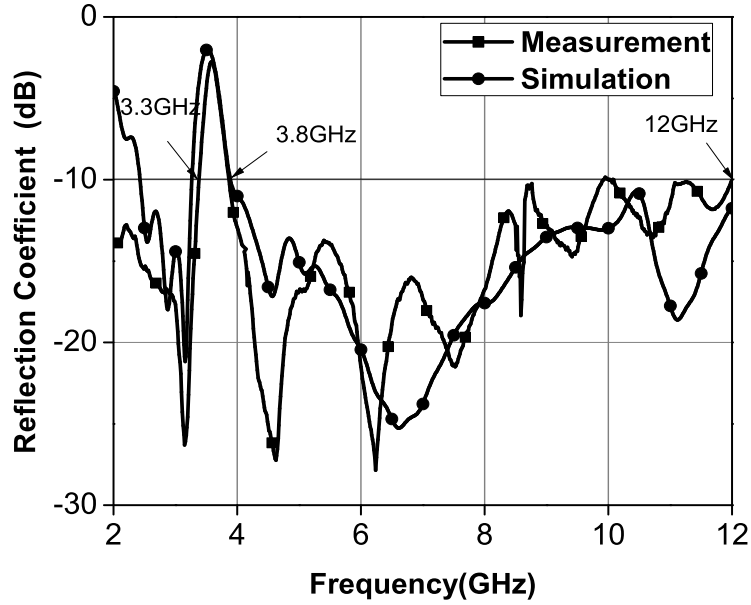


Figure 4.20: Measured reflection coefficient with frequency for notched semi octagon shaped diversity antenna 1

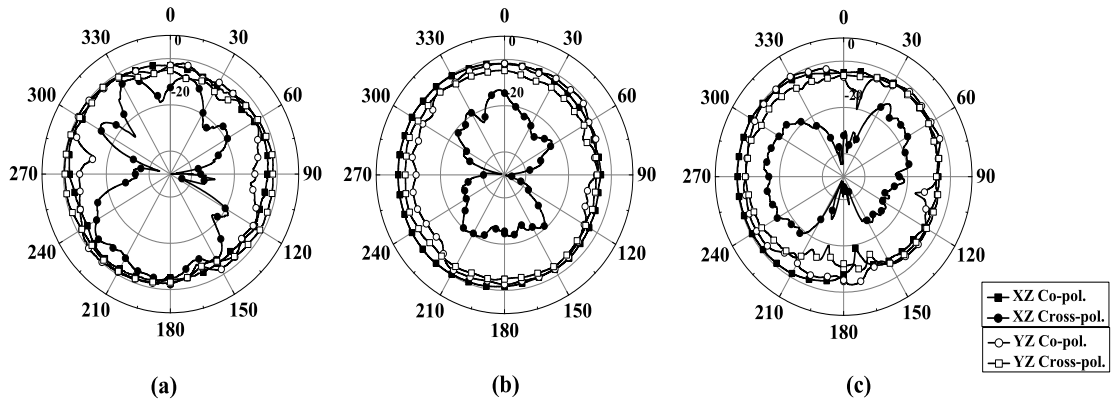


Figure 4.21: Measured radiation patterns of the antenna1 in X-Z and Y-Z plane at (a) 4GHz, (b) 6GHz and (c) 9.2GHz

E and H planes. During measurements, Port 2 is terminated with a 50Ω load when Port 1 is excited and vice versa. Comparing the patterns when Port 1 and Port 2 are separately excited, it can be observed that they cover complementary spatial regions symmetrically with respect to the y-z plane. The patterns are relatively stable across the impedance bandwidth.

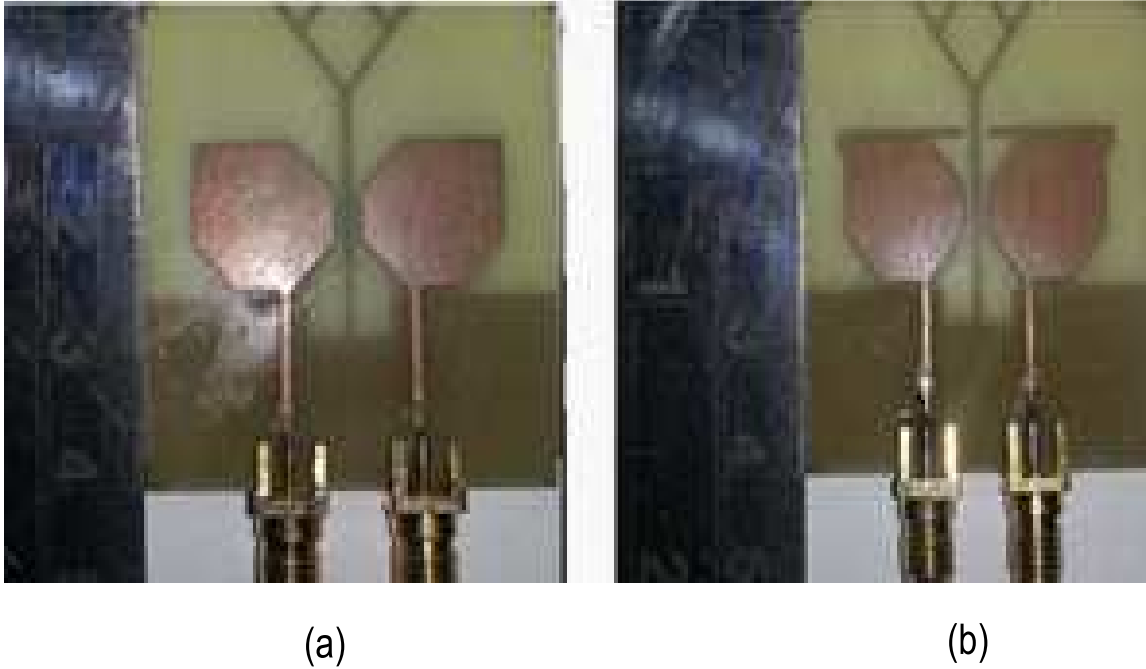


Figure 4.22: Photograph of proposed semi octagon shaped diversity antenna (a) without bandnotch, (b) with bandnotch

The photographs of the proposed antenna with and without bandnotch are shown in Figure 4.22. The antenna gain has been measured and presented in Figure 4.23. Only the gain for Port 1 is presented here. Due to the symmetry of the structure, the gains of the antenna2 are almost the same.

Diversity Performance

Antenna diversity techniques are used to increase the spectrum efficiency in mobile communication systems and the mutual coupling of the antenna degrades the performance of a diversity antenna system. Therefore the correlation coefficient is an important parameter in diversity antenna. The correlation coefficient is a statistical tool that measures the degree of similarity among the received signals. Its modulus varies from 0 to 1. Ideally, the diversity systems require a correlation coefficient of zero or low by default.

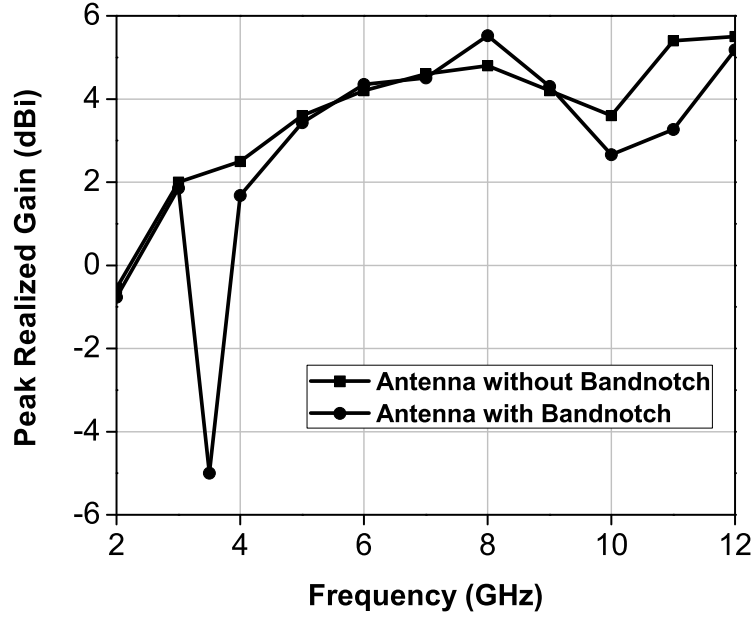


Figure 4.23: Measured peak gains of semi octagon shaped diversity antenna

These parameters can be viewed by three ways: complex, envelope and power correlation coefficients. Complex correlation coefficient gives the complex measure of correlation between received signals at the antennas. This is given by relationship [92]

$$\rho_c = \frac{\int_0^{2\pi} \int_0^\pi (XPRE_{\theta k}(\theta, \varphi) E_{\theta l}^*(\theta, \varphi) P_\theta(\theta, \varphi) + E_{\varphi k}(\theta, \varphi) E_{\varphi l}^*(\theta, \varphi) P_\varphi(\theta, \varphi)) \sin \theta d\theta d\varphi}{\sqrt{\sigma_k^2 \sigma_l^2}} \quad (4.1)$$

where σ_k^2 and σ_l^2 represent the variances of k^{th} and l^{th} branches which can be written mathematically as

$$\rho_c = \int_0^{2\pi} \int_0^\pi (XPRG_{\theta k}(\theta, \varphi) P_\theta(\theta, \varphi) + G_{\varphi k}(\theta, \varphi) P_\varphi(\theta, \varphi)) \quad (4.2)$$

also

$$G_{\theta k}(\theta, \varphi) = E_{\theta k}(\theta, \varphi) E_{\theta l}^*(\theta, \varphi) \quad (4.3)$$

$$G_{\varphi k}(\theta, \varphi) = E_{\varphi k}(\theta, \varphi) E_{\varphi l}^*(\theta, \varphi) \quad (4.4)$$

where ‘XPR’ is the cross polarization ratio, $E_{\theta k}$ and $E_{\varphi l}$ are the complex electric fields in the directions of θ and φ respectively for the k^{th} antenna. Similar expressions are valid for l^{th} antenna. Usually, the envelope correlation is presented to evaluate the diversity capabilities of MIMO systems [93]. These parameters are always real and by definition give the correlation among the amplitudes of the signals at antennas. For Rayleigh fading channel, the envelope correlation can be given as follows:

$$\rho_c = |\rho_c|^2 \quad (4.5)$$

It is clear that Envelope Correlation Coefficient (ECC) should be preferably computed from the 3D radiation patterns but it becomes tedious. However, assuming that the diversity system will operate in a uniform multi-path environment, the ECC can be calculated from the S-parameters using the relationship (4.6) [94].

$$\rho_c = \frac{|S_{11}^* S_{12} + S_{21}^* S_{22}|}{(1 - (|S_{11}|^2 + |S_{21}|^2)) (1 - (|S_{22}|^2 + |S_{12}|^2))} \quad (4.6)$$

The simulated and measured ECC across the desired frequency band are shown in the Figure 4.24. As can be seen, the value of ECC is well below the practical threshold value of 0.5 throughout the UWB band. Similarly, the capacity loss (bits/Hz) is another performance parameter which characterizes quality of a MIMO/Diversity antenna system. The channel capacity is the tightest upper bound on the rate of information that can be reliably transmitted over a communication channel. This can be defined using the correlation matrix given in [95], and is calculated by using the following equation.(4.7) [96].

$$C_{loss} = -\log_2 \det(\Psi^R) \quad (4.7)$$

where Ψ^R is the receiving antenna correlation matrix that is given by:

$$\Psi^R = \begin{pmatrix} \rho_{11} & \rho_{12} \\ \rho_{21} & \rho_{22} \end{pmatrix}$$

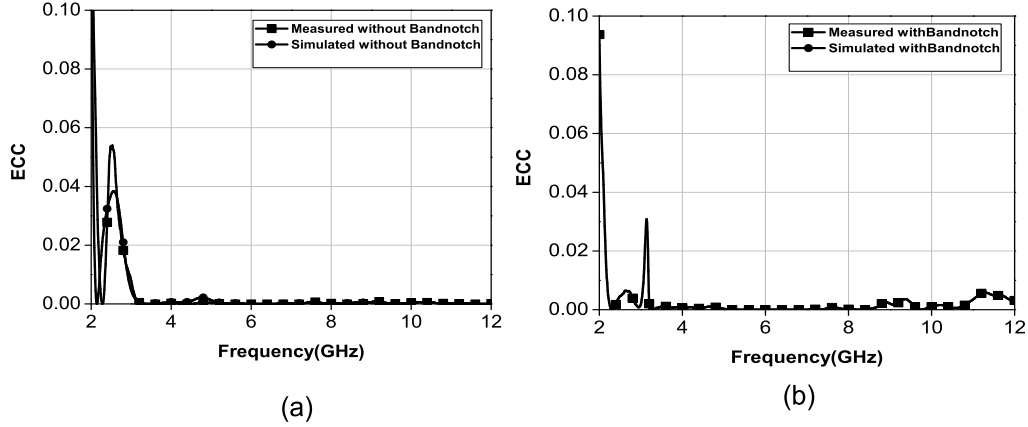


Figure 4.24: Simulated and measured (a) Envelope correlation coefficient(ECC) without bandnotched (b) Envelope correlation coefficient(ECC) with bandnotched.

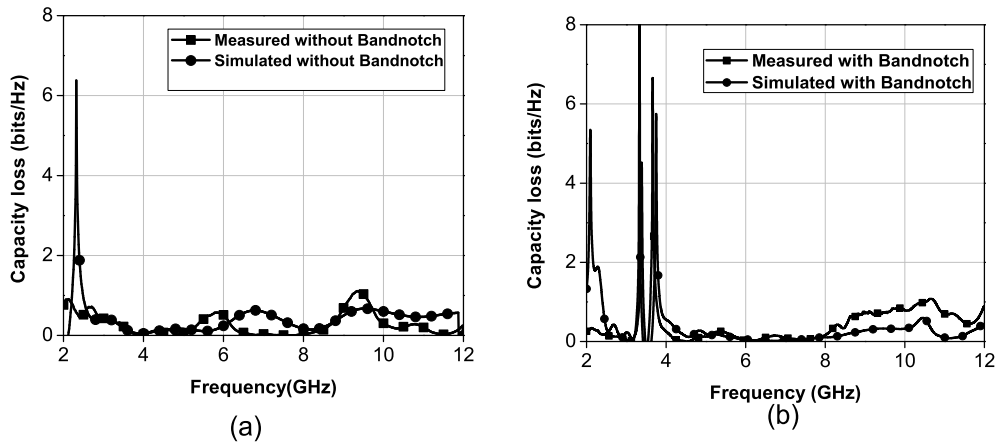


Figure 4.25: Simulated and measured (a) Capacity loss antenna without bandnotched (b) Capacity loss antenna with bandnotched

where, $\rho_{ii} = 1 - (|S_{ii}|^2 - |S_{ij}|^2)$ and $\rho_{ij} = -(|S_{ii}^* S_{ij} + S_{ji}^* S_{ij} |)$ for $i, j = 1$ or 2 .

The comparison of measured and simulated capacity loss values of the proposed antenna are shown in Figure 4.25. It can be observed that the capacity loss does not exceed 0.3 bits/Hz except bandnotched antenna and is well below the threshold value 0.4 bits/Hz for the throughout UWB band.

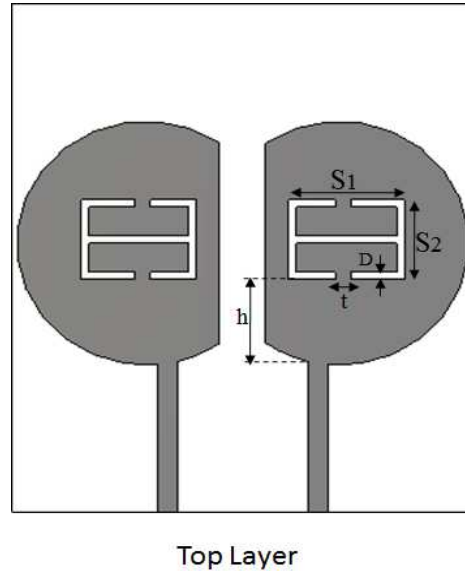


Figure 4.26: Geometry of a notched semi circular diversity antenna

4.4.2 Band-notched semi circular diversity antenna

The band rejection mechanism is achieved for the semi circle diversity antenna by introducing Complementary Electric Inductive Capacitive (CELC) resonator inside the patch as shown in Figure 4.26. According to the babinet principle, as CELC could provide a predominantly electric response, the predominantly magnetic response could be observed in the complement ELC. Based on current distribution, it is observed that the center part of the radiating element has low current density. Therefore as shown in Figure 4.26, the CELC placed near microstrip feed line at a height 'h'

Design and Simulation Results

The simulated reflection coefficient of the antenna for different slot parameters namely the slot width S_1 , length S_2 , and position 'h' and 't' from the edge of the radiator are plotted in Figure.4.27. The dimensions of circular antenna remain same as in Table 4.3. It is observed from Figure 4.27 (a) that the center frequency of the notched band is determined by the slot width S_1 and is approximately given by

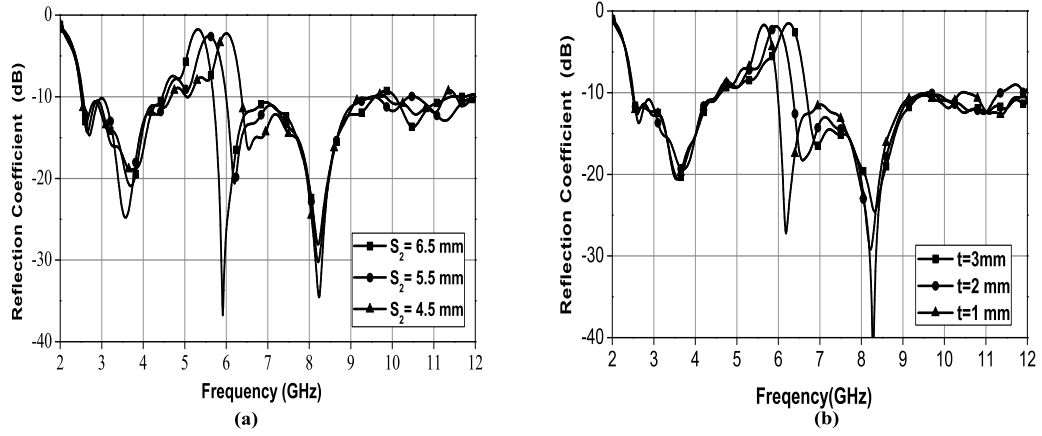


Figure 4.27: Simulated reflection coefficient and isolation coefficient with frequency for different values of S_2 and t

$$S_1 = \frac{\lambda_g}{2} \quad (4.9)$$

where $\lambda_g = \lambda_o / \sqrt{\epsilon_{eff}}$, $\epsilon_{eff} \approx (\epsilon_r + 1)/2$ and λ_o is free space wavelength at the rejection frequency. This is confirmed in Figure 4.27 (b) which shows that on keeping S_1 constant and changing the slot position, the notch frequency remains same but the matching varies. The dimension of the slot described in the radiator circle is deduced using equation (4.9) at a notch frequency of 5.5GHz and are as follows: $S_1 = 8\text{mm}$, $S_2 = 6\text{mm}$, $t = 1\text{mm}$, $h = 6.5\text{mm}$, $d = 0.5\text{mm}$. Figure 4.28 and 4.29 shows the simulated 3D radiation patterns and surface current distribution respective frequency at 3.3GHz, 5.8GHz, and 8.6GHz. It can be observed that the gain of the antenna at all the frequencies is more than 3dBi. The 3D patterns are omnidirectional towards the lower frequency band. In addition with 5.8GHz the current distribution mainly concentrated at the area of CELC resonator. It causes the antenna to be non-responsive at that frequency. The impedance changes make large reflection at the desired notched frequency.

The simulated and measured reflection coefficient and isolated coefficient curve for this antenna with and without the slot are plotted in Figure 4.30. Good agreement between the simulated and measured results is observed. It reveals a $|S_{11}| \leq 10\text{dB}$ reflection coefficient bandwidth from 3.2GHz to 12GHz. In the pass band, the reflec-

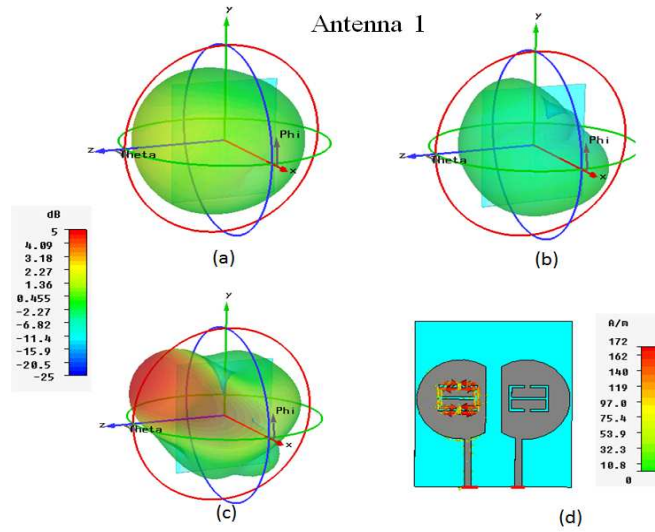


Figure 4.28: Simulated radiation patterns of a notched semi circular diversity antenna1 at (a) 3.3GHz, (b)5.8 GHz, (c) 8.6 GHz and (d) the current distribution at 5.8GHz

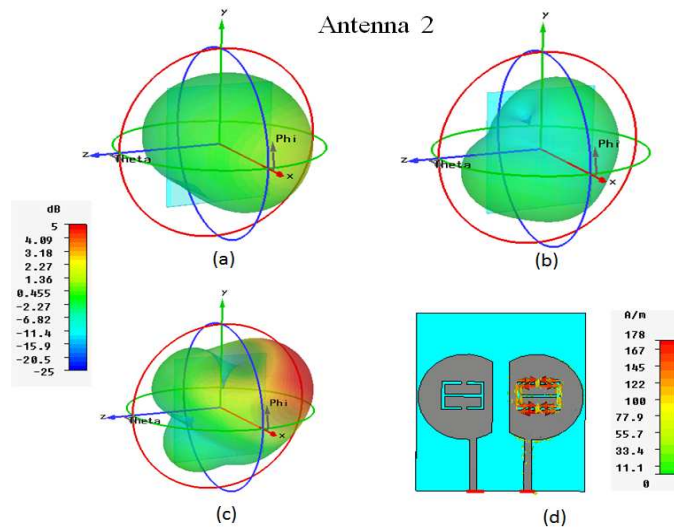


Figure 4.29: Simulated radiation patterns of a notched semi circular diversity antenna2 at (a) 3.3GHz, (b)5.8 GHz, (c) 8.6 GHz and (d) the current distribution at 5.8GHz

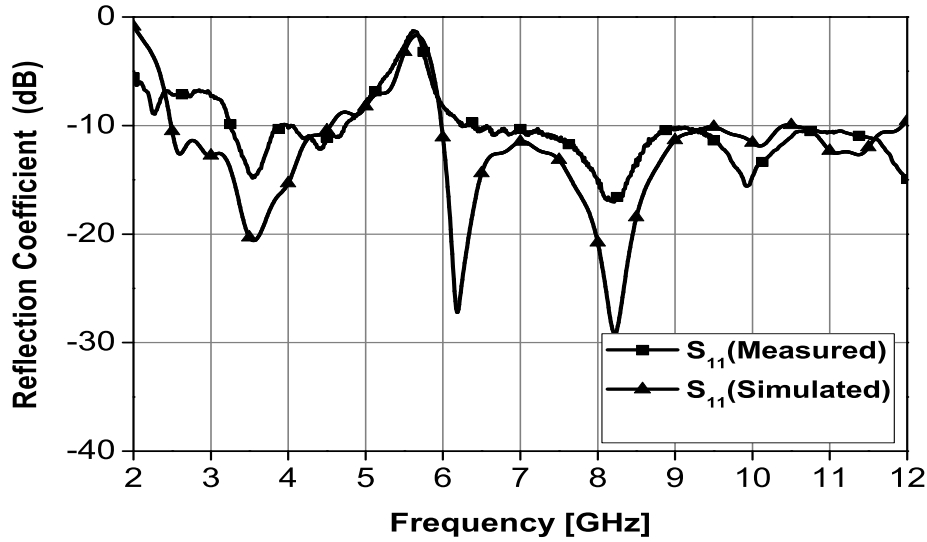


Figure 4.30: Measured reflection coefficient for a notched semi circular diversity antenna

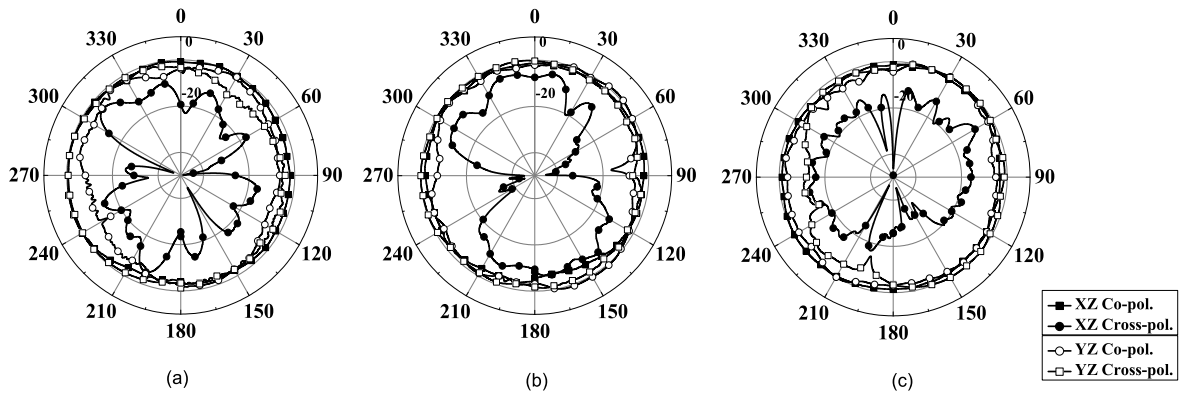


Figure 4.31: Measured radiation patterns of the antenna 1 in X-Z and Y-Z plane at (a) 3.3GHz, (b) 4.5GHz and (c) 8GHz

tion coefficient of the original UWB antenna is only slightly affected by the presence of the slot. The measured radiation patterns at XY and YZ cut planes are shown in Figure 4.31.

During the measurements, only antenna 1 is excited while antenna 2 is terminated with 50Ω load. It can be seen from Figure 4.31, those patterns are omni-directional but it is nearly omni-directional with some multiple lobe towards the higher frequency

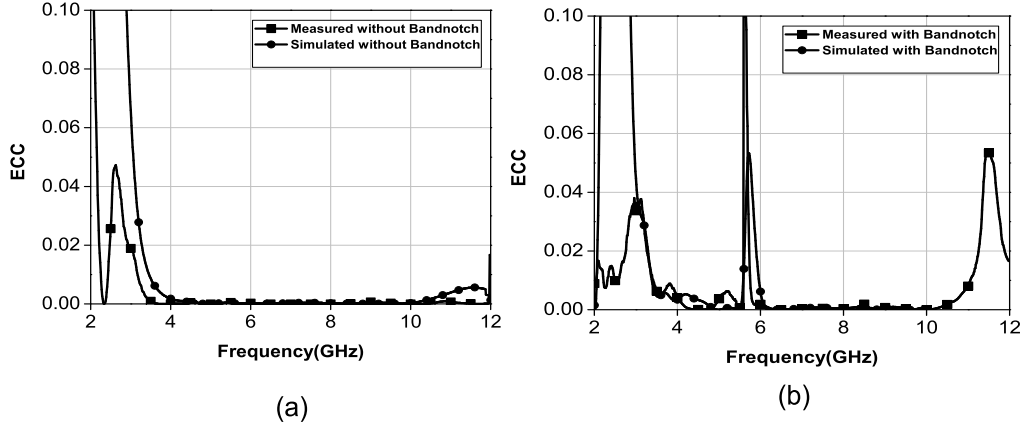


Figure 4.32: Simulated and measured (a) Envelope correlation coefficient (ECC) without bandnotched, (b) Envelope correlation coefficient(ECC) with bandnotched.

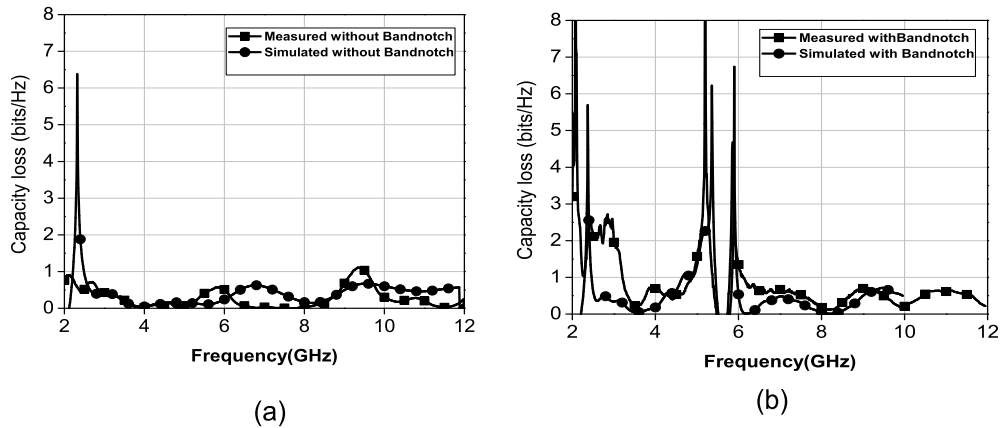


Figure 4.33: Simulated and measured (a) Capacity loss antenna without bandnotched, (b) Capacity loss antenna with bandnotched

band. In the proposed diversity antenna, the radiator is placed symmetrically, therefore, it will provide complementary patterns when one antenna is excited at a time and the other antenna is with match terminated.

The envelope correlation between antennas can be calculated using (4.6) as shown in Figure 4.32. The value of ECC is well below the practical threshold value of 0.5 except bandnotch frequency. Similarly the capacity loss (bits/Hz) is another parameter which characterizes quality of diversity antenna systems. Figure 4.33 shows the capacity loss of the proposed antenna system, using Equation.4.7, the capacity

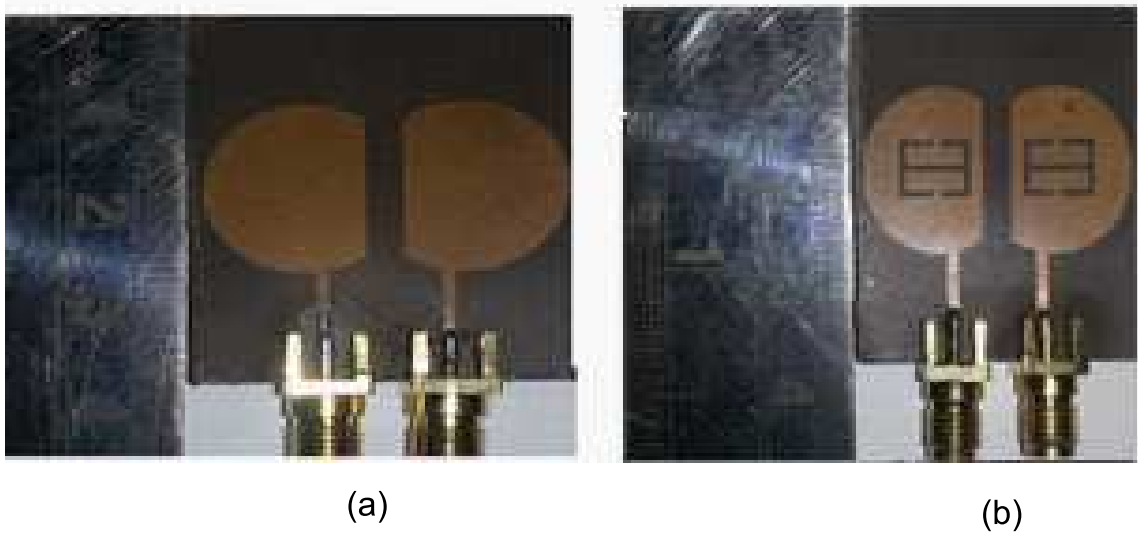


Figure 4.34: Photograph of proposed semi circular diversity antenna (a) without bandnotch, (b) with bandnotch

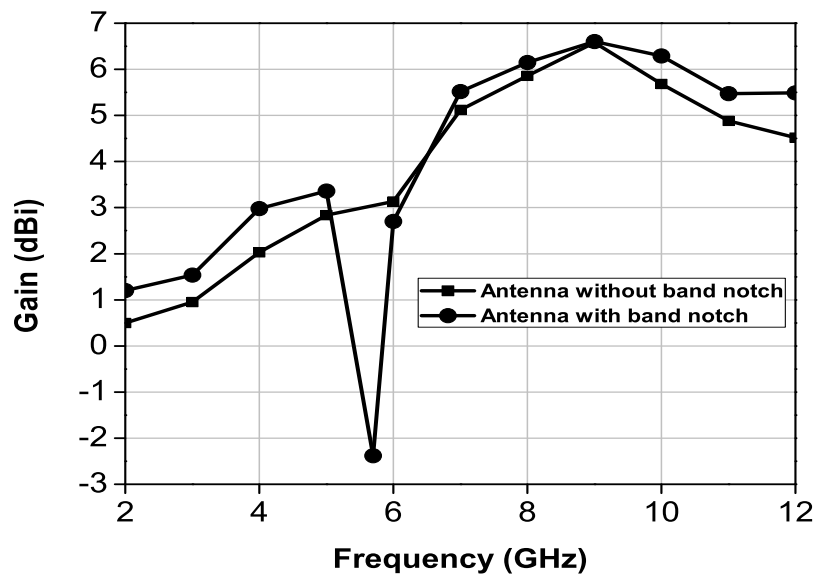


Figure 4.35: Measured peak realized gain of semi circular diversity antenna

loss calculated as below 0.3bits/Hz .

The photographs of the proposed antenna with and without bandnotch are shown in Figure 4.34. The measured gain for both antennas are plotted in Figure 4.35, the

Table 4.4: Comparison between proposed works with existing works.

Antenna type	Size(mm)	Bandwidth	Isolation loss	Gain
Compact wide-band MIMO antenna [97]	78×40×1.6	2.4GHz - 6.55GHz	-18dB	upto 5dBi
An ultra wide-band diversity antenna [98]	37×45×1.6	3GHz-5GHz	-20dB	6dBi
Printed ultra wideband diversity monopole antenna [99]	48×30×1.6	2.2GHz to 7.7GHz	-20dB	4dBi
Semi octagon shaped diversity antenna	40×40×1.6	3GHz-12GHz	-20dB	5dBi
Semicircular diversity antenna	35×30×1.6	2.8GHz to 12GHz	-18dB	5.5dBi

measured maximum peak realized gain is 6.5dBi. Due to symmetry of the antenna structure and their common fabrication tolerances; the gain values of the two radiators are almost same. Therefore, only the gain of the antenna 1 is measured, when the antenna 2 is terminated with a 50Ω matched load. Table (4.4) shows comparison of antenna performance between proposed works here along with existing works.

4.5 Summary

Two types of diversity antennas (a) semi octagon shaped diversity antenna and (b) semi circular diversity antenna are presented in this chapter. The compact semi octagon shaped antenna is designed to operate 3GHz to 12GHz. Simulated results show that adding branch lengths structure in ground plane for reduction of mutual coupling between two antennas. Use of a compact ground plane improves reduction in the overall size of the antenna. Measured results indicate a large impedance bandwidth with relatively stable and omnidirectional radiation patterns, which make the design suitable for broadband wireless communication applications. A quarter wavelength tuning stub is integrated with radiating element for filter action which in the case

is optimized to notch out 3 3GHz to 3.8GHz. In the final section, a semi circular diversity antenna for UWB application is presented. The impedance bandwidth of the designed antenna ranges from 2.8GHz to 12GHz. A half wave length slot inscribed on the radiating element for bandnotched function in the frequency of 5.5GHz. However, to ascertain the performance of the antenna for transmission of short UWB pulse in nano seconds duration, the UWB slot antenna need to be analyzed in time domain. This aspect of the antenna is studied in detail chapter 5.

CHAPTER 5

Time Domain Analysis of Planar Antennas

In Chapter 3 and Chapter 4, UWB planar monopole and diversity antennas have been investigated with an emphasis on their frequency domain performances. These antennas are well-matched in 3.1GHz to 10.6GHz communication bands. Since they have been behaving differently while transmitting and receiving large fractional bandwidth pulses, their time-domain studies of extreme importance for high speed pulse communications. In this thesis, the measurements are carried out in the frequency domain and the time domain parameters are deduced by taking inverse Fourier transform and is found equally accurate as the direct time domain measurements [100].

In this chapter, time domain characteristics of UWB planar monopole and diversity antennas are analyzed. Firstly, performances of these UWB antennas are evaluated for system point of view. Secondly, the transmitter and receiver responses of UWB antennas are investigated. And finally, a convolution approach is used to obtain the measured received pulses and the transmitting and receiving antenna systems are assessed for pulse fidelity.

5.1 Transfer Function Determination

In this thesis, the antenna is modeled as a Linear Time Invariant (LTI) system characterized by its transfer function $H(\omega, \theta, \phi)$ [101,102], whose magnitude and phase would completely define the antenna behavior. The antenna impulse response $h(t, \theta, \phi)$ can be calculated by inverse Fourier transformation of its transfer function.

Figure 5.1 presents a system model of a radio link made up of two antennas in

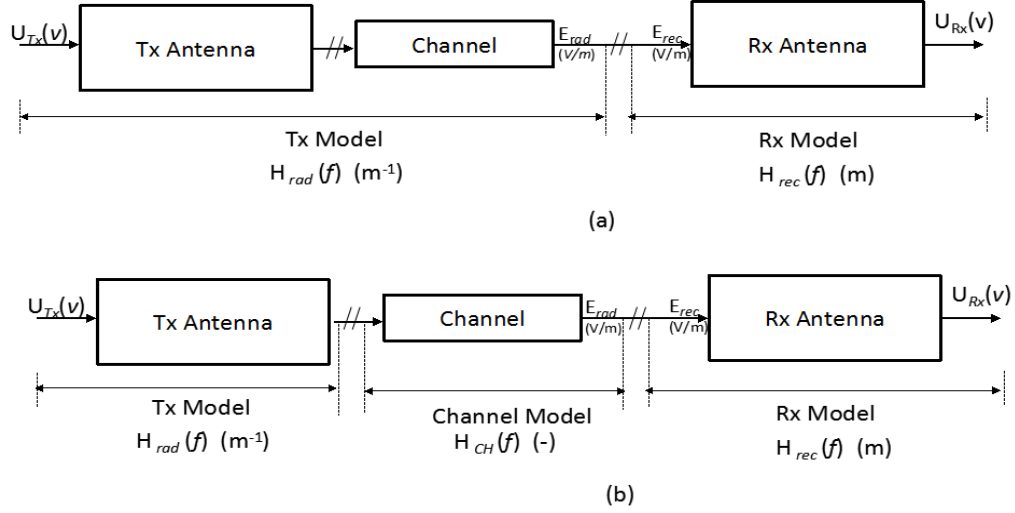


Figure 5.1: UWB channel model (a) classical (b) contemporary

free space under the approximation of far-field and line-of-sight propagation [103]. It consists of three blocks: the transmitting antenna (Tx), the free space channel and the receiving antenna (Rx). Each block is characterized by transfer functions $H_{Tx}(\omega, \theta, \phi)$, $H_{CH}(\omega)$ and $H_{Rx}(\omega, \theta, \phi)$, and associated impulse responses $h_{tx}(t, \theta, \phi)$, $h_{ch}(t)$ and $h_{rx}(t, \theta, \phi)$ respectively. The transient transmission is written in the frequency domain and the time domain given in (5.1) and (5.2)

$$s(\omega) = H(\omega, \theta, \phi)e(\omega) = H_{Tx}(\omega, \theta, \phi) \cdot H_{CH}(\omega) \cdot H_{Rx}(\omega, \theta, \phi) \cdot e(\omega) \quad (5.1)$$

$$s(t) = h(t, \theta, \phi) \otimes e(t) = H_{tx}(t, \theta, \phi) \otimes H_{CH}(t) \otimes h_{rx}(t, \theta, \phi) \otimes e(t) \quad (5.2)$$

where $H(\omega, \theta, \phi)$ and $h(t, \theta, \phi)$ are the overall system transfer function and impulse response, respectively. Figure 5.1 (a) presents the classical approach to characterize an ideal UWB channel. The emission model takes into account the Tx and the channel jointly, while in reception only the Rx antenna is considered [100]. The transmitting and receiving antennas are characterized by eliminating channel effects

which is adapted for the present study as shown in Figure 5.1 (b)

5.1.1 Transient reception and radiation

The time domain relation between the received voltage pulse $U_{Rx}(\omega, \theta, \phi)$ and the incident electric field pulse $E_{rad}(\omega, \theta, \phi)$ is shown in (5.3) and (5.4) [104]

$$\frac{U_{Rx}(\omega, \theta, \phi)}{\sqrt{Z_c}} = h_{Rx}(\omega, \theta, \phi) \frac{E_{rad}(\omega, \theta, \phi)}{\sqrt{Z_o}} \quad (5.3)$$

$$\frac{u_{rx}(\omega, \theta, \phi)}{\sqrt{Z_c}} = h_{rx}(\omega, \theta, \phi) \otimes \frac{E_{rad}(\omega, \theta, \phi)}{\sqrt{Z_o}} \quad (5.4)$$

The frequency domain relation between the transmitted electric field pulse and the incident voltage pulse is given in (5.5)

$$\frac{E_{rad}(\omega, \theta, \phi)}{\sqrt{Z_o}} = h_{Tx}(\omega, \theta, \phi) \otimes \frac{u_{Tx}(\omega, \theta, \phi)}{\sqrt{Z_c}} \quad (5.5)$$

where Z_c and Z_o are the characteristic impedance of the antenna port respectively. From (5.3) and (5.5), it is possible to determine the full input/output characteristics in both frequency and time domains

$$S_{21}(\omega) = \frac{U_{Rx}(\omega, \theta, \phi)}{U_{Tx}(\omega, \theta, \phi)} = H_{Tx}(\omega, \theta, \phi) H_{CH}(\omega) H_{Rx}(\omega, \theta, \phi) \quad (5.6)$$

$$\frac{u_{RX}(t\theta, \phi)}{u_{TX}(t, \theta, \phi)} = h_{tx}(\omega, \theta, \phi) \otimes h_{ch}(t) \otimes h_{rx}(t, \theta, \phi) \quad (5.7)$$

5.1.2 Implementation in CST microwave studio software

For the time domain characterization of the antenna discussed in this thesis, fourth derivative of the Gaussian pulse is chosen as input pulse whose mathematical form is given in Equation (5.8). This pulse is shown in Figure 5.2 (a)

$$S_i(t) = A \left[3 - 6 \left(\frac{4\pi}{T^2} \right) (t - \tau)^2 + \left(\frac{4\pi}{T^2} \right) (t - \tau)^4 \right] e^{-2\pi \left(\frac{t-\tau}{T} \right)^4} \left(\frac{V}{m} \right) \quad (5.8)$$

This pulse conforms to FCC spectral mask as shown in Figure 5.2 (b), where A =

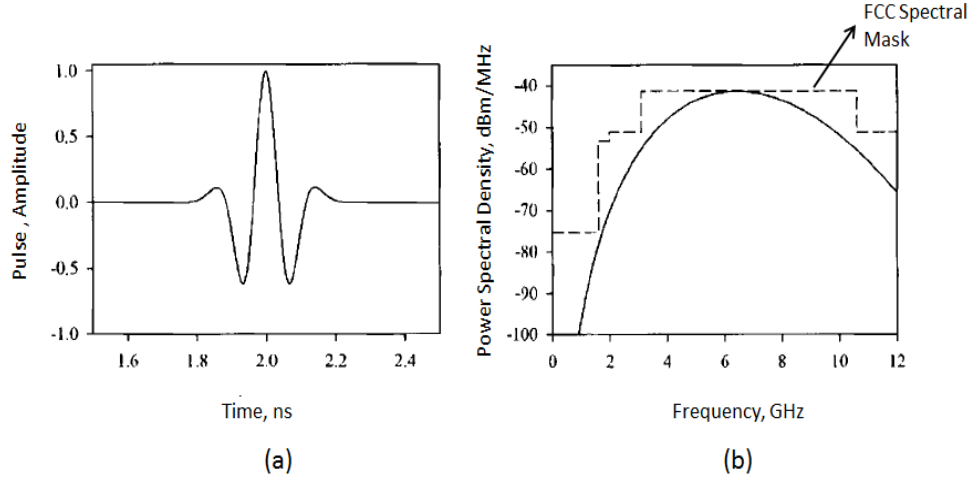


Figure 5.2: UWB channel model (a) Input pulse (b) Power spectral density

0.333 and $T = 0.175$ nS. For the antennas discussed in this thesis, the input voltage $h_{Tx}(t)$ ($=s_i(t)$) is specified in CST Microwave Studio suite and the radiated pulse $e_{rad}(t, \theta, \varphi)$ is calculated on face to face and side by side planes. Fourier transforms of these two quantities are then calculated using Equation (5.7) in order to calculate the transfer function $H_{Rx}(\omega, \theta, \phi)$. The impulse response $h_{Rx}(t, \theta, \phi)$ can be calculated using an IFFT.

In practice, from a simple measurement of the scattering parameter $|S_{21}|$ in the frequency domain, transfer functions of both the transmitting and receiving antennas can be deduced. Using two identical horn antennas oriented for bore sight transmission, the following relations are derived from Equation (5.7)

$$H_{TX}(\omega, \theta, \phi) = \sqrt{\frac{j}{2\pi} \left(\frac{\omega}{c}\right)^2 \frac{|S_{21}|(\omega, \theta, \phi)}{H_{CH}(\omega, \theta, \phi)}} (m^{-1}) \quad (5.9)$$

$$H_{RX}(\omega, \theta, \phi) = \sqrt{\frac{2\pi}{j} \left(\frac{c}{\omega}\right)^2 \frac{|S_{21}|(\omega, \theta, \phi)}{H_{CH}(\omega, \theta, \phi)}} (m) \quad (5.10)$$

$$H_{CH}(\omega) = \frac{c}{2d\omega} \exp\left(\frac{-j\omega d}{c}\right) \quad (5.11)$$

where the free space transfer function is shown in equation 5.11 with the reference antenna as the TX antenna and the AUT as the receiving antenna. The received transfer function of the AUT is deduced for multiple orientations and is given in Equation (5.12)

$$H_{AUT}(\omega, \theta, \phi) = \frac{|S_{21}|(\omega, \theta, \phi)}{H_{TX}(\omega) H_{CH}(\omega)} \quad (5.12)$$

5.2 Measurements with the Prototype Antennas

The measurement of the proposed antenna is carried out in an anechoic chamber with the help of vector network analyzer. The antenna system is comprised of two identical UWB antennas, as shown in Figure 5.3 (a). Since UWB technology is mainly employed in WPAN systems in the measurements, the transmitter and receiver are vertically placed with a separation of $d=0.3\text{m}$. Further, to investigate the system performance in different directions, two antennas are measured in two different orientations, namely face to face and side by side, respectively as shown in Figure 5.3 (b)

The measured antenna transfer function amplitudes are plotted in face to face and side by side plane as shown in Figure (5.4). It is observed that the magnitude of the transfer function has low ripples. The group delay deduced from the phase of the measured transfer function as in Equation (5.13) is plotted in Figure 5.5 for two face to face and side by side plane. Except at the notched frequencies of the band notched designs given in Figure 5.13, the measured group delay is within the tolerable range of $\pm 1\text{ns}$.

$$\tau_{g(\omega)} = -\frac{d\varphi(\omega)}{d\omega} \quad (5.13)$$

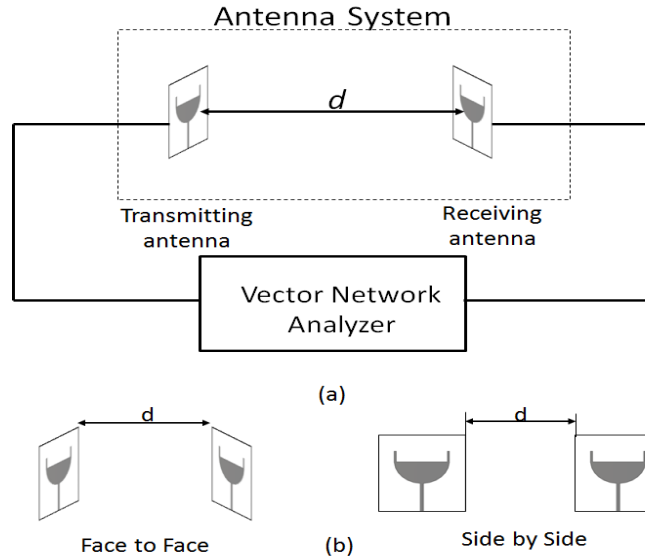


Figure 5.3: (a) System set-up (b) Antenna orientation: Face to Face and Side by Side

5.3 Impulse Responses of UWB Antennas

The transient behaviors of the antennas are assessed from their impulse responses which are obtained by taking the inverse Fourier transform of the transfer functions. The UWB antenna quality measures, namely the *FWHM* and ringing are directly deduced from the magnitude of the impulse responses.

5.3.1 Pulse distortion analysis: Fidelity factor

The antenna performance as a transmit-receive system is assessed based on Equation (5.14).

$$F = \max \frac{\int x(t) \int y(t - \tau) dt}{\sqrt{\int x(t)^2 dt \cdot \int y(t)^2 dt}} \quad (5.14)$$

The measured output pulses for both face to face and side by side orientations of the antennas are plotted with respect to the normalized face to face response and is plotted in Figure 5.6. It can be observed that the band notched designs exhibit ringing

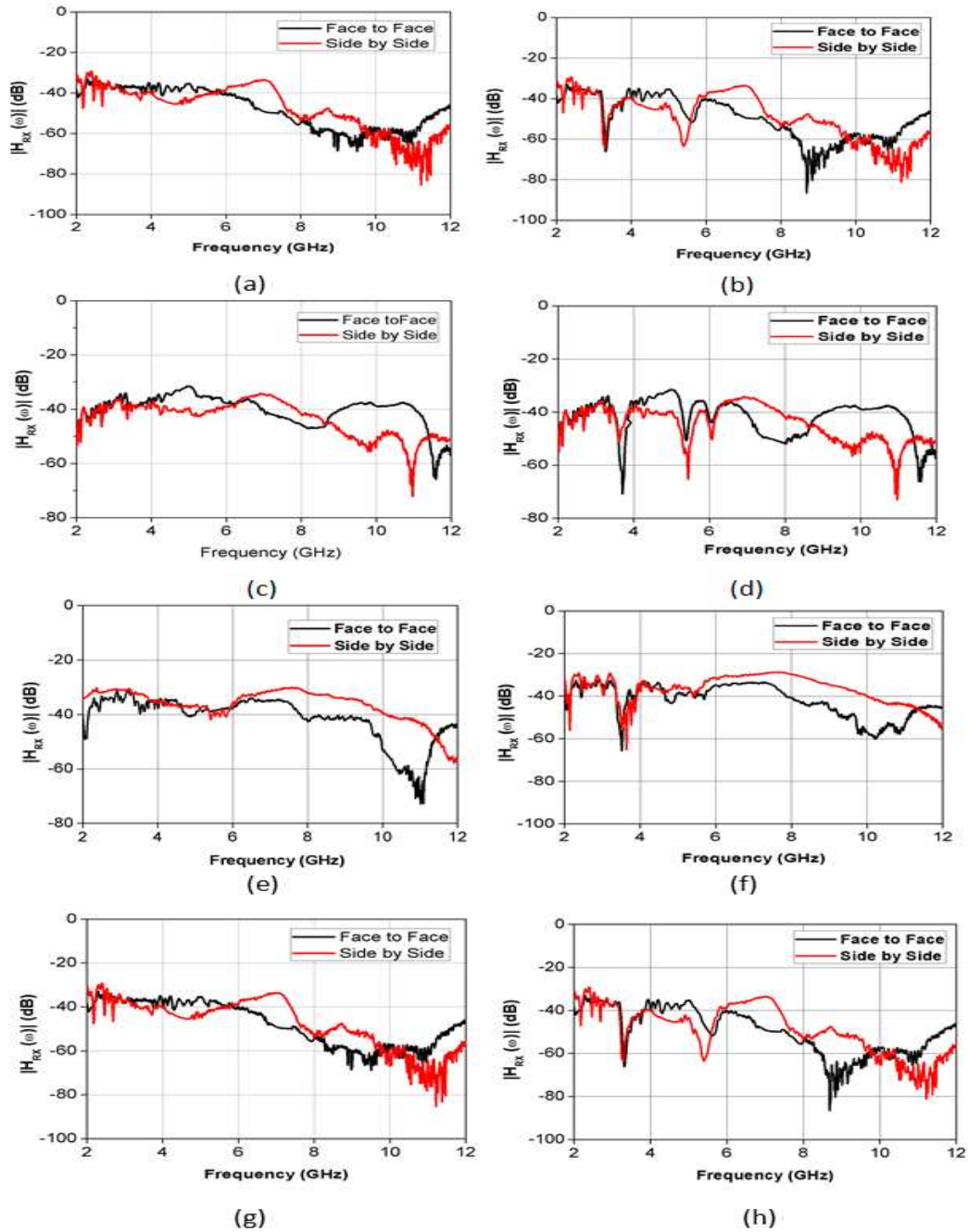


Figure 5.4: The measured transfer function in the face to face and side by side planes of the (a) octagon shaped monopole antenna (b) band notched octagon shaped monopole antenna (c) semi circular disk monopole antenna (d) band notched semi circular disk monopole antenna (e) semi octagon shaped diversity antenna (f) band notched semi octagon shaped diversity antenna (g) semi circular diversity antenna (h) band notched semi circular diversity antenna

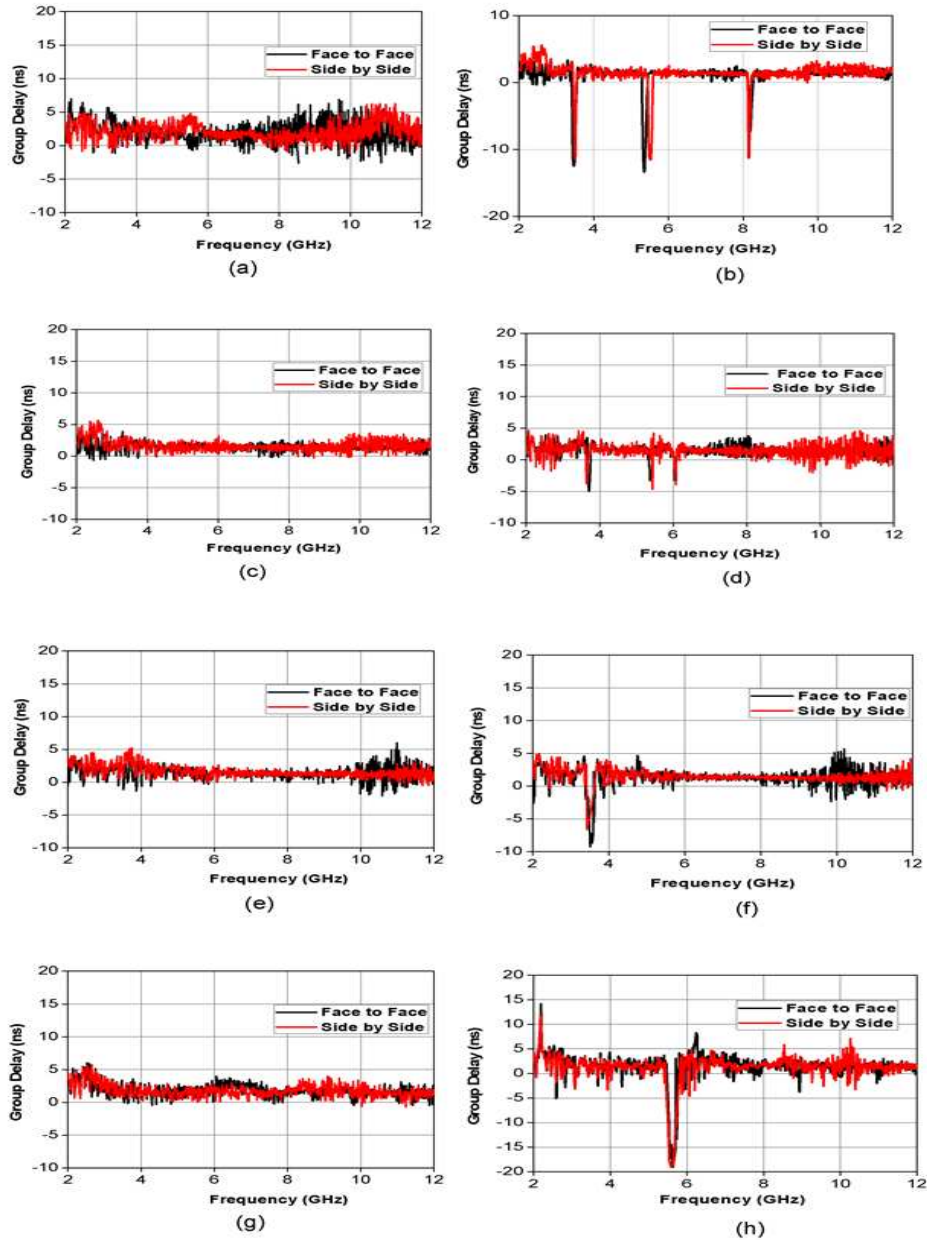


Figure 5.5: The measured group delays in the face to face and side by side planes of the (a) octagon shaped monopole antenna (b) band notched octagon shaped monopole antenna (c) semi circular disk monopole antenna (d) band notched semi circular disk monopole antenna (e) semi octagon shaped diversity antenna (f) band notched semi octagon shaped diversity antenna (g) semi circular diversity antenna (h) band notched semi circular diversity antenna

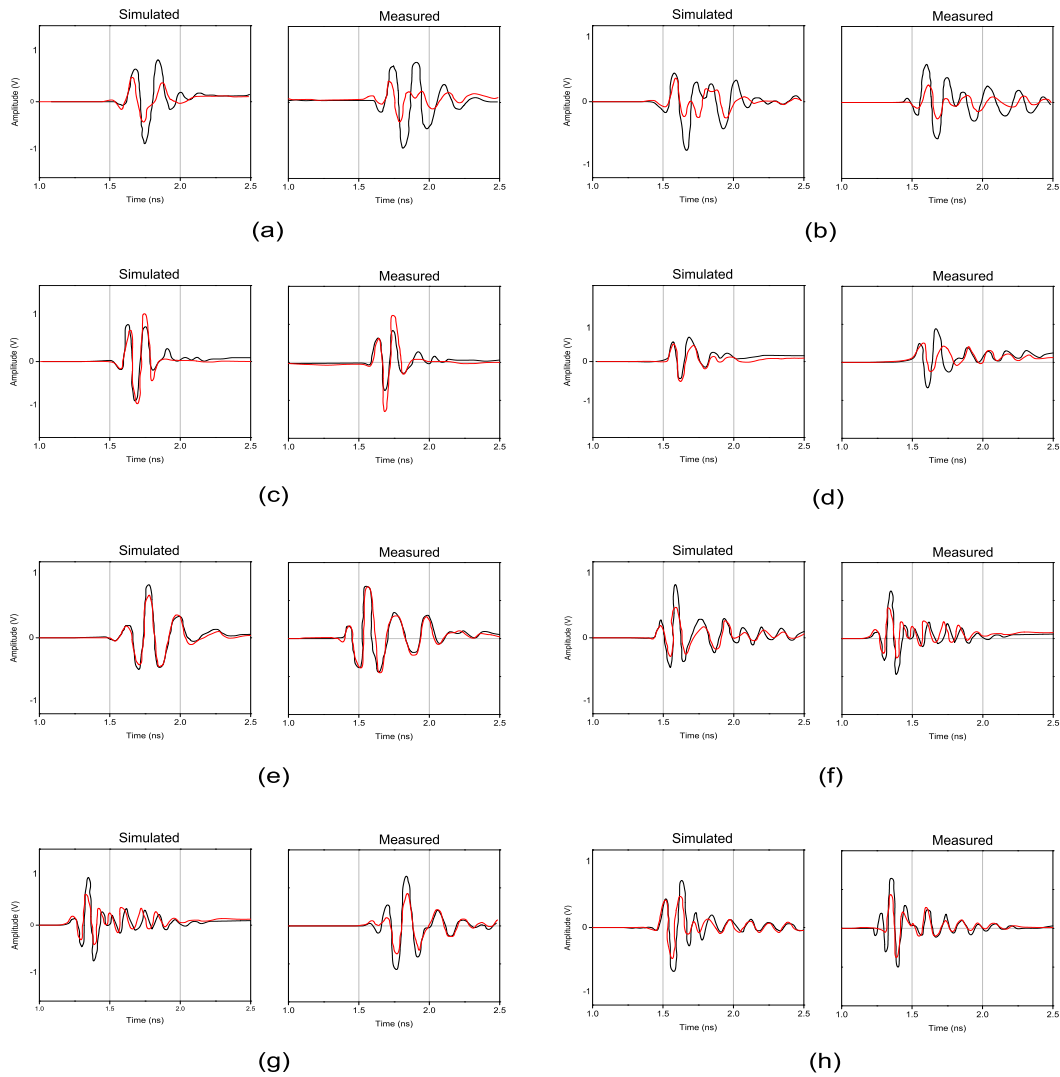


Figure 5.6: Simulated and measured transmitted pulses by two identical antennas in their face to face and side by side orientations (a) octagon shaped monopole antenna (b) band notched octagon shaped monopole antenna (c) semi circular disk monopole antenna (d) band notched semi circular disk monopole antenna (e) semi octagon shaped diversity antenna (f) band notched semi octagon shaped diversity antenna (g) semi circular diversity antenna (h) band notched semi circular diversity antenna.

effects. In case of the octagon shaped monopole antennas (Figure 5.6 (a) and (b) even though the output pulses are slightly distorted, they remain in acceptable range. But the maximum amplitude of the received waveform for the side by side case is about 20% lower than that of the face to face case.

The semi circular disk and circular diversity antennas show very little difference in

Table 5.1: Measured fidelity of the transmitted pulses

Antennas	Face to Face		Side by Side	
	Simulated	Measured	Simulated	Measured
Octagon shape monopole	95	88	83	80
Band notched octagon shape monopole	88	82	77	72
Semi circular disk monopole	95	91	94	92
Band notched semi circular disk monopole	91	87	91	86
Semi octagon shaped diversity	93	92	89	88
Band notched semi octagon shaped diversity	90	86	85	83
Semi circular diversity	89	88	86	84
Band notched semicircular diversity	85	83	82	81

the face to face and side by side cases. The fidelity factor for the measured pulses are tabulated in Table 5.1 for the antennas with face to face and side by side orientations.

5.3.2 Time domain parameters

The antenna effects on the signal transmission can be analyzed by considering the envelope of the transient response as shown in Figure 5.7, which localizes the distribution of energy versus time and is a direct measure for the dispersion of the antenna. The Fourier transform of the transfer function gives a complex response, so a real valued antenna impulse response, $h_r(t, \theta, \varphi)$ is as in equation 5.15

$$h_r(t, \theta, \varphi) = h_{RX}(t, \theta, \varphi) \quad (5.15)$$

The peak output voltage from an incident waveform depends on the peak value $p(\theta, \varphi)$ of the antenna's transient response and shown in Equation (5.16)

$$p(\theta, \varphi) = \max h_r(t, \theta, \phi) \quad (5.16)$$

The duration of the antenna transient response, which can be evaluated through its Full Width at Half Maximum (*FWHM*), defined as, Equation (5.17)

$$FWHM_{0.5}(\theta, \phi) = t_2 |p/2 - t_1|_{p/2} \quad t_1 < t_2 \quad (5.17)$$

The duration in ringing is defined as the time until the envelope has fallen from the peak value to below a fraction α of the main peak, Equation (5.18)

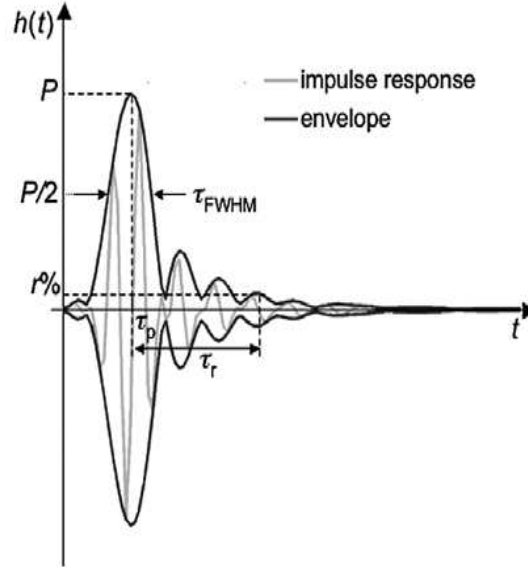


Figure 5.7: Impulse response, its envelope and time domain related parameters

$$Ringing_{\alpha} = t_2 |\alpha p - t_1|_p \quad t_1 < t_2 \quad (5.18)$$

The lower bound for α is chosen according to the noise floor of the measurement. In order to compare the ringing of antennas with different gains under the constraint of constant noise floor, the fraction α is chosen to be $\alpha = 0.22$. The UWB antenna quality measures, namely the *FWHM* and ringing are directly deduced from the magnitude of the impulse response envelop as in Equations (5.16),(5.17) and (5.18). An ideal antenna for UWB portable applications should show a uniform impulse response performance for different antenna orientations with minimum *FWHM* and ringing.

The impulse response deduced from the measured transfer functions are plotted in face to face and side by side orientation planes in Figure5.6. Most of the responses resemble the delta function. The increase in ringing is clearly observed in case of the band notched antenna designs in Figure5.6.(b), (d) and (f). To compare the antenna performance qualitatively, the measured *FWHM* and ringing, derived using Equations

5.17 and 5.18 and are tabulated in Table 5.2. Those appear to be well matched and a narrow *FWHM* ($<200\text{pS}$) is seen in face to face case, within ± 600 of side by side in most of the cases. The band-notched antenna designs record a clear increase in ringing ($> 400\text{pS}$). The planar octagon and the semi circular disk monopole show superior transient response with in the band which is having a uniform response and minimum spatial variations in the face to face. In the case of the diversity antenna, even though it shows a reasonably good performance in the face to face, it has a slightly narrower performance in the side by side plane. This matches well with the magnitude distortion noted in their transfer function plots in the face to face plane, shown in Figure 5.4

Table 5.2: *FWHM* and ringing in face to face and side by side planes

Antenna	Face to Face		Side by Side	
	FWHM		Ringing	
	Simulated	Measured	Simulated	Measured
Octagon shape monopole	104	117	316	327
Band notched octagon shape monopole	109	125	344	408
Semi circular disk monopole	183	160	413	440
Band notched semi circular disk monopole	189	152	426	442
Semi octagon shaped diversity	154	112	327	336
Band notched semi octagon shaped diversity	120	155	432	472
Semi circular diversity	180	152	410	430
Band notched semi circular diversity	189	160	420	438

5.4 Summary

In this chapter, the transfer characteristics of the antennas are presented for UWB applications and are studied. This would confirm their suitability for pulsed UWB applications and is quantified further by their pulse distortion analysis. Any distortion in the frequency domain and abrupt discontinuity in the antenna geometry are reflected in the time domain as dispersion, the *FWHM* and ringing measurement. Fidelity, which is the cross correlation of the transmitted and received pulses, measures the effects of the antenna on the transmitted pulse. The study reveals a close correspondence between the geometry of the antenna with its performance in the time domain. The surface current distribution analysis has revealed a relative shift in the

phase center for the different frequencies of operation in case of the planar octagon monopole shaped antenna which is relatively large in size compared to the rest (width $\approx 30mm$). So, for certain frequencies, the surface currents from different parts of the antenna combine out of phase while receiving a signal depending on the antenna orientations. By reciprocity, the antenna exhibits this feature in transmitting mode as well. This results in distorted radiation patterns which occur at the upper end of the UWB spectrum. Thus we can conclude here, that wider bandwidth is ensured by a smooth impedance transformation in the antenna geometry at the cost of its increased size. It is basically the antenna phase center location over the operating frequency which determines its suitability for the pulsed UWB operation. As studies reveal in case of the semi circular disk and the diversity antenna, a compact size with good impedance matching within the UWB 3.1 to 10.6GHz band and a uniform response in terms of the space coordinates would be better option for portable UWB applications than antennas with a large bandwidth and that consume PCB space. The retardation caused by any displacement in the antenna phase center location by such compact antennas (width $\approx 20mm$) is negligible for nano-sec pulses.

CHAPTER 6

Conclusion and Future Work

This chapter summarizes and highlights the conclusions drawn from the present study. This is followed by few suggestions for future work.

6.1 Summary

In this thesis, a comprehensive study on the design, simulation, testing and characterization of UWB antennas is presented, taking the extra constraints placed on the antenna designs to account for pulse based operations. Frequency and time domains analysis have been used for analyzing strengths and weaknesses of the antenna designs.

Four compact antennas have been designed and analyzed. These include octagon shaped monopole antenna, semi circular disk monopole antenna, semi octagon shaped diversity antenna and semi circular diversity antenna. The evolutions of the designed antennas are investigated in detail to have an insight into their wideband behavior. The design aspects based on the geometrical parameters of the antenna are firstly investigated. The simulation studies in terms of their return loss and current/field distribution on the antenna at different resonances, reveal their dependence on the antenna dimensions.

The design incorporate thin slot resonators inscribed within the radiator and /or ground patch to reject narrow frequency bands. Such embedded filters avoid the use of additional filter in the circuits which may not be desired for portable wireless systems with space constraints

A brief summary of the different antennas designed are;

(i) *Octagon shaped monopole antenna:*

This antenna has a simple structure providing wide band operation (3GHz to >11GHz), and omnidirectional radiation pattern especially at the lower end of the spectrum. The octagon shaped monopole as well as the ground plane forms a quasi-dipole antenna at its lowest resonance and the extremely wide impedance band is ensured by the gradual impedance transformation arrangement between the ground and the patch. The antenna uses microstrip line fed with a size of $36 \times 32 \text{mm}^2$ and gain ranging from 1 to 6dBi. The narrow slot resonators are incorporated in this design to reject single and multiple frequencies. A thin half wavelength long slot resonator is inscribed on the radiator patch to filter out bandnotched frequencies. A combination of such multiple slots are implemented (radiating patch as well as the ground) to adapt the antenna for triple band operation particularly suited for the 3.5GHz/ 5.5GHz/ 8GHz WiMAX standards.

(ii) *Semi circular disk monopole antenna:*

This antenna has a wide band of operation (3.05GHz to 11.2GHz). The radiating patch is printed in the shape of semi circular disk and ground plane is square shaped with radiator feed. The slot appears to have a significant influence on the antenna behavior by maintaining its region of radiation almost constant. It is also observed that the antenna performs well throughout the UWB band. Hence, it appears to be perfectly ideal for UWB band held applications with a compact size, stable and omnidirectional antenna pattern. The antenna gain averages around 2.5dBi. This design also incorporates triple quarter wavelength slot resonators placed near radiating element and ground to notch out the 3.5GHz/ 5.2GHz/ 5.8GHz WLAN frequencies.

(iii) *Semi octagon shaped diversity antenna:*

This is a compact two element UWB diversity antenna for diversity applications. The proposed antenna provides wideband response (3GHz to 12GHz) with low isolation. The simulation results produce the reflection coefficient, peak realized gain, envelope correlation coefficients, 3D radiation patterns and current distributions. The measured results are well matched with simulated ones. These designs also include a

quarterwave length slot inscribed on the tuning stub to notch out the 3.5GHz WiMAX band.

iv) *Semicircular diversity antenna:*

This is a compact 2 element UWB diversity antenna for diversity applications. The proposed antenna provides wideband response with low isolation. The goal of the design is to achieve low correlation values, low capacity loss, and high gain. The measured results match with the simulated ones. These designs also include a half wave length slot inscribed on the tuning slot to notch out the 5.5GHz WiMAX band.

The antennas designed for UWB operation from 3.1GHz to 10.6GHz have been further analyzed for their time domain response in the final section of the thesis to confirm their suitability for pulsed UWB applications. The transfer function measurements are performed for both in face to face and side by side planes and their impulse responses are deduced. The impulse response of the antennas is then characterized in terms of FWHM and ringing. A narrow FWHM ($<200\text{pS}$) is seen in face to face plane and within ± 600 of side by side plane. The band-notched antenna designs record a clear increase in ringing ($> 400\text{pS}$). The semi octagon shaped diversity antenna exhibits the minimum variation in FWHM and ringing values for face to face and side by side positions. The antenna's effects on nano-second pulses are measured in terms of the fidelity factor and values $> 90\%$ in the face to face plane are recorded for all antennas except in case of band-notched where it is more than 80%. The semi octagon shaped diversity antenna gives a superior performance with fidelity more than 92% reported uniformly in the face to face plane.

Lastly, all of the designs proposed in this thesis can be conveniently used for ultra-wideband systems. However, in the case of ground modified monopole and serrated monopoles, a distortion in the pattern is observed at higher frequencies since the region of radiation does not remain constant. This distortion in the frequency domain gets reflected in the transient response of the antenna. The performance of all the designed UWB antennas are within tolerable limits which makes them all suitable for pulsed UWB applications.

6.2 Limitations of the work

Some limitations of this research work are noted below,

- The transfer function measurement performed in this thesis have been restricted to two orthogonal planes.
- The time domain measurement is limited to direct measurement. .

6.3 Future Work

Antenna design is under rapid progress with the fast development in technology in this area. With the growing requirements of wireless communication, there are plenty of room for improvement of antenna design. The following points discuss some possible future research directions for the work reported in this thesis.

- 1) New techniques should be explored to further reduce the size of the UWB antennas to suit practical applications. Metamaterial is a promising entrant, since it can reduce the antenna size greatly in theory. Although most of current metamaterial antennas are used in narrow bandwidth application, this technique will be available for wideband operation in the near future.
- 2) Due to the low power level operation of UWB systems, a typical UWB receiver requires a low-noise amplifier. Antenna integration with low-noise amplifier may be investigated in future.
- 3) Future radio systems, such as software defined radio and cognitive radio concepts give rise to significant challenges for antenna design and in particular for reconfigurable antenna designs.

APPENDIX A

Design Methodology

A.1 Introduction

This Section deals with the techniques used for the design, fabrication and measurement of antennas. The design and simulations are performed using the CST MW Studio suite v12 and HFSS v14 packages. The antennas are fabricated using photolithographic method and milling machine techniques. Vector Network Analyzer (VNA) is used to measure antenna characteristics such as S-parameters, gain, radiation patterns etc.

A.1.1 Numerical and Analytical Approaches

Scientists and engineers use several techniques in solving continuum of electromagnetic field problems. The following methods are commonly used in electromagnetic (EM) theory.

Analytical method (exact solution)

1. Separation of variables
2. Series expansion
3. Conformal mapping
4. Integral solution, e.g. Laplace and Fourier transformation
5. Perturbation methods

Numerical methods (approximate solutions)

1. Finite difference method
2. Moment method
3. Finite element method
4. Transmission-line modeling

The principles of EM fields and waves are very important for the design and development of antennas as key elements of any wireless communication system. The need for numerical solutions of electromagnetic problems is the best expressed by Paris and Hurd [105]; “***Most problems that can be solved formally (analytically) have been solved.***” Until 1940s, the most EM problems were solved using well known Maxwell’s equations. These equations describe all electromagnetic phenomena of different structures and configurations. They can be expressed in their either differential or integral forms as given in equations (A.1 to A.8) [106].

Differential form

$$\nabla \cdot \vec{D} = \rho_v \quad (\text{A.1})$$

$$\nabla \cdot \vec{B} = 0 \quad (\text{A.2})$$

$$\nabla \times \vec{E} = -\frac{\partial \vec{B}}{\partial t} - \vec{M} \quad (\text{A.3})$$

$$\nabla \times \vec{H} = \vec{J} + \frac{\partial \vec{D}}{\partial t} \quad (\text{A.4})$$

Integral form

$$\oiint \vec{D} \cdot d\vec{s} = Q_{enc} \quad (\text{A.5})$$

$$\oiint \vec{B} \cdot d\vec{s} = 0 \quad (\text{A.6})$$

$$\oint \vec{E} \cdot d\vec{l} = -\frac{\partial \phi_B}{\partial t} \quad (\text{A.7})$$

$$\oint \vec{H} \cdot d\vec{l} = i_{enc} + \epsilon \frac{\partial \phi_E}{\partial t} \quad (\text{A.8})$$

where the vectors \vec{E} and \vec{H} are the electric and magnetic field intensities and are measured in units of [V/m] and [A/m], respectively. The vectors quantities \vec{D} and \vec{B} are the electric and magnetic flux densities and are in units of [C/m²] and [Wb/m²]. The scalar quantities $\phi_E = \iint \vec{D} \cdot d\vec{S}$ and $\phi_B = \iint \vec{B} \cdot d\vec{S}$ are the electric and magnetic fluxes and are in units of [C] and [Wb], respectively.

When the EM field problem is complex, an exact solution in a closed form may be difficult to obtain and hence we should solve them by applying numerical techniques. In this thesis, all proposed antenna structures are complex. Hence they can be modeled using commercial simulation software programs which enable us to design, simulate, tune and optimize structure's physical parameters to reach the best design before fabricating prototypes. Currently, there are several numerical techniques those can be used to solve the EM problems, such as the Finite Element (FE) method [107], the Method of Moments (MoM) [108], the Finite Difference Time Domain (FDTD) [109] and the Finite Integration Technique (FIT) [110] etc. The first two methods solve the EM problems in the frequency domain while the other two methods use the time domain.

A.1.2 Finite Element Method using Ansoft HFSS

The first simulation software program is Ansoft High Frequency Structure Simulator (HFSS) [111]. Ansoft HFSS is currently considered to be one of the top industry-standard software programs and a powerful EM field simulation tool for many years. It is based on a three-dimensional (3D) full-wave finite element (FE) method which is a frequency-domain numerical technique for solving Maxwell's equations. Because of its high accuracy and performance, Ansoft HFSS can be used by engineers in industry or researchers and scientists in academia to analyze and design different

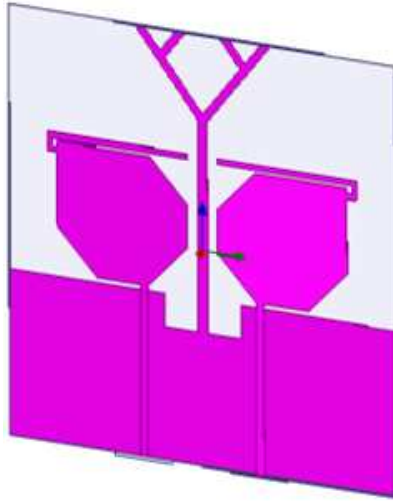


Figure A.1: Antenna structure in Ansoft HFSS.

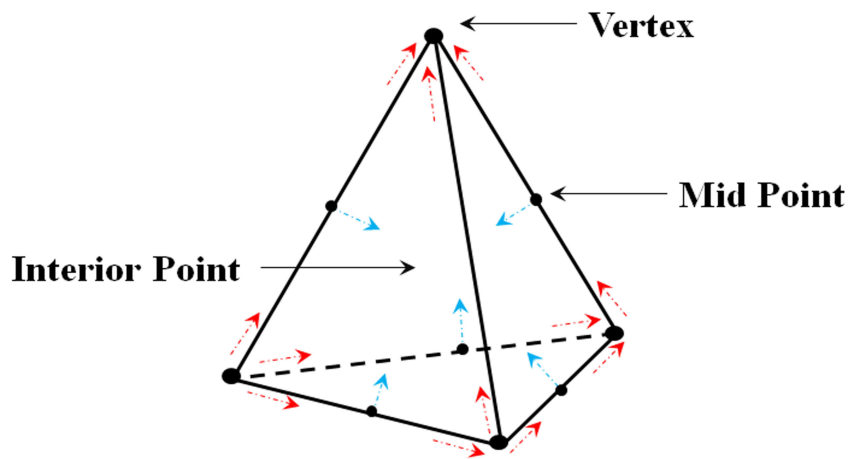


Figure A.2: A single mesh shape used in Ansoft HFSS

complex structures for high-frequency applications.

Ansoft HFSS uses the FE numerical technique in order to generate an EM field solution for different 3D problems. At first, the finite element technique is based on dividing the whole big problem space into small regions or sub-regions called elements. Then the fields in each finite element are formulated by local functions. Ansoft HFSS automatically converts the whole problem structure into a finite element mesh which

consists of a large number of very small 3D tetrahedral shapes as shown in Figure A.1. Each single tetrahedron is a four-sided pyramid as presented in Figure A.2. It can be noticed that the meshing or discretization operation done by Ansoft HFSS is very coarse in almost the whole structure while it is very fine at some regions which need more accuracy such as near wave port, metallic edges or discontinuities. After finalizing the mesh operation of the whole structure, the solution process starts with two-dimensional (2D) port solutions as the structure excitation then followed by the field solution of the full 3D problem including fields at all verticals, midpoints and interior points as in Figure A.2. The program exploits the computed 2D fields on ports to be used as boundary conditions to solve the 3D fields of the whole structure.

During the numerical iterative solution, Ansoft HFSS solves the electric field for a given problem based on the following matrix equation (for a lossless case) [111]:

$$[A]\bar{x} + [B]K_0^2 = c \quad (\text{A.9})$$

where $[A]$ and $[B]$ are square matrices and their sizes depend on the geometry of the problem and the size of the mesh, \bar{x} is the electric field vector, K_0 is wave number in free space and c is the value of the source or excitation defined for the given problem. Then the magnetic field solution is calculated from the following relationship with the electric field:

$$\vec{H} = -\frac{1}{j\omega\mu}(\nabla \times \vec{E}) \quad (\text{A.10})$$

A.1.3 Finite Integration Technique using CST

The other simulation software program is called Computer Simulation Technologies Microwave Studio (CST MWS) [112]. CST MWS is a tool for fast and accurate 3D EM simulation of high frequency problems. Currently, it is considered to be industry-standard software programs and a powerful 3D EM field simulation tool. CST MWS is based on the Finite Integration Technique (FIT) [113] which is equivalent to FDTD. Unlike the FE method, FIT is a time-domain numerical technique for

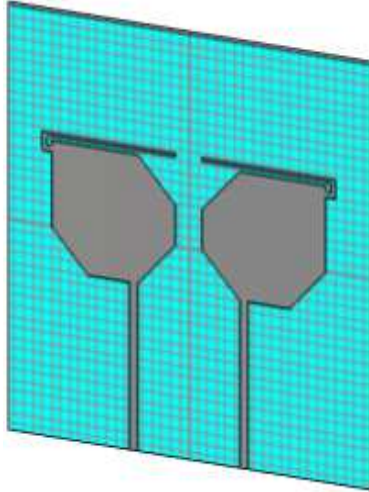


Figure A.3: Antenna structure in CST MW studio

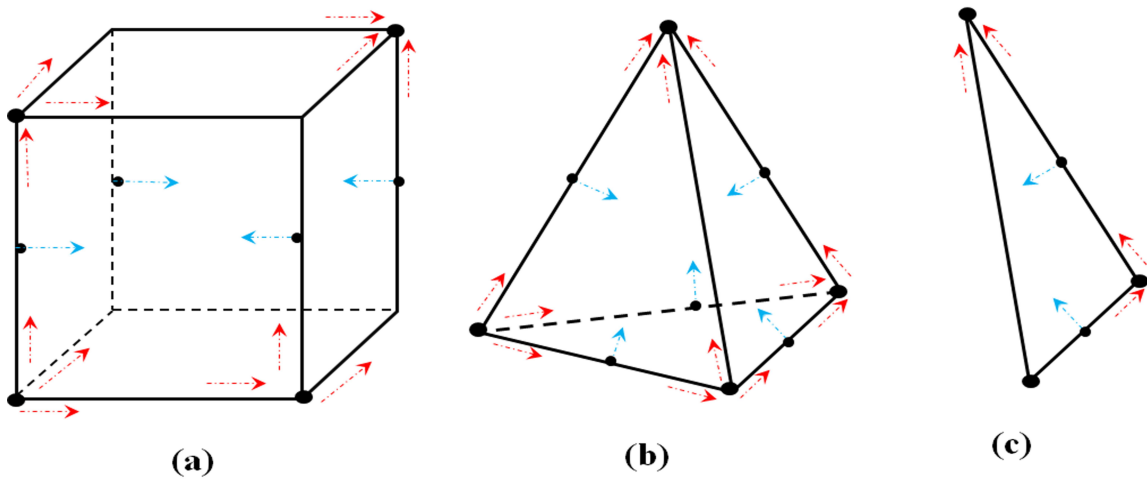


Figure A.4: A single (a) hexahedral, (b) tetrahedral and (c) surface mesh element used in CST MW Studio.

solving Maxwell's equations. Using the function of parametric study in both Ansoft HFSS and CST MWS simulation programs, we can tune and optimize the structure physical parameters to obtain the best design before going to the fabrication process. CST MWS has different kind of solvers not only a transient solver but also a frequency domain solver, an Eigen mode solver and an integral equation solver.

In a transient or time-domain solver, the value of the vector electric \vec{E} or magnetic \vec{H} field quantities are computed through time at discrete spatial locations and at discrete time samples. The maximum time step Δt used in the simulation program depends on the minimum mesh step size which can be determined by the density of the mesh used in the meshing process of the whole structure. Therefore the program takes more time to run simulation if the mesh is dense. Once the spatial mesh or discretization is performed by the CST program, the finite integration method is employed. CST has two different mesh types available, i.e. hexahedral and tetrahedral meshes. Another type of mesh used by the Integral Equation (IE) solver is called surface mesh. Figure A.3 shows an antenna structure in CST Figure A.4 shows a single hexahedral, tetrahedral and surface mesh element used in CST program. For complex structures, CST uses a hexahedral mesh in meshing or discretization because it is considered to be very robust. Other solvers use a tetrahedral or surface mesh method. .

The finite integration technique converts the well-known Maxwell equations in their integral form into set of discrete matrix equations called Maxwell grid equations (MGE) as follows [113]:

Integral form \Rightarrow Matrix form

$$\oiint \vec{D} \cdot d\vec{A} = \iiint_v \rho_v dV \Rightarrow [\tilde{S}] = q \quad (\text{A.11})$$

$$\oiint \vec{B} \cdot d\vec{A} = 0 \Rightarrow [S]b = 0 \quad (\text{A.12})$$

$$\oint \vec{E} \cdot d\vec{l} = - \iiint_A \frac{\partial \vec{B}}{\partial t} d\vec{A} \Rightarrow [C]e = -\frac{d}{dt}b \quad (\text{A.13})$$

$$\oint \vec{H} \cdot d\vec{l} = - \iint_A \left[\frac{\partial \vec{A}}{\partial t} + J \right] d\vec{A} \Rightarrow [\tilde{C}]h = -\frac{d}{dt}d + j \quad (\text{A.14})$$

where $[\tilde{C}]$, $[C]$, $[S]$ and $[\tilde{S}]$ are square matrices represent the discrete curl and divergence operators, respectively and their sizes depend on the problem geometry. ‘e’ and ‘h’

represent the electric and magnetic grid voltages and they are related to the electric and magnetic fields according to $e = \int_{\partial A} \vec{E} \cdot d\vec{l}$ and $h = \int_{\partial \tilde{C}} \vec{H} \cdot d\vec{l}$, d and b are the electric and magnetic facet flux vectors over the mesh cell.

A.1.4 Antenna Fabrication

The accuracy of the antenna dimension is very critical in microwave frequencies. Therefore photolithographic technique is used to fabricate the antenna geometry. Photo-lithography is the process of transferring geometrical shapes from a photo-mask to as surface. The various steps involved in the photolithographic technique are illustrated in Figure A.5

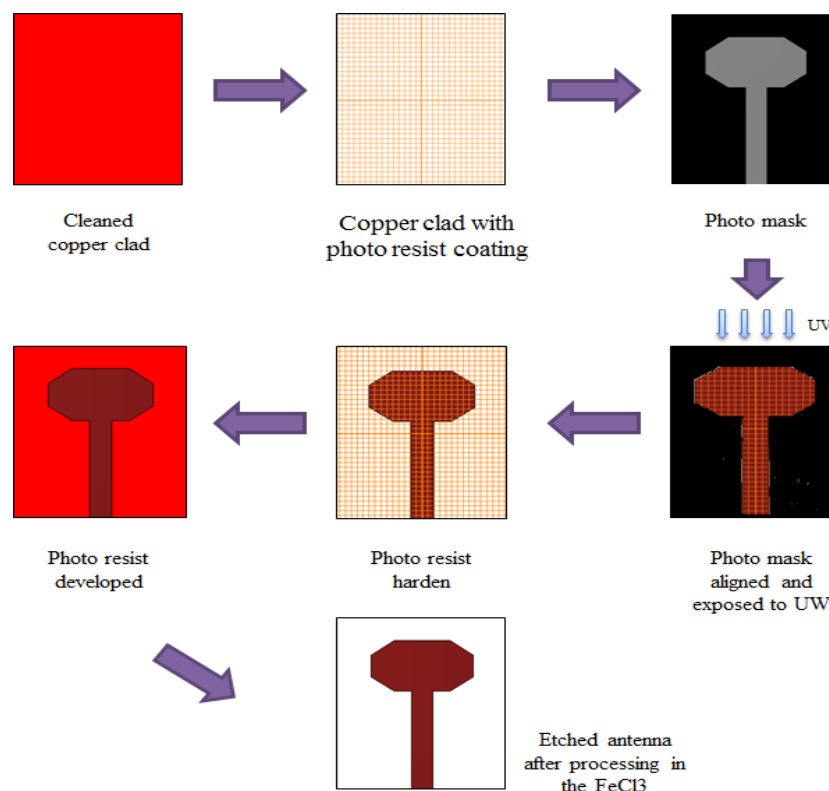


Figure A.5: Various steps involved in the fabrication process

The CAD drawing of the antenna is printed on a high quality butter paper with a high resolution laser printer. The copper clad of suitable dimension is cleaned with a suitable chemical like acetone to remove any chemical impurities. A thin layer of photo resist material is the applied over the copper clad using a high speed spinner. The antenna mask is carefully aligned over the photo resist coated clad and exposed to Ultraviolet (UV). An extreme care must be taken to ensure that no dust or impurities are present in between the mask and copper clad. The layer of photo resist material in the exposed portions hardens, while the unexposed region remains the same and it can be removed by carefully rinsing with a suitable developer solution. The unwanted copper over the copper clad can be removed by processing the copper clad in a ferric chloride ($FeCl_3$) solution. The laminate is the cleaned to remove the hardened photo resist using acetone solution.

A.1.5 Input Reflection Coefficient and VSWR

The reflection coefficient (Γ) at the antenna input is the ratio of the reflected voltage (current) to the incident voltage (current) and is same as the S_{11} , when the antenna is connected at the port 1 of the network analyzer. It is a measure of the impedance mismatch between the antenna and the source line. The degree of mismatch is usually described in terms of input VSWR or the reflection coefficient. The Reflection coefficient (RC) is the ratio of the reflected power to the incident power, expressed in dB as

$$RC = -20\log(\Gamma) = -20\log(|S_{11}|) \quad (\text{A.15})$$

The voltage standing wave ratio (VSWR) is the ratio of the voltage maximum to minimum of the standing wave existing on the antenna input terminals. A well-matched condition will have return loss of 15dB or more. A VSWR equal to 2 gives a return loss of $\approx 10dB$ and it is set as the reasonable limits for a matched antenna.

The antenna input impedance is a complex quantity with a real and imaginary part, namely the antenna resistance and antenna reactance respectively. It is again a measure of the efficiency with which the antennas act as a transducer between the

source and the propagating medium. The AUT is connected at the calibrated ports of the analyzer and reflection mode is selected from the parameter menu. The input reflection coefficient, VSWR and input impedance are characterized using a single port calibration. The display is then set to give the $|S_{11}|_{dB}$ as a function of frequency. The return loss curve indicates good impedance matching at some frequencies (dips on the reflection coefficient curve) and they are regarded as the resonances of the antenna. The bandwidths are measured between the 2:1 VSWR or $|S_{11}|_{dB} \leq -10dB$ points of the plot. Similarly, VSWR, antenna impedance can as well be plotted against frequency by changing the output format.

A.1.6 Anechoic Chamber

The measurement setup in an anechoic chamber is shown in Figure A.6. The anechoic chamber provides a quiet zone and used to measure the antenna characteristics accurately. All the antenna characterizations are done in an anechoic chamber to avoid reflections from nearby objects. The absorbers fixed on the walls are highly loss at microwave frequencies. They have tapered shapes to achieve good impedance matching for the microwave power impinges upon it. The chamber is made free from the surrounding EM interferences by covering all the walls and the roof with aluminum sheet.

A.1.7 Radiation Pattern Measurement

The radiation pattern of an antenna is graphical representation of its radiation properties as a function of the space coordinates. This assumes a three dimensional (3-D) pattern. Because of the limits set by the practical measurement setup for measuring the 3-D pattern, usually patterns are measured in the three principal coordinate planes (XY, YZ, and XZ) for antennas with omni-directional patterns. The far field patterns are measured at a distance $d > 2D^2/\lambda$, where 'D' is the largest dimension of the antenna and the smallest operating wavelength. As shown in Figure A.6, the AUT is connected to Port 1 and the standard ridged horn is connected to Port 2. The height and polarization of both antennas are aligned for maximum transmission

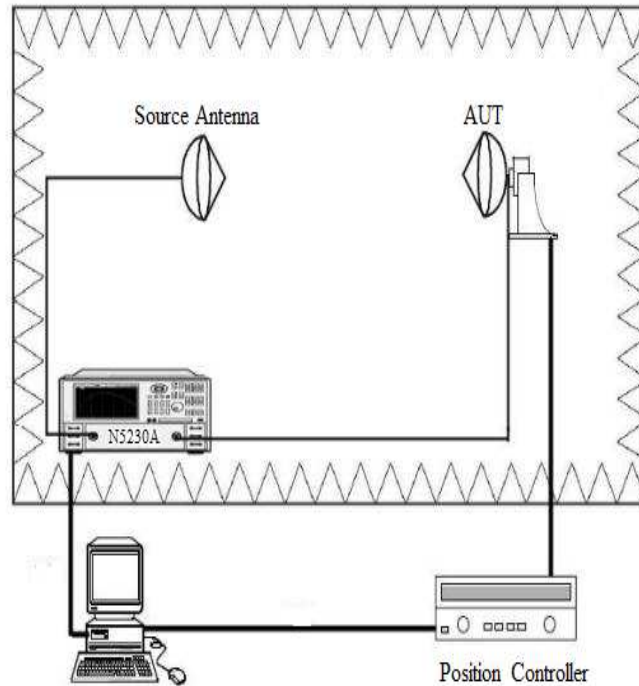


Figure A.6: Antenna measurement setup

($|S_{21}|$) between them. The desired frequency points are selected for measurements. A through calibration is performed in this position which calibrates the ($|S_{21}|$) data to 0dB for every frequency point selected. In order to avoid any spurious reflections from the nearby objects, the time domain gating facility of the analyzer is implemented. The gate span is selected according to the largest dimension of the radiator. The antenna positioned is now set to home which sets the current position as 00. The radiation pattern measurement software, 'cremasoft' developed in-house, controls the automated radiation pattern measurement process. The software is next evoked and the normalized $|S_{21}|$ is measured. The number of frequency points is set according to convenience. The start angle, stop angle and step angle of the motor is also configured in 'cremasoft' which then stores the measurements as a text file.

A.1.8 Antenna Gain Measurement

Gain transfer method is employed to measure the gain of the antenna. The experimental setup for determining the gain is similar to the radiation pattern measurement setup. The gain of the AUT is measured relative to the power levels detected by a standard gain antenna. In order to measure the gain of AUT, the standard gain antenna is mounted on the turntable and a thorough calibration is performed at bore-sight direction. The AUT is carefully mounted over the turntable and extreme care is taken for the exact alignment. The relative power level is obtained from the analyzer and this provides the gain with respect to the standard antenna. The gain of the standard antenna is added to the relative gain to obtain the gain of the AUT. The gain measurement method basically based on Friis transmission formula as given by equation A.16 [5]

$$(G_t + G_r)_{dB} = 20 \log_{10} \left(\frac{4\pi R}{\lambda} \right) + 10 \log_{10} \left(\frac{P_r}{P_t} \right) \quad (\text{A.16})$$

where,

$(G_t)_{dB}$ = gain of the transmitting antenna (dB)

$(G_r)_{dB}$ = gain of the receiving antenna (dB)

P_r = received power (W)

P_t = transmitted power (W)

R = antenna separation (m)

λ = operating wavelength (m)

If transmitting and receiving antennas are identical ($(G_t)_{dB} = (G_r)_{dB}$). So, the equation can be written as

$$(G_t + G_r)_{dB} = (G_r)_{dB} = 20 \log_{10} \left(\frac{4\pi R}{\lambda} \right) + 10 \log_{10} \left(\frac{P_r}{P_t} \right) \quad (\text{A.17})$$

By measuring R , λ and P_r/P_t , the gain of the antenna can be calculated using the equation A.17.

Bibliography

- [1] Federal Communication Commission, *First report and order, revision of part 15 of commission's rule regarding UWB transmission systems*. FCC 02-48, 2002.
- [2] Zhi Ning Chen, *Antennas for portable devices*. Wiley Publisher, 2007.
- [3] Chia-Chin Chong, Fujio Watanabe, and Hiroshi Inamura, "Potential of UWB Technology for the Next Generation Wireless Communications," in *IEEE Ninth International Symposium on Spread Spectrum Techniques and Applications*, USA, 2006.
- [4] N.E.Lindenblad, "Wide band antenna." U.S. Patent 2284434 A, 1941.
- [5] C. A. Balanis, *Antenna theory analysis and design*. John Wiley & Sons, Inc, 1982.
- [6] Victor H. Rumsey, "Frequency-independent antennas," *IRE National Convention Record*, vol. 5, pp. 114–118, 1957.
- [7] Lodge, O.J., "Electric telegraphy." U.S. Patent 609154 A, 1898.
- [8] R.W.Masters, "Multichannel antenna system." U.S. Patent 2634371 A, 1953.
- [9] H.G.Schantz, "A brief history of UWB antennas," *IEEE Aerospace and Electronic System Magazine*, vol. 2, pp. 22–26, 2004.
- [10] O. E. Allen, D. A. Hill, and A. R. Ondrejka, "Time-domain antenna characterizations," *IEEE Trans Electromagnetic Compatibility*, vol. 35, pp. 339–346, August, 1993.
- [11] Kuo, J-S; Huang, C-Y, "Triple-frequency planar monopole antenna for side feed communication device on GSM/DCS/PCS operation," *Electronics Letters*, vol. 42, pp. 268–270, 2006.
- [12] Liang,X-L; Zhong,S-S; Wang, W, "Elliptical planar monopole antenna with extremely wide bandwidth," *Electronics Letters*, vol. 42, pp. 441–442, 2006.
- [13] J. Winters, "On the capacity of radio communication systems with diversity in a Rayleigh fading environment," *IEEE Journal Selected Areas in Communications*, vol. 5, p. 871878, 1987.
- [14] G. Foschini, "Layered space-time architecture for wireless communication in a fading environment when using multiple antennas," *Journal of Bell Labs Technical*, vol. 01, pp. 41–59, 1996.

- [15] E. Telatar, N. Seshadri, and A. Calderbank, "Space-time codes for high data rate wireless communication: performance criterion and code construction," *IEEE Transactions on Information Theory*, vol. 44, pp. 744–765, 1998.
- [16] S. Alamouti, "A simple transmit diversity technique for wireless communications," *IEEE Journal on Selected Areas in Communications*, vol. 16, pp. 1451–1458, 1998.
- [17] J. R. James and P. S. Hall, *Handbook of microstrip antennas*. London: Peter Peregrinus (IEE), 1988.
- [18] Z. N. Chen and M. Y.W. Chia, *Broadband planar antennas: design and applications*. John Wiley & Sons Ltd, 2006.
- [19] CARTER, P. S, "Wideband shortwave antenna and transmission." U.S. Patent 2181870 A, 1939.
- [20] Stutzman, *Antenna theory and design*. John Wiley & Sons, Inc, 2012.
- [21] L. Paulsen, J. West, W. Perger, and J. Kraus, "Recent investigations on the volcano smoke antenna," in *IEEE Antennas and Propagation Society International Symposium*, USA, 2003.
- [22] W. Stohr, "Broadband ellipsoidal dipole antenna ." U.S. Patent 3364491 A, 1968.
- [23] Agrawall, N.P. and Kumar, G. and Ray, K. P, "Wide-band planar monopole antennas," *IEEE Transactions on Antennas and Propagation*, vol. 46, no. 2, pp. 294–295, 1998.
- [24] Lee.E, Hall.p.s, Gardner P, "Compact wideband planar monopole antenna," *Electronics Letters*, vol. 35, pp. 2157–2159, 1999.
- [25] Anob, P. V. and Ray, K. P. and Kumar, G, "Wideband orthogonal square monopole antennas with semi-circular base," in *IEEE Antennas and Propagation Society International Symposium*, vol. 3, pp. 294–297 vol.3, 2001.
- [26] Ammann, and Max , "Control of the impedance bandwidth of wideband planar monopole antennas using a beveling technique," *Microwave and Optical Technology Letters*, vol. 30, pp. 229–232, 2001.
- [27] Antonino-Daviu, "Wideband double-fed planar monopole antenna," *Electronics Letters*, vol. 34, pp. 1635–1636, 2003.
- [28] Kin-Lu Wong, Yun-Wen Chi, Chih-Ming Su, Fa-Shian Chang, "Band-notched ultra-wideband circular-disc monopole antenna with an are shaped slot," *Microwave and Optical Letter*, vol. 45, pp. 188–191, 2005.
- [29] K.P. Ray, Y. Ranga and P. Gabhale, "Printed square monopole antenna with semicircular base for ultra-wide bandwidth," *Electronics Letters*, vol. 43, 2007.

- [30] Peyrot-Solis, M. A. and Tirado-Mendez, J.A. and Jardon-Aguilar, H, "Design of multiband UWB planarized monopole using DMS technique," *IEEE Antennas and Wireless Propagation Letters*, vol. 6, pp. 77–79, 2007.
- [31] Ray, K.P. and Ranga, Y, "Ultra-wideband printed modified triangular monopole antenna," *Electronics Letters*, vol. 42, no. 19, pp. 1081–1082, 2006.
- [32] S. H. Choi, J. K. Park, S. K. Kim and J. Y. Park, "A new ultrawideband antenna for UWB applications," *Microwave and Optical Technology Letters*, vol. 40, pp. 399–401, 2004.
- [33] Lin, C.-C. and Kuo, L.-C. and Chuang, H. -R and Kan, Y.-C., "A planar triangular monopole antenna for UWB communication," *IEEE Microwave and Wireless Components Letters*, vol. 15, pp. 624–626, 2005.
- [34] K. G. Thomas and N. Lenin, "Ultra wideband printed monopole antenna," *Microwave And Optical Technology Letters*, vol. 49, pp. 1082–1085, 2007.
- [35] Ching-Wei Ling and Wen-Hsin Lo and Ran-Hong Yan and Shyh-Jong Chung, "Planar binomial curved monopole antennas for ultrawideband communication," *IEEE Transactions on Antennas and Propagation*, vol. 55, no. 9, pp. 2622–2624, 2007.
- [36] M. Gopikrishna, D. D. Krishna, C. K. Aanandan, P. Mohanan and K. Vasudevan, "Square monopole antenna for ultra wideband communication applications," *Journal of Electro-Magnetic Waves and Application*, vol. 21, pp. 1525–1537, 2007.
- [37] Yuan-Dan Dong and Wei Hong and Zhen-Qi Kuai and Ji Xin Chen, "Analysis of planar ultrawideband antennas with on-ground slot band-notched structures," *IEEE Transactions on Antennas and Propagation*, vol. 57, no. 7, pp. 1886–1893, 2009.
- [38] Qi Wu and Ronghong Jin and Junping Geng and Min Ding, "Printed omni-directional UWB monopole antenna with very compact size," *IEEE Transactions on Antennas and Propagation*, vol. 56, no. 3, pp. 896–899, 2008.
- [39] X. L. Bao and M. J. Ammann, "Investigation on UWB printed monopole antenna with rectangular slitted ground plane," *Microwave and Optical Technology Letters*, vol. 49, pp. 1585–1587, 2007.
- [40] Thomas, K.G. and Lenin, N. and Sivaramakrishnan, R, "Ultrawideband planar disc monopole," *IEEE Transactions on Antennas and Propagation*, vol. 54, no. 4, pp. 1339–1341, 2006.
- [41] Y.-T. L. Saou-Wen Su, Austin Chen, "Wide band omnidirectional L-shaped monopole antenna for a wireless USB dongle," *Microwave and Optical Technology Letters*, vol. 49, pp. 625–628, 2007.
- [42] Saou-Wen Su and Jui-Hung Chou and Kin-Lu Wong, "Internal ultrawideband monopole antenna for wireless USB dongle applications," *IEEE Transactions on Antennas and Propagation*, vol. 55, no. 4, pp. 1180–1183, 2007.

- [43] B. L. Ooi, Irene Ang, X. C. Shan, Albert Lu, R. Fieck, and H. D. Hristov, "Wide-slot waveguide antenna on ltcc technology," *Microwave And Optical Technology Letters*, vol. 50, pp. 2181–2184, 2008.
- [44] Jin-Ping Zhang and Xu, Yun-Sheng and Wei-Dong Wang, "Microstrip-fed semi-elliptical dipole antennas for ultrawideband communications," *IEEE Transactions on Antennas and Propagation*, vol. 56, no. 1, pp. 241–244, 2008.
- [45] Zaker, Reza and Abdipour, A., "A very compact ultrawideband printed omnidirectional monopole antenna," *IEEE Antennas and Wireless Propagation Letters*, vol. 9, pp. 471–473, 2010.
- [46] Sim, C. and Wen-Tsan Chung and Ching-Her Lee, "Compact slot antenna for UWB applications," *IEEE Antennas and Wireless Propagation Letters*, vol. 9, pp. 63–66, 2010.
- [47] Mahdi Moosazadeh, Changiz Ghobadi and Massoud Dousti, "Small monopole antenna with checkedred-shaped patch for UWB application," *IEEE Antennas and Wireless Propagation Letters*, vol. 9, pp. 1014–1017, 2010.
- [48] F.Muge, Altuncan Hizal and Ligthart, "On the operating principles of UWB, CPW-fed printed antennas," *IEEE Antennas and Propagation Magazine*, vol. 52, pp. 46–50, 2010.
- [49] K.G.Thomas and M.Sreenivasan, "Wideband planar printed antenna with end-fire radiation pattern," *IET Microwave. Antennas and Propagation*, vol. 5, pp. 831–836, 2011.
- [50] Yang Lu, Yi Huang and Ping Cao, "Reducing ground-plane effects on UWB monopole antennas," *IEEE Antennas and Wireless Propagation Letters*, vol. 10, pp. 147–151, 2011.
- [51] Mohammad Reza and Farzad Mohajeri, "A compact hexagonal wide-slot antenan with microstrip-fed monopole for UWB application," *IEEE Antennas and Wireless Propagation Letters*, vol. 10, pp. 682–686, 2011.
- [52] Wei Liu, YinZeng Yin, WenLong Xu and ShaoLi Zuo, "Compact open-slot antenna with bandwidth enhancement," *IEEE Antennas and Wireless Propagation Letters*, vol. 10, pp. 850–854, 2011.
- [53] Deepti Das Krishna, *Investigations on broadband planar monopole and slot radiations and their suitability for UWB applications*. PhD thesis, Department of Electronics, CUSAT, India, 2010.
- [54] M .Gopikrishna, *Investigations on the radiation characterostocs planar printed UWB antennas with modified ground planes*. PhD thesis, Department of Electronics, CUSAT, India, 2010.
- [55] H.J.Zhou, B.H.Sun, Q.Zh and J.Y.Deng, "Implementation and investigation of u-shaped aperture UWB antenna with dual band-notched characteristics," *Electronics Letters*, vol. 44, pp. 1387 – 1388, 2008.
- [56] N.Farrokh Heshmat, J.Nourinia and C.Ghobadi, "Band-notched ultra-wideband printed open slot antenna using variable on ground slits," *Electronics Letters*, vol. 45, 2009.

- [57] J.Liu, S.Gong, Y.Xu, X.Zhang, C.Feng and N.Qi, "Compact printed ultra-wideband monopole antenna with dual band-notched characteristics," *Electronics Letters*, vol. 44, pp. 710–711, 2008.
- [58] Kenny Seungwoo Ryu, Ahmed A. Kishk, "UWB antenna with single or dual band-notches for lower WLAN band and Upper WLAN Band," *IEEE Transactions on Antennas and Propagation*, vol. 57, pp. 3942–3950, 2009.
- [59] Wen Tao Li, Xiao Wei Shi and Yong Qiang Hei, "Novel planar UWB monopole antenna with triple band-notched characteristics," *IEEE Antennas and Wireless Propagation Letters*, vol. 8, pp. 1094–1098, 2009.
- [60] D.O.Kim and C.Y.Kim, "CPW-fed ultra wideband antenna with triple-band notch function," *Electronics Letters*, vol. 46, 2010.
- [61] Ming-Chun Tang ,Shaoqiu Xiao , Tianwei Deng , Duo Wang ,Jian Guan , Bingzhong Wang and Guang-Ding Ge, "Compact UWB Antenna With Multiple Band-Notches for WiMAX and WLAN," *IEEE Transactions on Antennas and Propagation*, vol. 59, no. 4, pp. 1372–1376, 2011.
- [62] Subbarao, Akkala and Raghavan, S, "Printed planar UWB antenna with rejection of WLAN and WiMAX bands," *Microwave and Optical Technology Letters*, vol. 55, no. 4, pp. 740–744, 2013.
- [63] J. I. Kim, Y. J. Chong, and J. I. Choi, "Printed multiband terminal antenna for multiple wireless services," *12th International Conference on Antennas and Propagation*, Exeter University, 2003.
- [64] C. Y. Mo and J. C. Cheng, "A novel tri-band dual-port coplanar waveguide-fed slot loop antenna for WLAN and WiMAX applications," *6th Asia-Pacific Microwave Conference*, Macau, 2008.
- [65] Zong Xian-zheng; Nie Zai-ping and Yang Xue-heng, "Novel dual feed broadband antennas with a combined shape," *4th Asia-Pacific Conference on Environmental Electromagnetics*, Dalian, 2006.
- [66] D. Guha, S. Biswas, C. Kumar, "Annular ring shaped DGS to reduce mutual coupling between two microstrip patches," In proceeding of Applied Electromagnetics Conference (AEMC), Kolkata, 2009.
- [67] J. Cho, C.W. Jung and K. Kim, "Frequency-reconfigurable two-port antenna for mobile phone operating over multiple service bands," *Electronics Letters*, vol. 45, pp. 1009–1011, 2009.
- [68] Z.H. Hu, C.T.P. Song, J. Kelly, P.S. Hall and P. Gardner, "Wide tuneable dual-band reconfigurable antenna," *Electronics Letters*, vol. 45, pp. 1109–1110, 2009.
- [69] H. Wong, K.-L. Lau and K.-M. Luk, "Design of dual-polarized l-probe patch antenna arrays with high isolation," *IEEE Transaction Antennas and Propagation*, vol. 52, pp. 45–51, 2004.

- [70] C.-Y. Chiu, J.-B. Yan and R. D. Murch, "Compact three-port orthogonally polarized MIMO antennas," *IEEE Antennas and Wire*, vol. 6, pp. 619–622, 2007.
- [71] K.-L. Wong, S.-W. Su, and Y.-L. Kuo, "A printed ultra-wideband diversity monopole antenna," *Microwave and Optical Technology Letters*, vol. 38, no. 4, pp. 257–259, 2003.
- [72] Gaoming Chi, Binhong Li, and Dongsheng Qi, "Dual-band printed diversity antenna for 2.4/5.2-ghz wlan application," *Microwave And Optical Technology Letters*, vol. 45, pp. 561–563, 2005.
- [73] Liu, L. and Zhao, H. and See, T. S P and Zhi Ning Chen, "A printed ultra-wideband diversity antenna," in *IEEE International Conference Ultra Wideband*, pp. 351–356, Waltham, MA, 2006.
- [74] Diallo, A. and Luxey, C. and Le-Thuc, P. and Staraj, R. and Kossiavas, G, "Study and reduction of the mutual coupling between two mobile phone pifas operating in the dcs1800 and umts bands," *IEEE Transactions on Antennas and Propagation*, vol. 54, no. 11, pp. 3063–3074, 2006.
- [75] Chi-Yuk Chiu and Chi-Ho Cheng and Murch, R.D. and Rowell, C.R, "Reduction of Mutual Coupling Between Closely-Packed Antenna Elements," *IEEE Transactions on Antennas and Propagation*, vol. 55, no. 6, pp. 1732–1738, 2007.
- [76] Ding Yuan and Zhengwei Du and Ke Gong and Zhenghe Feng, "A novel dual-band printed diversity antenna for mobile terminals," *IEEE Transactions on Antennas and Propagation*, vol. 55, no. 7, pp. 2088–2096, 2007.
- [77] Seokjin Hong, Kyungho Chung, Jaewon Lee, Sangwook Jung, Sang-Sun Lee, and Jaehoon Choi, "Design of a diversity antenna with stubs for uwb applications," *Microwave And Optical Technology Letters*, vol. 50, pp. 1352–1356, 2008.
- [78] Jaewon Lee, Seokjin Hong, and Jaehoon Choi, "Design of an ultra-wideband MIMO antenna for pda applications," *Microwave And Optical Technology Letters*, vol. 52, pp. 2165–2170, 2010.
- [79] Wang, A. and Zhenghe Feng and Luk, Kwai-Man, "Pattern and polarization diversity antenna with high isolation for portable wireless devices," *IEEE Antennas and Wireless Propagation Letters*, vol. 8, pp. 209–211, 2009.
- [80] See, T. S P and Zhi Ning Chen, "An ultrawideband diversity antenna," *IEEE Transactions on Antennas and Propagation*, vol. 57, no. 6, pp. 1597–1605, 2009.
- [81] Ali Nezhad, S.M. and Hassani, H.R, "A novel triband E-shaped printed monopole antenna for MIMO application," *IEEE Antennas and Wireless Propagation Letters*, vol. 9, pp. 576–579, 2010.
- [82] Shuai Zhang and Zhinong Ying and Jiang Xiong and Sailing He, "Ultrawideband mimo/diversity antennas with a tree-like structure to enhance wideband isolation," *IEEE Antennas and Wireless Propagation Letters*, vol. 8, pp. 1279–1282, 2009.

- [83] S. Baek and S. Lim, "Compact planar MIMO antenna array with polarisation diversity on single layer," *Electronics letters*, vol. 46, pp. 528–530, 2010.
- [84] Q. Luo, J.R. Pereira and H.M. Salgado, "Reconfigurable dual-band C-shaped monopole antenna array with high isolation," *Electronics letters*, vol. 46, pp. 210–212, 2010.
- [85] Sonkki, M. and Salonen, E, "Low mutual coupling between monopole antennas by using two slots," *IEEE Antennas and Wireless Propagation Letters*, vol. 9, pp. 138 –141, 2010.
- [86] Gaojian Kang and Zhengwei Du and Ke Gong, "Compact broadband printed slot-monopole-hybrid diversity antenna for mobile terminals," *IEEE Antennas and Wireless Propagation Letters*, vol. 10, pp. 159–162, 2011.
- [87] XueMing Ling and RongLin Li, "A novel dual-band MIMO antenna array with low mutual coupling for portable wireless devices," *IEEE Antennas and Wireless Propagation Letters*, vol. 10, pp. 1039–1042, 2011.
- [88] H.K. Yoon, Y.J. Yoon, H. Kim, C.-H. Lee, "Flexible ultra-wideband polarisation diversity antenna with band-notch function," *IET Microwave. Antennas Propagation*, vol. 5, pp. 1463–1470, 2011.
- [89] A. Najam, Y. Duroc, and S. Tedjni, "UWB-MIMO antenna with novel stub structure," *Progress In Electromagnetics Research*, vol. 19, pp. 245–257, 2011.
- [90] Yuan Yao and Xing Wang and Xiaodong Chen and Junsheng Yu and Shaohua Liu, "Novel diversity/MIMO PIFA antenna with broadband circular polarization for multimode satellite navigation," *IEEE Antennas and Wireless Propagation Letters*, vol. 11, pp. 65–68, 2012.
- [91] P.A. Agrawal, G.Kumar and K.P.Ray, "Wideband planar monopole antenna," *IEEE Transaction on Antennas and Propagation*, vol. 46, pp. 294–295, 1998.
- [92] G. Pedersen and J. Andersen, "Handset antennas for mobile communications: intergration diversity and performance," *Review Of Science Radio*, pp. 119–138, 1999.
- [93] A. N. Kulkarni and S. K. Sharma, "A multiband antenna with MIMO implementation for USB dongle size wireless devices," *Microwave And Optical Technology Letters*, vol. 54, pp. 1990–1994, 2012.
- [94] S. Blanch, J. Romeu and I. Corbella, "Exact representation of antenna system diversity performance from input parameter description," *Electronics Letters*, vol. 9, pp. 705–707, 2003.
- [95] D valderas, P.Crespo, and C. Ling, "UWB portable printed monopole arry design for MIMO-communications," *Microwave and Optical Technology Letters*, vol. 52, pp. 889–895, 2010.
- [96] H.Shin and J.H. Lee, "Capacity of Multiple antenna fading channels: spatial fading correlation double scattering and key hole," *IEEE Transactions on Information Theory*, vol. 10, pp. 2636–2647, 2003.

- [97] Jian-feng Li Qing-xin Chu and Tian-gui Huang, "A compact wideband mimo antenna with two novel bent slits," *IEEE Transactions On Antennas And Propagation*, vol. 60, pp. 482–489, 2012.
- [98] Terence S. P. See and Zhi Ning Chen, "An Ultrawideband Diversity Antenna," *IEEE Transactions on Antennas and Propagation*, vol. 57, pp. 1597–1604, 2009.
- [99] Kin-Lu Wong, Saou-Wen Su, and Yen-Liang Kuo, "A Printed Ultra Wideband Diversity Monopole Antenna," *Microwave and Optical Technology Letters*, vol. 38, pp. 257–259, 2003.
- [100] W. Sorgel, C. Waldschmidt and W. Wiesbeck, "Transient responses of a vivaldi antenna and a logarithmic periodic dipole array for ultra wideband communication," pp. 592–595, Proc. IEEE AP-S Int. Symp, 2003.
- [101] A. H. Mohammadian, A. Rajkotia and S. S. Soliman, "Characterization of UWB transmit-receive antenna systems," pp. 157–161, IEEE Conf. on Ultra-wideband Systems and Technology, 2003.
- [102] S. Zwierzchowski and P. Jazayeri, "Derivation and determination of the antenna transfer function for use in ultra-wideband communications," pp. 533–543, Proc. Wireless, Calgary, Alberta, Canada, 2003.
- [103] Y. Duroc, A. Ghiotto, T.-P. Vuong and S. Tedjini, "UWB antennas: systems With transfer functions and impulse response.," *IEEE Transation on Antennas and Propagation*, pp. 1449–1451, 2007.
- [104] W. Sorgel and W. Wiesbeck, "Influence of antennas on ultrawideband transmisson," *EURASIP J. App. Signal Processing*, pp. 296–305, 2005.
- [105] D. Paris and F. Hurd, *Basic elctromagnetics theory*. McGraw-Hill, Newyork, 1969.
- [106] D. Pozar, *Microwave engineering*. Wiley, New York, 2005.
- [107] N. Bastos, J. P. A. and Sadowski, *Electromagnetic modeling by finite element methods*. New York: Marcel Dekker, Inc, 2003.
- [108] W. C. Gibson, *The method of moments in electromagnetics*. Taylor & Francis, 2008.
- [109] A. Taflove and S. C. Hagness, *Computational electrodynamics: the finite-difference time-domain method*. Artech House, 2005.
- [110] D. Swason, *Microwave circuit modeling using electromagnetic field simulation*. Artech House, 2003.
- [111] *User manual for HFSS*. Ansoft Corporation Pittsburg, PA, USA, 2000.
- [112] *User manual for CST*—. CST Germony, 2004.
- [113] M. Clements and T. Weiland, "Discrete electromagnetism with the finite integration technique," *Progress In Electromagnetics Research*, vol. 32, pp. 65–87, 2001.

Disseminations

Journal papers Published

1. **S.Natarajamani**, S K Behera and S K Patra, “A triple band-notched planar monopole antenna for ultra wide band applications”, *Microwave and Optical Technology Letters (Wiley Publication)*, 54(2):539-543, 2011
2. **S.Natarajamani**, S K Behera and S K Patra, “A Compact planar diversity antenna for ultrawideband application with bandnotched function”, *Microwave and Optical Technology Letters(Wiley Publication)*, 54(4):758-764, 2013
3. **S.Natarajamani**, S K Behera and S K Patra, “A triple band-notched planar antenna for UWB applications”, *Journal of Electromagnetic Wave and Application(Taylor Francis Publication)*, 27(9):1178-1186, 2013
4. **S.Natarajamani**, S K Behera and S K Patra, “Planar ultra-wideband fractal antenna with 3.4 and 5.5 GHz dual band-notched characteristics”, *International Journal of Signal and Imaging Systems Engineering(InderScience Publication)*, 6(1):46-51, 2013

Conference papers Published

1. **S.Natarajamani**, S K Behera and S K Patra, “A Planar UWB antenna with band notch characteristics”, *International Conference on Electronic Systems*, 2011, India.
2. **S.Natarajamani**, S K Behera and S K Patra, “A Planar Ultrawideband antenna with 5.5GHz band dispensation characteristics”, *Annual IEEE India Conference*, 2010, India.
3. **S.Natarajamani**, S K Behera and S K Patra, “A Compact wide band patch Antenna for WLAN application”, *IEEE second International Conference on Computing, Communication and Networking Technologies*, 2010, India.
4. **S.Natarajamani**, S K Behera and S K Patra, “Compact CPW-fed dual-band antenna for WLAN/UWB application”, *IEEE International Conference on Communication Control and Computing Technology* , 2010, India.

5. **S.Natarajamani**, S K Behera and S K Patra, “Compact slot antenna for UWB application and band-notch designs”, *IEEE 5th International Conference on Computational Intelligence and computer networks* , 2010, India
6. **S.Natarajamani**, S K Behera and S K Patra, “Design of multi slotted and multi frequency patch antenna”, *IEEE Applied Electromagnetics Conference*, 2009, India
7. **S.Natarajamani**, S K Behera and S K Patra, “CPW-FED octagon shape slot antenna for UWB application”, *IEEE 5th International conference on Microwaves, Antenna Propagation and Remote Sensing*, 2009, India

BIO-DATA

Natarajamani.S

Date of Birth: 15th May, 1984

Correspondence:

Research Scholar,

Department of Electronics and Communication Engineering,
National Institute of Technology Rourkela, India – 769 008.

Ph: +91 8807867611(M)

E-mail: natarajamani@gmail.com

Qualification

- Ph.D. (RF and Microwave Engineering)
National Institute of Technology Rourkela, Odisha, India
- M.E. (Communication Systems)
Anna University, Tamilnadu, India [First division]
- B.E. (Electronics and Communication)
Anna University, Tamilnadu, India [First division]
- Diploma (Electronics and Communication)
Govt. polytechnic college-Kanchipuram, India [First division]

Publications

- 04 Journal Articles
- 07 Conference Articles